RADIONUCLIDE SORPTION TECHNICAL ASSISTANCE ACTIVITIES AT THE CENTER FOR NUCLEAR WASTE REGULATORY ANALYSES

Prepared for

U.S. Nuclear Regulatory Commission
Contract NRC–02–07–006

Prepared by

Paul Bertetti
Roberto Pabalan
David Pickett
David Turner

Center for Nuclear Waste Regulatory Analyses
San Antonio, Texas

September 2011

ABSTRACT

The potential release of radionuclides as dissolved constituents in groundwater is a primary concern in performance assessment of proposed high-level nuclear waste geologic repositories. Sorption onto mineral surfaces is an important mechanism for reducing radionuclide concentrations along groundwater flow paths and retarding radionuclide migration. Radionuclide sorption is, in turn, influenced by the physical and chemical conditions of the groundwater system. Beginning in 1990, Center for Nuclear Waste Regulatory Analyses (CNWRA®) staff initiated experimental and modeling programs to evaluate processes that influence radionuclide sorption and to identify key geochemical and physical parameters that have the greatest effects. As the sorption program evolved, CNWRA staff focused on two main sorption mechanisms: (i) ion exchange, which has the greatest effects on alkali and alkaline earth radionuclides, such as Cs^{+} and Sr^{2+} and (ii) surface complexation, the process that exerts the most control on the sorption of long-lived actinides, such as uranium, neptunium, plutonium, americium, and thorium. In addition, fine-scaled analysis (extended x-ray absorption fine structure and molecular dynamics simulations) were used to better understand radionuclide sorption reactions at the molecular scale. CNWRA staff used the results from the experimental program to calibrate detailed ion-exchange and surface complexation process models that were used to inform CNWRA understanding of how radionuclide sorption could be abstracted into performance assessment models. The purpose of this knowledge management report is to capture insights gained during more than 20 years of CNWRA experience in evaluating radionuclide sorption processes and incorporating the results of detailed modeling into the performance assessment codes U.S. Nuclear Regulatory Commission and CNWRA staffs developed. A list of sorption-related reports and publications CNWRA staff produced is included as an appendix.

CONTENTS

CONTENTS (continued)

CONTENTS (continued)

FIGURES

FIGURES (continued)

FIGURES (continued)

TABLES

ACKNOWLEDGMENTS

This report was prepared to document work performed by the Center for Nuclear Waste Regulatory Analyses (CNWRA®) for the U.S. Nuclear Regulatory Commission (USNRC) under Contract No. NRC–02–007–006. The studies and analyses reported here were performed on behalf of the NRC Office of Nuclear Material Safety and Safeguards, Division of High-Level Waste Repository Safety. The report is an independent product of the CNWRA and does not necessarily reflect the views or regulatory position of USNRC.

The authors thank James Myers for technical review and English Pearcy for programmatic review. The authors also thank Arturo Ramos for support in report preparation and Lauren Mulverhill for editorial review.

QUALITY OF DATA, ANALYSES, AND CODE DEVELOPMENT

DATA: All CNWRA-generated original data contained in this report meet the quality assurance requirements described in the Geosciences and Engineering Division Quality Assurance Manual. Sources for other data should be consulted for determining the level of quality for those data.

ANALYSES AND CODES: No scientific and engineering software was used in the analyses contained in this report.

1 INTRODUCTION

1.1 Background

The potential release of radionuclides as dissolved constituents in groundwater is a primary concern in performance assessment of proposed high-level nuclear waste geologic repositories. Sorption onto mineral surfaces is an important mechanism for reducing radionuclide concentrations along groundwater flow paths and retarding radionuclide migration to a receptor location [such as the reasonably maximally exposed individual (RMEI)].

Early in the high-level nuclear waste program, U.S. Nuclear Regulatory Commission (NRC) staff recognized the importance of understanding processes that may influence radionuclide sorption in the engineered and natural barrier components of a geologic repository system at Yucca Mountain, Nevada. As part of its charter program work to support NRC in meeting its responsibilities under the Nuclear Waste Policy Act of 1982, as amended, the Center for Nuclear Waste Regulatory Analyses (CNWRA®) has been engaged since 1990 in experimental and modeling programs designed to understand how physical and chemical conditions can affect radionuclide sorption. A list of sorption-related reports and publications CNWRA produced staff is included as an appendix.

The purpose of this knowledge management report is to capture insights gained during more than 20 years of CNWRA experience in evaluating radionuclide sorption processes and incorporating the results of detailed modeling into the performance assessment codes developed by NRC and CNWRA staffs.

1.2 History of Radionuclide Sorption Technical Assistance at the CNWRA

Beginning in 1990, CNWRA staff initiated experimental and modeling programs to evaluate processes that might influence radionuclide sorption, and to identify key geochemical and physical parameters that have the greatest effects. As the sorption program evolved, CNWRA staff focused on two main sorption mechanisms: (i) ion exchange, which has the greatest effects on alkali and alkaline earth radionuclides such as Cs^+ and Sr^{2+} and (ii) surface complexation, the process that exerts the most control on the sorption of long-lived actinides such as uranium, neptunium, plutonium, americium, and thorium.

1.2.1 Experimental Program(s) and Developing Process Models

1.2.1.1 Ion Exchange

Zeolite minerals are naturally occurring aluminosilicate compounds with a characteristic three-dimensional pore structure that allows exchange of cations between aqueous solutions and intracrystalline sites. Because of their favorable ion-exchange selectivity for certain cations such as Cs^+, Sr^{2+}, and NH_4^+, zeolite minerals are of interest for potential use in the remediation of sites contaminated with fission products such as Sr-90, Cs-135, and Cs-137. Zeolites are also of interest because Yucca Mountain is underlain by diagenetically altered, zeolite-rich (predominantly clinoptilolite) rhyolitic tuffs that could serve as barriers to radionuclide migration to the accessible environment. Ion-exchange equilibria are a function of solid and aqueous phase composition and aqueous solution concentration. Because these parameters can vary

substantially for the chemical system of interest, it is essential to have chemical models that allow accurate description and prediction of ion-exchange equilibria.

To investigate the key aspects of ion-exchange processes and to develop the parameters needed to test different thermodynamic ion exchange models, CNWRA conducted experiments on ion exchange between clinoptilolite and aqueous solutions of Na^+, K^+, Sr^{2+}, and Ca^{2+} to examine binary, ternary, and quaternary exchanges. One thermodynamic approach that CNWRA staff found useful for this purpose combined the Pitzer electrolyte solution model to describe nonideal behavior in the aqueous phase with Wilson and Margules solid solution formulations to account for nonideality effects in the zeolite. The thermodynamic approach, detailed in Section 3.2, was successful in describing and predicting ion-exchange equilibria between clinoptilolite and aqueous solutions over wide ranges of solution composition and concentration.

1.2.1.2 Surface Complexation

In contrast to fission products like Cs-137 and Sr-90, sorption studies by CNWRA staff and other groups indicate that actinides, such as uranium and neptunium, sorb onto most silicate and oxide minerals not through ion exchange, but through a surface complexation mechanism. This type of sorption behavior has been well simulated using a class of chemical equilibrium models called surface complexation models. In a surface complexation approach, the sorbing radionuclides are assumed to form complexes with functional surface sites at the mineral–water interface that are analogous to actinide speciation in the bulk aqueous phase (Davis and Kent, 1990). An example of a general type of surface complexation reaction for an actinide (An) sorbing on a functional surface site $>SOH^0$ would be

$$>SOH^0 + pAn^{m+} + nH_2O = \left[>SOH_q^- - (An)_p(OH)_n\right]^{pm+q-n-1} + (1+n-q)H^+ \qquad (1.2\text{-}1)$$

The strength of the surface complex, and therefore the amount of sorbed radionuclide, depends on the speciation of the actinide in the bulk aqueous phase as well as the physical and electrostatic characteristics of the sorbing mineral. The surface complexation modeling approach is detailed in Section 3.3.

The surface complexation approach works well at simulating sorption onto relatively simple pure mineral phases, but the dependence of sorption on aqueous solution properties (e.g., pH, radionuclide concentration, ionic strength, and complexing ligands) and sorptive phase characteristics (e.g., composition, surface area, and sorption site density) makes prediction of radionuclide retardation and transport difficult in natural geologic systems that are mineralogically and chemically heterogeneous.

CNWRA staff conducted batch experiments to examine uranium and neptunium sorption on alumina, quartz, clinoptilolite, and montmorillonite. These phases were selected because they represent minerals that occur at Yucca Mountain, and because they represent a relatively broad range in surface properties. To evaluate the effects of key geochemical parameters, the experiments were conducted over a wide range in radionuclide concentrations, solution chemistry, and partial pressure of CO_2 gas chemistry (see Section 2.2). CNWRA experiments indicated that actinide sorption onto silicates, aluminosilicates, and oxides tended to be strongest where the chemistry of the system (including complexing ligands such as carbonate) favors the formation of hydroxy complexes in the aqueous phase, and the magnitude of sorption is controlled primarily by the number of available sorption sites (see Section 2.4). Data from

these experiments were used to derive the parameters necessary to implement a simplified and internally consistent surface complexation model, that was then abstracted to provide input into performance assessment calculations (see Section 4).

1.3 Process Model Abstraction for Total-system Performance Assessment

Traditionally, performance assessment models have simulated radionuclide sorption using constant empirical relationships between the mass of radionuclide sorbed on the solid (S) to the mass of radionuclide dissolved in solution (C). The most common of these empirical relationships is the relatively straightforward linear sorption coefficient {K_d in mL/g [fl. oz/oz]}

$$K_d = \left(\frac{S}{C}\right)\left(\frac{V}{M}\right) \tag{1.3-1}$$

where S is the amount of radionuclide sorbed on the mineral surface {g/g or [oz/oz]}, C is the amount of radionuclide dissolved in the solution [g/mL (oz/fl. oz)]. V represents the solution volume (mL [fl. oz]), and M represents the mass of solid in g. The K_d is then used to represent the relative contaminant transport velocity through a retardation factor, R_f (unitless) (Freeze and Cherry, 1979), such that

$$R_f = \frac{\text{groundwater velocity}}{\text{contaminant velocity}} = 1 + \left(\frac{\rho_b}{\theta}\right)K_d \tag{1.3-2}$$

where ρ_b = bulk density, and θ = porosity. For performance assessment calculations, the K_d value for a given radioelement is typically assumed to be a property of the geologic medium, much like permeability and porosity. In actuality, the K_d value is a derived property that is known to be a function of system chemistry. The K_d approach assumes the amount of radionuclide sorbed on a solid is directly proportional to the amount dissolved in solution, but does not explicitly consider changes in system chemistry or variations in the mineral–water interface that may affect radionuclide sorption. For actinides, however, sorption is a complex function of chemistry, particularly pH, mineral surface area, and total carbon concentration (Bertetti, et al., 1998; Pabalan, et al., 1998; Turner, 1995; Wang, et al., 2001a,b; Davis and Curtis, 2003). For this reason, it is difficult to extrapolate experimentally derived sorption coefficients (Turner, 1995; Davis and Curtis, 2003).

In performance assessment analyses, uncertainty and variability in sorption coefficients are represented by statistical parameter distributions based, at least in part, on expert judgment that is in turn based on experimental determinations of K_d. The parameter distributions for sorption coefficients and other uncertain parameters are sampled during individual numerical simulations or realizations.

The principal goal of CNWRA sorption work has been to develop performance assessment methods that incorporate, at least indirectly, the effects of chemistry on radionuclide sorption coefficients. Turner, et al. (2006, 2002) identified two methods for doing this. In the first approach, a surface complexation model was applied with available site-specific hydrochemistry data to develop frequency histograms and the accompanying statistics for calculated K_d. These statistics provide more realistic constraints on the probability distributions used in performance assessment to describe radionuclide sorption. The model results suggest that lognormal

distributions of actinide sorption coefficients are appropriate. This approach allows the user to estimate statistical relationships correlating among the different calculated radionuclide sorption parameters and provides for an indirect inclusion of geochemical effects on sorption in performance assessment calculations.

In the second approach, CNWRA staff used calibrated surface complexation models to simulate actinide sorption over a wide range of geochemical conditions. This approach allows the user to develop a sorption response surface for a given radionuclide as a function of key geochemical parameters. For each performance assessment realization, key geochemical parameters, such as pH and P_{CO2}, are sampled from distributions based on site-specific data, and the corresponding K_d is estimated from the response surface. There is uncertainty in extrapolating beyond the experimental conditions used for parameterizing the model, but even so, the extrapolation is based on a more sound theoretical basis than strictly empirical approaches.

1.4 References (Section 1)

Bertetti, F.P., R.T. Pabalan, and M.G. Almendarez. "Studies of Neptunium^{V} Sorption on Quartz, Clinoptilolite, Montmorillonite, and α-alumina." *Adsorption of Metals by Geomedia*. E.A. Jenne, ed. New York City, New York: Academic Press, Inc. pp. 131–148. 1998.

Davis, J.A. and G.P. Curtis. NUREG/CR–6820, "Application of Surface Complexation Modeling to Describe Uranium(vi) Adsorption and Retardation at the Uranium Mill Tailings Site at Naturita, Colorado." Washington, DC: NRC. 2003.

Davis, J.A. and D.B. Kent. "Surface Complexation Modeling in Aqueous Geochemistry. Reviews in Mineralogy. Vol. 23." *Mineral-Water Interface Geochemistry*. M.F. Hochella, Jr. and A.F. White, eds. Washington, DC: Mineralogical Society of America. pp. 77−260. 1990.

Freeze, R.A. and J.A. Cherry. *Groundwater*. Englewood Cliffs, New Jersey: Prentice-Hall, Inc. 1979.

Kent, D.B., V.S. Tripathi, N.B. Ball, J.O. Leckie, and M.D. Siegel. NUREG/CR–4807, "Surface-Complexation Modeling of Radionuclide Adsorption in Subsurface Environments." Washington, DC: NRC. 1988.

Pabalan, R.T., D.R. Turner, F.P. Bertetti, and J.D. Prikryl. "UraniumVI Sorption onto Selected Mineral Surfaces." *Adsorption of Metals by Geomedia*. E.A. Jenne, ed. New York City, New York: Academic Press, Inc. pp 99–130. 1998.

Turner, D.R. CNWRA 95-001, "A Uniform Approach to Surface Complexation Modeling of Radionuclide Sorption." San Antonio, Texas: CNWRA. 1995.

Turner, D.R., R.T. Pabalan, and F.P. Bertetti. Applying Surface Complexation Modeling to Radionuclide Sorption." *Surface Complexation Modeling*. F. Lützenkirchen, ed. Amsterdam: Elsevier, Ltd: pp. 553–604. 2006.

Turner, D.R., F.P. Bertetti, and R.T. Pabalan. "The Role of Radionuclide Sorption in High-Level Waste Performance Assessment: Approaches for the Abstraction of Detailed Models." Soil Science Society of America Proceedings Volume: Soil Geochemical Processes of Radionuclides. pp. 211–252. Pittsburgh, Pennsylvania: Soil Science of America. 2002.

Wang, P., A. Anderko, and D.R. Turner. "Thermodynamic Modeling of Radionuclide Adsorption on Selected Minerals. I: Cations." *Industrial and Engineering Chemistry Research*. Vol. 40. pp. 4,428–4,443. 2001.

Wang, P., A. Anderko, and D.R. Turner. "Thermodynamic Modeling of Radionuclide Adsorption on Selected Minerals. II: Anions." *Industrial and Engineering Chemistry Research*. Vol. 40. pp. 4,444–4,453. 2001.

2 RADIONUCLIDE SORPTION EXPERIMENTS

In a generic sense, the term sorption refers to the removal of a dissolved contaminant from solution through interaction with a solid substrate to which the solution is exposed. Sorption may involve several physicochemical processes including precipitation, co-precipitation, ion exchange, and surface complexation. Because of their long half-lives and radiotoxicity, the Center for Nuclear Waste Regulatory Analyses (CNWRA®) experimental program on sorption generally focused on actinide sorption through a process of surface complexation.

The CNWRA sorption experiments were designed to identify, characterize, and reduce uncertainties of features and processes important to assessing the safety of high-level waste disposal. The experimental program was not intended to provide a comprehensive characterization of sorption and sorption parameters related to Yucca Mountain. Instead, work was focused on improving knowledge in critical areas as guided by the risk-informed prelicensing process.

To develop an understanding of specific important physical and chemical parameters that affect sorption behavior in the Yucca Mountain environment, experiments were conducted to investigate the sorption behavior of uranium, neptunium, and other radionuclides on geologic media. The experiments were designed to determine the effects of pH, initial radionuclide concentration in solution, solid mass to solution volume ratio, solution ionic strength, and partial pressure of CO_2(g) on sorption. The minerals selected for these sorption experiments were representative of matrix and fracture lining minerals in Yucca Mountain stratigraphic units (Bish and Chipera, 1989).

Results of the experimental and associated sorption modeling program were used to (i) provide input and guidance for the development and review of performance assessment models, (ii) provide confirmatory results for review of U.S. Department of Energy (DOE) activities, and (iii) identify and reduce uncertainty in parameters deemed important to repository performance.

2.1 Chemical Systems Considered

Initial DOE investigations of the Yucca Mountain region indicated that the potential radionuclide flow paths within the volcanic and alluvial aquifers are dominated by sodium-calcium-bicarbonate waters of relatively low ionic strength (~0.003 M) (e.g., Ogard and Kerrisk, 1984). In addition, the groundwaters are generally oxidizing and ranged in pH from about 6 to 9. Subsequent data derived from DOE field studies and independent CNWRA field sampling confirmed these general characteristics for the volcanic and alluvial aquifers (e.g., Perfect, et al., 1995; Turner and Pabalan, 1999; Bertetti, et al., 2004; McMurry and Bertetti, 2005). The type and variations of the chemistry of Yucca Mountain groundwaters were carefully considered in the CNWRA experimental program on sorption, and experimental solution chemistries were tailored as needed for the goals of a particular sorption experiment.

Early experimental efforts focused on developing a general understanding of sorption behavior over a wide range of pH conditions (e.g., Pabalan, et al., 1998). The influence of carbonate complexation of actinides on sorption was also considered by varying the CO_2(g) concentrations of the experimental solutions. Because of the potential confounding effects of ion-exchange processes in assessing the complexation of radionuclides on mineral surfaces, many of the sorption experiments were conducted using a background electrolyte of 0.1 M $NaNO_3$ (Pabalan, et al., 1998; Bertetti, et al., 1998), which helped to minimize ion exchange by providing an excess of Na^+ in solution. In some experiments, however, ionic strength of solution

was varied to examine its effects on sorption. All experiments were conducted under oxidizing conditions, which predominated along expected flow paths from Yucca Mountain to the accessible environment (e.g., Ogard and Kerrisk, 1984; Bertetti, et al., 2004). Radionuclide concentrations in experiments were constrained by the need to maintain concentrations low enough to remain below solubility limits (to prevent the potential confounding effects of precipitation) yet high enough to effectively quantify radionuclide concentrations with the analytical tools available.

The sorption experimental program evolved as data were collected from DOE characterization of the Yucca Mountain region, and the conceptual understanding of the Yucca Mountain groundwater system and its transport processes matured. Initial experiments assessed the sorption influence of saturated volcanic strata below the proposed repository horizon by focusing on common minerals (quartz, clinoptilolite, calcite, and montmorillonite) identified in those units (Bish and Chipera, 1989). Later, as focus shifted to the saturated alluvium as a potentially important natural barrier, analyses were conducted to evaluate and confirm the mineralogy of potential sorptive surface in the alluvium (Bertetti and Werling, 2005; McMurry and Bertetti, 2005). As a result, experiments were expanded to include calcite and samples of alluvium collected in the field (e.g., Bertetti, 2002; Bertetti and Werling, 2005). Additionally, experiments were modified to assess sorption using actual groundwater collected from the Fortymile Wash region or using simulated groundwater that mimicked the composition of the alluvial aquifer (Bertetti and Werling, 2005).

2.1.1 Alkaline/Alkaline Earths (Na–Ca–K–Sr–Cs)

The sorption of fission products, such as Sr-90 and Cs-137, was studied primarily as part of the ion-exchange experimental program, which included many other alkaline and alkaline-earth cations. These experiments and their results are discussed in Section 3.2.

2.1.2 Uranium

Sorption experiments focused primarily on the actinides uranium and neptunium. Uranium was an important component of the experiments because (i) by mass it was the most prevalent radionuclide in spent fuel, (ii) there were known instances in groundwaters of the contamination and transport of oxidized U(VI), and (iii) the long half-life of various uranium isotopes meant that uranium would be part of the spent-fuel inventory and a potential contributor to dose for a long period of time. Moreover, aqueous chemistry data for uranium were more readily available, and there were numerous methods available for analyzing and quantifying uranium in solution. In the oxidizing Yucca Mountain groundwaters relevant to the sorption experimental program, U(VI) is expected to exist as the uranyl species (UO_2^{2+}) (e.g., Allard, et al., 1984).

Experiments investigating uranium sorption utilized the isotope U-233, which was available in a National Institute of Standard and Technology-traceable purified form from Isotope Products Laboratories (Burbank, California). Like the other radionuclides used in the sorption experimental program, the U-233 was quantified in solution by liquid scintillation analysis. Liquid scintillation analysis enabled analyses of a relatively high throughput of experimental solutions with a minimum of sample chemical pretreatment.

Uranium at various concentrations (~10^{-6} to 10^{-7} M) was reacted with the minerals α-alumina, clinoptilolite, montmorillonite, and quartz to understand uranium sorption behavior, produce data that enabled the development of surface complexation models, and confirm DOE analyses. Results of the numerous uranium sorption experiments indicated uranium sorption is highly

dependent on the pH of solution and, when CO_2(g) is present, on the formation of uranium carbonate complexes. Uranium sorption increases with increasing solution pH and, when CO_2(g) is present, displays maximum sorption at about pH of 6 before decreasing with further increases in pH. Specific sorption results for various experiments are discussed in Section 2.2. Uranium-related sorption experiments are summarized in Table 2.1.2-1.

2.1.3 Neptunium

Because of its long half-life (2.14×10^6 yr), radiotoxicity, occurrence in high-level waste, and reported low sorption characteristics, Np-237 was a particular concern to the safety suitability of the Yucca Mountain repository. Under the oxidizing conditions typical of the Yucca Mountain environment, neptunium is expected to exist in solution primarily in one oxidation state (V) as the neptunyl species, NpO_2^+ (e.g., Allard, et al., 1984; Fuger, 1992). Early in the sorption experimental program there were relatively few published investigations of the sorption behavior of neptunium (e.g., Allard, et al., 1984; Bidoglio, et al., 1988; Lieser and Mühlenweg, 1988; Nakayama and Sakamoto, 1991). As DOE characterization activities progressed (e.g., Triay, et al., 1993), it was clear that neptunium exhibited relatively low K_d values, and the range of reported neptunium K_d values suggested that neptunium could potentially be transported through the natural system within regulatory time frames. Thus, an extensive effort was made in the CNWRA program to reduce uncertainties in the magnitude and sorption behavior of neptunium.

Experiments investigating neptunium sorption utilized the isotope Np-237, which was available in a NIST-traceable purified form from Isotope Products Laboratories (Burbank, California). Like the other radionuclides used in the sorption experimental program, the Np-237 was quantified in solution by liquid scintillation analysis. The liquid scintillation analysis equipment used (Packard 2550TR/AB and later 3100TR/AB) enabled separation of the alpha activity signal of Np-237 and the beta activity signal of its immediate daughter Pa-233 so that no chemical separation or preprocessing of experimental solution samples was required.

Like the early uranium experiments, the early neptunium experiments were conducted using a background electrolyte of $NaNO_3$ or $NaClO_4$. Later experiments used actual groundwater collected from the Yucca Mountain region or synthetic groundwater at ionic strengths of about 1×10^{-3} M. Solutions with neptunium concentrations of approximately 2×10^{-6} M or less were reacted with quartz, clinoptilolite, α-alumina, montmorillonite, calcite, and alluvium over the course of the experiments.

Results of the neptunium sorption experiments indicated neptunium sorption was highly dependent on solution pH and carbonate concentration. Similar to observations of uranium sorption, neptunium speciation (hydrolysis and carbonate complexation) play key roles in neptunium sorption behavior. Maximum measured neptunium K_d values were much lower (more than two orders of magnitude) than those observed for uranium, and the neptunium sorption peak in solutions where CO_2(g) was present occurred at pH between 8–8.5.

Specific sorption results for various experiments are discussed in Section 2.2. Neptunium-related sorption experiments are summarized in Table 2.1.3-1.

2.1.4 Technetium

Under chemically oxidizing conditions typical of Yucca Mountain groundwaters, technetium has high solubility and exists as the pertechnetate anion (TcO_4^-), which has a low sorption potential.

The fission product Tc-99 has a relatively long half-life (2×10^5 yr) and sufficient mass inventory in spent fuel to make it a potential contributor to dose at regulatory time scales. Limited experiments were conducted to investigate the potential for the sorption of Tc-99 onto aquifer materials. The experiments were conducted on clinoptilolite and calcite over a range of pH at technetium concentrations of $3–4 \times 10^{-7}$ M. The results of both sets of experiments show that for the conditions studied there was no discernable sorption of Tc-99 (Figure 2.1-1), which was consistent with the representation of Tc-99 in performance assessment as a nonsorbing radionuclide.

2.2 Batch Experiments

The laboratory sorption investigations were conducted as batch experiments in which the solid substrate was immersed in a solution of known composition containing the radionuclide(s) of interest. In general, experiments were conducted so that sorption reactions and solutions would come to equilibrium before the solutions were sampled for radionuclide concentration and chemistry. Several confirmatory kinetics experiments were conducted with uranium, neptunium, and technetium to evaluate the minimum required duration of experiments. In all cases, the sorption reactions equilibrated within 48 hours. The limiting factor for solution equilibration was the rate of gas exchange between the experimental solutions and atmosphere, which took several days. Thus, care was taken to ensure adequate exposure to atmosphere and mixing of the solutions, and experiments were conducted for typical periods of 7–10 days.

The batch experiments were conducted using polycarbonate bottles or test tubes. Polycarbonate was selected based on results of tests to evaluate sorption of uranium and neptunium on container materials including Teflon-FEP, polypropylene, and polycarbonate. The results of those tests showed that in the absence of a competing substrate, the polycarbonate sorbed less uranium than the other materials tested. When a competing substrate was added, sorption on the container was reduced further (Figure 2.2-1). Some uranium sorption results were corrected as needed to account for container sorption (Pabalan, et al., 1998). Neptunium sorption onto containers was negligible in the presence of even a minimally sorbing competing substrate.

A main goal of the sorption experiments was to evaluate the effects of variations in solution chemistry on sorption behavior. Varying pH conditions were typically established by adding small amounts of acid or base to solutions. The partial pressure of CO_2(g) in solutions was established by exposing the experimental solutions to lab atmosphere or conducting the experiments inside an atmosphere-controlled glove box in which a known P_{CO2} (higher or lower than atmosphere) was maintained. As an alternative to glove box experiments, some low-CO_2(g) conditions were tested by using tightly capped vials to prevent gas exchange with lab atmosphere.

Minerals used in the majority of experiments were selected based on (i) expected or identified occurrences in Yucca Mountain strata or (ii) differences in surface characteristics. For example, the reported points of zero charge (pH_{pzc})—the pH at which the net electrical surface charge of the mineral is neutral or zero—for quartz, clinoptilolite, and α-alumina are 2.9, 3.0, and 9.1, respectively (Davis and Kent, 1990; Gainer, 1990), and pH_{pzc} values reported for montmorillonite range from 6.5 to 8 depending on the ionic strength of the background electrolyte (Wanner, et al., 1994). Single component minerals were acquired from readily available, commercial sources. Except for the α-alumina, all were physically and/or chemically pretreated to isolate particular size fractions and to remove unwanted mineral impurities and grain coatings. Natural alluvium used in later experiments was collected from Early Warning

Drilling Program well core samples and was treated as necessary for a particular experiment design. The Early Warning Drilling Program was conducted by Nye County, in part, to characterize the geology and hydraulic properties of the alluvial aquifers south of Yucca Mountain.

The external surface areas of the sorbent materials were determined using a multipoint N_2-BET isotherm measured using a Coulter SA3100 surface area analyzer. The surface area samples were prepared by outgassing for 24 hours at 350 °C [662 °F] {100 °C [212 °F] in the case of montmorillonite}. The composition and purity of the mineral sorbents were checked by petrographic examination and x-ray diffraction, scanning electron microscope/energy dispersive x-ray spectroscopy, x-ray fluoresence, and inductively coupled plasma analyses.

2.2.1 Quartz

Quartz was obtained as quartz sand (Wedron #510) from Wedron Silica Company (Illinois). The quartz sand was sieved to isolate the 60–100 mesh fraction {0.250–0.149 mm [0.0098–0.0059 in]} and was pretreated to remove impurities in a fashion similar to that used for clinoptilolite. A portion of the 60–100 mesh fraction was crushed using an agate mortar and pestle to create a fine-grained fraction {0.044–0.004 mm [0.0017–0.00016 in]} with higher surface area for use in evaluating the effects on sorption due to changes in surface area. The N_2-BET-measured surface areas of the 60–100 mesh fraction and the fine-grained fraction were 0.03 ± 0.01 and 0.5 ± 0.05 m^2/g, respectively.

Sorption experiments involving quartz were conducted for both U-233 and Np-237. Variables tested included pH, solid mass to solution volume ratio, radionuclide concentration, P_{CO2}, and surface area. Results of the experiments investigating U-233 sorption on quartz revealed patterns similarly observed for all other minerals studied in the sorption program: (i) in the absence of $CO_2(g)$, sorption increased with increasing pH (see Figure 2.2-2); (ii) in the presence of $CO_2(g)$, a sorption maximum was observed at pH values of ~6.5 and decreased with further increase in pH (see Figure 2.2-4); (iii) increasing the P_{CO2} content of solutions reduced the observed maximum sorption and shifted the pH of peak sorption to lower pH values (not shown); (iv) for the pH range and uranium concentration ranges studied, uranium sorption can be represented as a Freundlich isotherm at constant pH values (not shown); and (v) normalization of sorption data to effective surface area produces an overlap of sorption data for minerals of different surface types (see Figure 2.2-4) (Pabalan, et al., 1998). Because of its relatively low specific surface area, quartz sorbed the least uranium of the minerals tested in the experiments (Pabalan, et al., 1998).

Results of the experiments studying Np-237 sorption on quartz revealed patterns similarly observed for all other minerals studied in the sorption program: (i) in the absence of $CO_2(g)$, sorption increased with increasing pH (see Figure 2.2-3); (ii) in the presence of $CO_2(g)$, a sorption maximum was observed at pH values of ~8.25 and decreased with further increase in pH (see Figure 2.2-3); (iii) increasing the P_{CO2} content of solutions reduced the observed maximum sorption and shifted the pH of peak sorption to lower pH values (not shown); (iv) over the range of neptunium concentrations studied, neptunium sorption appeared to be linear (not shown); and (v) normalization of sorption data to effective surface area produces an overlap of sorption data for minerals of different surface types (see Figure 2.2-5) (Bertetti, et al., 1998). Because of its relatively low specific surface area, quartz sorbed the least neptunium of the minerals tested in the experiments (Bertetti, et al., 1998).

2.2.2 Alumina

The α-alumina (α-Al_2O_3) samples used in the experiments were obtained as powders from NIST, which issued the material as a certified reference material for measurements of specific surface area of powders. Reference materials 8005, 8006, and 8007, with reported surface areas of 2.09, 0.229, and 0.0686 m^2/g, were used in the sorption experiments. To minimize altering the surface of the α-alumina, the powder was not washed or pretreated prior to its use.

Sorption experiments involving quartz were conducted for both U-233 (atmospheric CO_2 only) and Np-237 (no CO_2 only). Variables tested included pH and surface area. Results of experiments investigating U-233 sorption on α-alumina indicated the pH-related sorption behavior was typical of that observed for quartz and other aluminosilicate minerals (Pabalan, et al., 1998). In the presence of CO_2(g), U-233 sorption peaked at pH of ~6.5 and decreased at higher and lower pH values (Figure 2.2.-4). Modeling indicated that the decrease in sorption at high pH resulted from formation of uranium-carbonate complexes in solution (Prikryl, et al., 1993).

Results of studies of Np-237 sorption on α-alumina showed that in the absence of CO_2(g), sorption increased with increases in pH throughout the pH range studied (Figure 2.2-5) (Bertetti, et al., 1998). Normalization of sorption data to account for effective surface area of the α-alumina resulted in an overlap of similarly processed data for silicate minerals (Figure 2.2-5). Because the α-alumina samples had known surface areas, their results provided confidence in the process of normalizing sorption data to effective surface areas to represent sorption across multiple mineral types.

2.2.3 Clinoptilolite

Clinoptilolite was obtained from a clinoptilolite-rich tuff from Death Valley Junction, California (Minerals Research Company). The tuff was crushed and sieved to separate the 100–200 mesh fraction {0.150–0.074 mm [0.0059–0.0029 in]} and chemically pretreated to remove soluble salts, carbonates, iron-oxides, and mineral impurities. The pretreatment is detailed in Pabalan (1994). The clinoptilolite was then converted to sodium-form by ion exchange with 3 M NaCl solutions. The measured N_2-BET surface area for the clinoptilolite was 10.1 ± 0.3 m^2/g.

Results of experiments investigating the sorption of U-233 on clinoptilolite revealed the similar pH-related behavior observed for other minerals (quartz, α-alumina, and montmorillonite) (Pabalan, et al., 1998) (Figures 2.2-2 and 2.2-4). Sorption maximum was reached at about a pH of 6 in the presence of CO_2(g), while sorption increased with increasing pH throughout the pH range tested under conditions where CO_2(g) was absent. The uranium sorption behavior is linked to U(VI)-speciation in solution (e.g., Pabalan, et al., 1998). Sorption occurs when the UO_2^{2+} species undergoes significant hydrolysis (pH ~6), and sorption is diminished with the formation of uranium-carbonate species at higher pH values (~7–8) (see Figure 2.2-4). For the ionic strengths tested in the experiments (0.1 and 1.0 M $NaNO_3$), results indicate that ionic strength of the solution had little influence on U-233 sorption on clinoptilolite. It is likely that some ion exchange of uranium in clinoptilolite will occur at lower pH values (below 5) in more dilute solutions (Zachara and McKinley, 1993; McKinley, et al., 1995), but this was not tested in the experiments.

Similar to the data for quartz, results of experiments investigating the sorption behavior of Np(V) onto clinoptilolite (Figure 2.2-6) also show pH dependence (Bertetti, et al., 1998; Bertetti and

Werling, 2005). Significant sorption begins near pH 7 for conditions with and without atmospheric P_{CO2} present. For solutions at equilibrium with atmospheric P_{CO2}, Np-237 sorption onto clinoptilolite reaches a maximum near pH 8 and decreases again to a minimum near pH 9.5. Experimental solutions with no CO_2(g) exhibit a continued increase in sorption as solution pH increases, with the maximum sorption attained at the highest pH studied. There is little observable uptake of Np(V) below pH 7. Additional information garnered from the Np-237 sorption experiments showed that variation in ionic strength of the $NaNO_3$ matrix from 0.1 to 0.01 M did not promote any discernible increase in sorption for the pH range studied. However, at lower pH and ionic strengths Np(V) may be sorbed through an ion-exchange mechanism (e.g., Kozai, 1994). This behavior may be reflected in the results of the neptunium–alluvium sorption experiments (see Figure 2.2-11) (Bertetti and Werling, 2005), which show net positive sorption on clinoptilolite and montmorillonite-bearing alluvium at pH values between 4 and 6.5, below the pH range where significant surface adsorption is expected for NpO^+.

2.2.4 Montmorillonite

Montmorillonite (SAz-1, Apache County, Arizona) was obtained from the Source Clays Mineral Repository. The clay was processed using ion exchange with 3 M NaCl to make a sodium–montmorillonite form, and the less than 2-μm [3.9×10^{-5} in] sized fraction was isolated and saved for use. The clay was lyophilized for storage prior to use in experiments. The N_2-BET-measured surface area of the sodium–montmorillonite was 97 ± 2 m^2/g, (Bertetti, et al., 1998).

Results of experiments studying U-233 sorption on montmorillonite revealed pH-dependent sorption of U(VI) similar to that observed for quartz, clinoptilolite, and α-alumina (Figure 2.2-4) (Pabalan, et al., 1998). The uranium-speciation drive sorption effects produced sorption maxima near pH 6 under conditions where CO_2(g) was present. The magnitude of U-233 sorption on montmorillonite was the greatest of any of the minerals studied, reaching K_d values on the order of 10^4 mL/g at atmospheric P_{CO2}. Like the experiments with clinoptilolite, U(VI)-sorption experiments with montmorillonite used solutions at ionic strengths of 0.1 and 0.01 M $NaNO_3$, which inhibited the ion exchange of U(VI) at lower pH values (below 5). Normalization of the uranium–montmorillonite sorption data to effective surface area [10 percent of the measured surface area (Pabalan, et al., 1998; Wanner, et al., 1994)] resulted in an overlap with similarly normalized data from other minerals, suggesting that the $K_{A,eff}$ parameter (see Section 2.4.3) would be useful in performance assessment models (Figure 2.2-4) (Pabalan, et al., 1998).

Over the pH range considered in experiments, the magnitude of Np-237 sorption onto sodium–montmorillonite is greater than that observed for the other minerals studied (Figure 2.2-7) (Bertetti, et al., 1998; Bertetti and Werling, 2005; Turner, et al., 1999). However, the sorption trends with change in pH are very similar to the behavior observed for quartz and clinoptilolite (Figures 2.2-5 and 2.2-7). Np(V) sorption onto montmorillonite begins to increase significantly at a solution pH of about 7. For solutions in equilibrium with atmospheric P_{CO2}, the magnitude of sorption peaks near a pH of 8.25 and decreases as pH increases, forming a high pH sorption edge. Solutions undersaturated with respect to atmospheric P_{CO2} show a continuous increase in sorption with increasing pH through the pH range examined. Unlike the sorption behavior observed in experiments with quartz and clinoptilolite, there is a net positive uptake (K_d values on the order of 10 mL/g) of Np-237 from pH values of about 4 to 7, regardless of P_{CO2} conditions. This net positive sorption may be attributed to ion exchange between NpO_2^+ and Na^+ in the clay. Similar sorption occurred at lower pH values in the neptunium–alluvium

experiments likely due to the montmorillonite content (which is interpreted to control sorption in alluvium) of those samples (Bertetti and Werling, 2005).

Results of the neptunium–montmorillonite sorption experiments were used to develop and test the applicability of a diffuse-layer model surface complexation modeling approach to represent sorption in the Yucca Mountain region (Figure 2.2-7) (Turner, et al., 2002, 1998). The diffuse-layer model is detailed in Sections 3.3 and 4.4.

2.2.5 Calcite

Reagent-grade calcite [$CaCO_3$(s), Fischer Scientific], aged, dried, and separated for storage, was used in the calcite sorption experiments. The calcite was chemically and mineralogically free of impurities. Details of calcite preparation and analyses are provided in Bertetti (2002, 2001). The calcite had a surface area of approximately 0.23 ± 0.02 m^2/g as measured using N_2-BET analysis, which was consistent with results of similarly prepared calcite from other studies (e.g., Stipp, et al., 1992; Zachara, et al., 1991).

Results of Np-237 and calcite sorption experiments conducted at ~1.6×10^6 M Np-237 for a range of pH from 7.25 to 9, at equilibrium with atmospheric P_{CO_2} and at or near equilibrium with calcite in solution. The results confirmed the pH dependence of Np-237 sorption on calcite and showed calcite is an effective sorber of Np-237 for the pH range studied (Bertetti, 2002, 2001) (Figure 2.2-8). The Np-237 sorption magnitude observed on calcite was similar to or greater than the sorption of Np-237 by montmorillonite for the same pH range (Bertetti, 2002, 2001; Bertetti, et al., 1998). The experiments also indicated that the magnitude of sorption on calcite was more variable between repeat experiments than observed for other minerals tested. This behavior was possibly due to the sensitivity of the calcite surfaces to changes in solution chemistry.

A constant capacitance surface complexation model [used because of the availability of thermodynamic data from Van Cappellen, et al. (1993)] provided a good fit to experimental data but was less successful in predicting sorption of other solid mass to solution volume ratios (Bertetti, 2002). Model results indicate that Np-237 uptake was reduced by sorption of Ca^{2+} onto the calcite surface and by formation of neptunyl carbonate complexes in solution. These results were confirmed by later studies (e.g., Zavarin, et al., 2005)

2.2.6 Iron (Hydr)oxides (Corrosion Products)

Radionuclides may attach to carbon steel corrosion products (e.g., iron oxyhydroxides) produced by the degradation of carbon steel components within waste packages. Iron oxyhydroxides have been shown to have a high sorption affinity for many metals including some radionuclides (Dzombak and Morel, 1990). As a preliminary test of the capability of carbon steel corrosion products to sorb neptunium, sorption experiments were conducted using the carbon steel corrosion products and solutions produced in corrosion test cells described in He, et al. (2007).

The experiments consisted of removing a quantity of corrosion product grains from the test cells and reacting the solids with Np-237 at concentrations of ~1×10^{-6} M in filtered water from the test cells (simulated J-13 well water) (He, et al., 2007).

The resulting Np-237 K_d values for the carbon steel corrosion products ranged from 350 to 790 mL/g (Figure 2.2-4). Experimental group A, whose solutions generally had lower

equilibrium pH values, has an average Np-237 K_d of 514 mL/g, while group B had an average Np-237 K_d of 650 mL/g. The measured K_d values for each experimental group were not statistically different from each other; there is substantial overlap between the values. The magnitude of neptunium sorption is substantial {by comparison, montmorillonite clay has a measured K_d for neptunium of about 40 mL/g at similar pH values} and is somewhat expected for iron oxyhydroxides (Dzombak and Morel, 1990).

Unfortunately, chemical analyses of the solutions and x-ray diffraction analyses of the solids revealed trace amounts of calcite (He, et al., 2007). Although unlikely given the amounts present, the potential confounding effects of the sorption of Np-237 on the calcite could not be dismissed with the data available (Figure 2.2-9) and further investigations were recommended.

2.2.7 Mineral Mixtures

2.2.7.1 Quartz and Clinoptilolite

Uranium sorption experiments involving quartz and clinoptilolite mixtures were conducted to evaluate the ability of surface complexation models to predict U(VI) sorption onto mineral mixtures based on parameters derived from single mineral experiments (Prikryl, et al., 1999). The experiments were conducted at an initial uranium aqueous concentration of $\sim 2.0 \times 10^{-7}$ mol·L^{-1} (in a 0.1 mol·L^{-1} $NaNO_3$ matrix) and over the pH range ~2.5 to ~9.5. The experiments were carried out under atmospheric P_{CO2} conditions (in loosely capped containers) or under limited or low P_{CO2} conditions (in capped containers or in a glove box).

Results of the experiments were consistent with the magnitude and pH and P_{CO2}-dependent behavior observed in previous work (Pabalan, et al., 1998) (Figure 2.2-10). Data from sorption experiments on quartz at atmospheric P_{CO2} conditions were used to derive binding constants for a diffuse-layer model. The diffuse-layer model was then used with surface area as a scaling factor to predict sorption of U(VI) onto clinoptilolite and clinoptilolite/quartz mixtures under both atmospheric and low P_{CO2} conditions. The calculations reproduced many aspects of the pH-dependent sorption behavior. This approach could be used as a relatively simple method for improving radionuclide transport models in performance assessment calculations.

2.2.7.2 Alluvium

Multiple sorption experiments were conducted using groundwater and alluvium samples collected from the Fortymile Wash region to gain preliminary insight into the sorption behavior of Np-237 onto alluvium and to help corroborate K_d values used in performance assessments. To enhance understanding of Np-237 sorption onto alluvium under varying groundwater compositions, simulated groundwaters were created and used in the experiments (Bertetti and Werling, 2005).

Results of the sorption experiments with natural alluvium substrate and groundwater or simulated groundwater show a Np-237 sorption maximum {K_d values of approximately 25 to 30 mL/g over a range of pH from about 7.5 to 8.5 (Figure 2.2-11). Although Np-237 sorption generally decreases away from the pH range of peak sorption, at high pH (greater than 8.7) some experiments produced apparent K_d values that were as much as two orders of magnitude greater than those observed in the range of 7.5 to 8.5. The presence of both calcite and small amounts of iron oxides in the alluvium samples likely contributed to these larger sorption values. The broad Np-237 sorption peak and the location of that peak may be influenced by the

presence of clinoptilolite or small amounts of calcite in the alluvium samples—alluvium samples with calcite removed exhibited sorption behavior more similar to that observed in previous experiments on aluminosilicates (Figure 2.2-11).

A comparison of the alluvium sorption data to a diffuse-layer model developed to describe Np-237 sorption on montmorillonite (Turner, et al., 2002, 1998) reveals that the model does an excellent job of reproducing the experimental observations for Np-237 sorption on alluvium (Figure 2.2-11). In this case the model was scaled using the effective surface area for montmorillonite and replotted using the estimated effective surface area for the alluvium samples (Bertetti, et al., 2004). The comparison provides confidence in the generic diffuse-layer model approach used to represent sorption in alluvium in performance assessment modeling.

2.3 References

Allard, B., U. Olofsson, and B. Torstenfelt. "Environmental Actinide Chemistry. *Inorganica Chimica Acta.* Vol. 94. pp. 205–221. 1984.

Bechtel SAIC Company, LLC. "EBS Radionuclide Transport Abstraction." ANL–WIS–PA-000001. Rev. 1. Las Vegas, Nevada: Bechtel SAIC Company, LLC. 2004.

Bertetti, F.P. "Laboratory and Modeling Studies of Neptunium Uptake on Calcite." San Antonio, Texas: CNWRA. 2002.

Bertetti, F.P. "Laboratory Experiments of Neptunium Uptake on Calcite—Letter Report." San Antonio, Texas: CNWRA. 2001.

Bertetti, F.P. and B. Werling. "Sorption of Neptunium-237 on Alluvium Collected from Fortymile Wash, Nye County, Nevada—Status Report." San Antonio, Texas: CNWRA. 2005.

Bertetti, F.P., J. Prikryl, and B. Werling. "Development of Updated Total-System Performance Assessment Parameter Distributions for Radionuclide Transport in the Saturated Zone." San Antonio, Texas: CNWRA. 2004.

Bertetti, F.P., R.T. Pabalan, and M.G. Almendarez. "Studies of Neptunium(V) Sorption on Quartz, Clinoptilolite, Montmorillonite, and α-alumina." *Adsorption of Metals by Geomedia: Variables, Mechanisms, and Model Variations*. E. Jenne, ed. New York, City, New York: Academic Press, Inc. pp. 131–148. 1998.

Bidoglio, G., A. Avogadro, A. DePlano, and G.P. Lazarri. "Reaction Pathways of Pu and Np in Selected Natural Water Environments." *Radiochimica Acta.* Vol. 44/45. pp. 29–32. 1988.

Bish D.L. and S.J. Chipera. "Revised Mineralogic Summary of Yucca Mountain, Nevada." LA–11497–MS. Los Alamos, New Mexico: Los Alamos National Laboratory. 1989.

Davis, J.A. and D.B. Kent. "Surface Complexation Modeling in Aqueous Geochemistry. Reviews in Mineralogy: Volume 23." *Mineral-Water Interface Geochemistry*. M.F. Hochella, Jr., and A.F. White, eds. Washington, DC: Mineralogical Society of America. pp. 177–260. 1990.

Dzombak, D.A. and F.M.M. Morel. *Surface Complexation Modeling: Hydrous Ferric Oxide*. New York City, New York: John Wiley & Sons. 1990.

Fuger, J. "Thermodynamic Properties of Actinide Species Relevant to Geochemical Problems. *Radiochimica Acta.* Vol. 59. pp. 81–91. 1992.

Gainer, G.M. "Boron Adsorption on Hematite and Clinoptilolite. M.S. Thesis. University of Texas at El Paso. p. 122. 1990.

He, X., V. Jain, F.P. Bertetti, and D. Pickett. "Evolution of Fluid Chemistry Inside a Waste Package Due to Carbon Steel and Simulated High-Level Waste Glass Corrosion-Progress Report." San Antonio, Texas: CNWRA. 2007.

Kozai, N. "Sorption Characteristics of Neptunium by Smectite." In Progress Report on Safety Research on Radioactive Waste Management for the Period April 1992 to March 1993. S. Muraoka, M. Senoo, and K. Sekine, eds. Tokai, Japan: Japan Atomic Energy Research Institute. pp. 39–41. 1994.

Lieser, K.H. and U. Mühlenweg. "Neptunium in the Hydrosphere and Geosphere. I. Chemistry of Neptunium in the Hydrosphere and Sorption of Neptunium From Groundwaters on Sediments Under Aerobic and Anaerobic Conditions." *Radiochimica Acta.* Vol. 43. pp. 27–35. 1988.

McKinley, J.P., J.M. Zachara, S.C. Smith, and G.D. Turner. "The Influence of Hydrolysis and Multiple Site-Binding Reactions on Adsorption of U(VI) on Montmorillonite." *Clays and Clay Minerals.* Vol. 43. pp. 586–598. 1995.

McMurry, J. and F.P. Bertetti. "Selection of Sorption-Related Values For Unsaturated Zone and Saturated Zone Transport In Total-System Performance Assessment." CNWRA Letter Report. San Antonio, Texas: CNWRA. June 2005.

Nakayama, S. and Y. Sakamato. "Sorption of Neptunium on Naturally-Occurring Iron-Containing Minerals. *Radiochimica Acta.* Vol. 52/53. pp. 153–157. 1991.

Ogard, A.E. and J.F. Kerrisk. LA–10188-MS, "Groundwater Chemistry Along Flow Paths Between a Proposed Repository Site and the Accessible Environment." Los Alamos, New Mexico: Los Alamos National Laboratory. 1984.

Pabalan, R.T. "Thermodynamics of Ion-Exchange Between Clinoptilolite and Aqueous Solutions of Na^+/K^+ and Na^+/Ca^{2+}." *Geochimica et Cosmochimica Acta*. Vol 58. pp. 4,573–4,590. 1994.

Pabalan, R.T., D.R. Turner, F.P. Bertetti, and J.D. Prikryl. "Uranium(VI) Sorption onto Selected Mineral Surfaces: Key Geochemical Parameters." *Adsorption of Metals by Geomedia: Variables, Mechanisms, and Model Variations*. E. Jenne, ed. New York City, New York: Academic Press. pp. 99–130. 1998.

Perfect, D.L., C.C. Faunt, W.C. Steinkampf, and A.K. Turner. "Hydrochemical Data Base for the Death Valley Region, California and Nevada. USGS Open-File Report 94-305. Denver, Colorado: U.S. Geological Survey. 1995.

Prikryl, J.D., A. Jain, R.T. Pabalan, and D.R. Turner. "Uranium (VI) Sorption Behavior on Mixed Silicate Minerals." *Journal of Contaminant Hydrology*. Vol. 47, Issues 2–4. pp. 241–253. 1999.

Prikryl, J.D., R.T. Pabalan, and B.W. Leslie. "Uranium Sorption on Alumina: Effects of pH and Surface Area/Solution Volume Ratio." Fourth International Conference on the Chemistry and Migration Behavior of the Actinides and Fission Products in the Geosphere Abstract, MIGRATION '93. Charleston, South Carolina: December 12–17, 1993. 1993.

Stipp, S.L., M.F. Hochella, G.A. Parks, and J.O. Leckie. "Cd2+ Uptake by Calcite, Solid-State Diffusion, and the Formation of Solid-Solution: Interface Processes Observed with Near-Surface Sensitive Techniques (XPS, LEED, and AES)." *Geochimica et Cosmochimica Acta*. Vol. 56. pp. 1,941–1,954. 1992.

Triay, I.R., B.A. Robinson, R.M. Lopez, A.J. Mitchell, and C.M. Overly. "Neptunium Retardation With Tufts and Groundwaters From Yucca Mountain." Proceedings of the 4th Annual International Conference on High-Level Radioactive Waste Management, Las Vegas, Nevada, April 1993. La Grange Park, Illinois: American Nuclear Society. pp. 1,504–1,508. 1993.

Turner, D.R. and R.T. Pabalan. "Abstraction of Mechanistic Sorption Model Results for Performance Assessment Calculations at Yucca Mountain, Nevada." *Waste Management*. Vol. 19. pp. 375–388. 1999.

Turner, D.R., F.P. Bertetti, and R.T. Pabalan. "The Role of Radionuclide Sorption in High-Level Waste Performance Assessment: Approaches for the Abstraction of Detailed Models." *Geochemistry of Soil Radionuclides. Special Publication 59.* Soil Science Society of America. P.-C. Zhang and P.V. Brady, eds. Madison, Wisconsin. pp. 211–252. 2002.

Turner, D.R., R.T. Pabalan, J.D. Prikryl, and F.P. Bertetti. "Radionuclide Sorption at Yucca Mountain, Nevada - Demonstration of an Alternative Approach for Performance Assessment." J. Lee and D. Wronkiewicz, eds. *Materials Research Society Symposium Proceedings: Scientific Basis for Nuclear Waste Management—XXII*. Pittsburgh, Pennsylvania: Materials Research Society: 583-590. 1999.

Turner, D.R., R.T. Pabalan, and F.P. Bertetti. "Neptunium (V) Sorption on Montmorillonite: An Experimental and Surface Complexation Modeling Study." *Clays and Clay Minerals*. Vol. 46. pp. 256–269. 1998.

Van Cappellen, P., L. Charlet, W. Stumm, and P. Wersin. "A Surface Complexation Model of the Carbonate Mineral-Aqueous Solution Interface." *Geochimica et Cosmochimica Acta*. Vol. 57. pp. 3,505–3,518. 1993.

Wanner, H., Y. Albinsson, O. Kml, E. Wieland, P. Wersin, and L.Charlet. "The Acid Base Chemistry of Montmorillonite. *Radiochimica Acta*. Vol. 66/67. pp. 733–738. 1994.

Zachara, J.M. and J.P. McKinley. "Influence of Hydrolysis on the Sorption of Metal Cations by Smectites: Importance of Edge Coordination Reactions." *Aquatic Sciences.* Vol. 55. pp. 250–261. 1993.

Zachara, J.M., C.E. Cowan, and C.T. Resch. "Sorption of Divalent Metals on Calcite." *Geochimica et Cosmochimica Acta*. Vol. 55. pp. 1,549–1,562. 1991.

Zavarin, M., S.K. Roberts, N. Hakem, A.M. Sawvel, and A. B. Kersting. "Eu(III), Sm(III), Np(V), Pu(V), and Pu(IV) Sorption to Calcite." *Radiochimica Acta.* Vol. 93. pp. 93–102. 2005.

2.4 X-Ray Absorption Fine-Structure Spectroscopy Study of Uranium(VI) Sorption

Traditional sorption methods focus on the macroscopic aspects of the interaction of an aqueous species with a mineral surface (i.e., K_d), but give no direct information on the structural and chemical environment around a single atom or ion. X-ray absorption fine structure spectroscopy, which includes extended x-ray absorption fine structure and x-ray absorption near-edge structure spectroscopy, is an ideal tool for the direct determination of the structure of surface-adsorbed complexes and can be used to probe the mechanism of adsorption on the molecular scale. In this study, x-ray absorption fine structure spectroscopy was used to elucidate the structure and oxidation state of uranium species sorbed onto the clay mineral montmorillonite and the zeolite mineral clinoptilolite, which are important minerals at Yucca Mountain. Understanding of specific surface complexes on those minerals offered some insights into the most appropriate surface reactions to be incorporated into detailed sorption process models. Both minerals contain two types of sorption sites: (i) permanently charged cation-exchange sites and (ii) variably charged surface hydroxyl groups. The former is due to isomorphic substitution in the structure [e.g., of Al(III) for Si(IV)] within the tetrahedral layer of montmorillonite or within the zeolite framework causing a permanent negative charge that is compensated by cations interacting with the interlayer or intracrystalline exchange sites. The latter is due to partially coordinated aluminum and silicon exposed at the clay crystallite edges or zeolite surfaces, which hydrolyze to form aluminol (AlOH) and silanol (SiOH) groups. These hydroxylated sites exhibit acid/base behavior and coordinative properties similar to those of oxide (e.g., SiO_2) surfaces.

Uranium(VI) sorption onto mineral surfaces is a strong function of pH [Figure 2.3-1(a)]. At atmospheric P_{CO2}(g), uranyl sorption is highest at near-neutral pHs where aqueous uranyl species are mainly in the form of hydroxyl complexes [Figure 2.3-1(b)]. Uranyl sorption is low at alkaline pHs where uranyl-carbonate species are predominant. For minerals with no permanently charged cation-exchange sites, such as quartz, uranyl sorption is also low at acidic pHs where aqueous uranyl exists primarily as the mononuclear, ionic species UO_2^{2+}. However, uranyl sorption onto negatively charged cation-exchange sites of montmorillonite and clinoptilolite from solutions of low pH and low ionic strength has been shown to be important (Zachara and McKinley, 1993; Andreeva and Chernyavskaya, 1982).

2.4.1 Experimental

The Ca–montmorillonite (SAz-1; source locality: Cheto, Arizona) and Na–clinoptilolite (source locality: Death Valley Junction, California) used in the study were pretreated to remove carbonates and iron oxides, and dried prior to the experiments. Samples for x-ray absorption fine structure analysis were prepared by reacting 1 gram of mineral powder with 450 mL of uranyl nitrate solution (4.6×10^{-5} or 9.2×10^{-5} M U-238). Samples were prepared at pH ~3 and ~6 so the effect of pH on the sorption mechanism could be evaluated. The reaction bottles were placed on a gyratory shaker, and air was bubbled through the solutions to maintain atmospheric P_{CO2}. Periodic adjustments of pH were made with HNO_3 or NaOH to maintain a pH of ~3 or ~6. After about 2 weeks, the mixtures were centrifuged and the moist pastes were loaded onto x-ray absorption fine structure sample holders. The uranium concentrations before the addition of solid and after sorption equilibrium was achieved were analyzed by inductively coupled plasma to determine the uranyl uptake.

X-ray absorption fine structure spectra were collected on the moist paste samples at beamline X11A of the National Synchrotron Light Source at Brookhaven National Laboratory. Data collection and analysis are described in Reeder, et al. (2001).

2.4.2 Results

The near-edge regions of the uranium L_2-edge absorption spectra are shown in Figure 2.3-2(a). For all samples, the edge positions, relative to U(IV) and U(VI) reference standards, and the presence of a characteristic shoulder above the absorption maximum confirm the uranium remains in the 6+ oxidation state as the O=U=O moiety. No obvious difference in the near-edge structure is observed among the samples. Fourier transform magnitudes are shown in Figures 2.3-2(b) and 2.3-2(c). All Fourier transform magnitudes show a principal peak at 1.4 Å, corresponding to two axial oxygens at ~1.8 Å in the uranyl moiety. Peaks at ~2 Å in the Fourier transform correspond to equatorial oxygen shells. For the montmorillonite and clinoptilolite reacted at pH ~3, the Fourier transform magnitudes show a single peak well separated from the axial oxygen component. In contrast, both minerals at pH ~6 show separate and weaker peaks, suggesting split equatorial oxygen coordination. No significant peaks are apparent at higher *R*, indicating no significant backscattering from silicon, aluminum, or other uranium atoms and unlikely formation of a second uranyl-containing solid phase. A weak peak at ~3 Å in the Fourier transform reflects a multiple-scattering path within the UO_2 moiety. For all fits, a multiple-scattering contribution at ~3.58 Å was fitted with the four-legged O_{ax1}-U-O_{ax2}-U path.

Best fit results are reported in Table 2.3-1. All fits show two axial oxygens in the range 1.77–1.79 Å. The uranyl sorbed onto montmorillonite at pH 3.3 shows a single equatorial shell of five–six oxygens at 2.41 Å. At pH 6.3, the montmorillonite is best fitted with two equatorial shells (each with ~three oxygen atoms) at 2.28 and 2.44 Å. Generally similar fit results were found for the uranyl sorbed on clinoptilolite. The clinoptilolite reacted at pH 6.4 shows two equatorial oxygen shells at 2.28 and 2.45 Å. For the clinoptilolite sample reacted at pH 3.2, the single peak in the Fourier transform suggested a single equatorial oxygen shell, and fitting yielded ~five oxygen atoms at 2.45 Å. However, the fit quality was not as good as for the montmorillonite at pH 3.3. The fit was improved by an additional, weak equatorial oxygen component, giving best fit results of ~one oxygen at 2.21 Å and ~four oxygens at 2.42 Å. The significance of the weak contribution at 2.21 Å needs additional clarification. Attempts to fit uranium–aluminum and uranium–silicon paths generally resulted in very small coordination number values that were significantly less than the estimated errors. The lack of uranium backscattering also suggests that sorbed uranyl species are mononuclear.

The results on montmorillonite derived from this study are in agreement with the results Sylwester, et al. (2000) published. As shown in Table 2.3-2, for montmorillonite reacted with uranium solutions at a pH near 3, both studies indicate the presence of a single equatorial shell, with five to six oxygens at a distance of ~2.42 Å. Sylwester, et al. (2000) interpreted their results as an indication of an outer-sphere mechanism for uranyl sorption, with the uranyl existing as a monomeric oxo-cation surrounded by an outer hydration shell. For uranium sorbed onto montmorillonite at a pH near 6, both studies observe a split equatorial shell in the uranyl structure. Sylwester, et al. (2000) interpreted this equatorial splitting as evidence of an inner-sphere complexation with the surface.

The results of Sylwester, et al. (2000) for uranyl sorbed onto silica are also shown in the Table 2.3-2 for comparison with data from this study. Silica does not have permanently charged cation-exchange sites, as found in montmorillonite and clinoptilolite. In contrast to uranyl sorbed

on montmorillonite, uranyl sorbed on amorphous silica exhibits equatorial splitting over the pH range 3 to 6.5, which Sylwester, et al. (2000) interpreted as evidence of inner-sphere surface complexes at that pH range.

Also tabulated are the results of Hudson, et al. (1999) for uranyl sorbed onto vermiculite and hydrobiotite, which both have a layer structure. The results for these minerals are quite similar to those for montmorillonite. At low pH, a single equatorial shell is observed, with coordination numbers and uranium–oxygen distances about the same as those observed for uranium sorbed on montmorillonite. At near-neutral pH, vermiculite and hydrobiotite both show equatorial splitting as observed for montmorillonite, although the coordination number and uranium–oxygen distances are somewhat different compared to montmorillonite.

2.4.3 Conclusions

The results of this study show that the uranium remains in the 6+ oxidation state as the uranyl ion moiety, with two axial oxygens ~1.8 Å distance from the uranium atom. There is a difference in the equatorial coordination of the uranyl sorbate as a function of pH for both montmorillonite and clinoptilolite. Split equatorial shells are evident for both samples at pH ~6, whereas primarily a single shell exists at pH ~3. The results for montmorillonite are consistent with the extended x-ray absorption fine structure data Sylwester, et al. (2000) reported. The structure of U(VI) sorbed on montmorillonite is similar to that of U(VI) sorbed on vermiculite and hydrobiotite (Hudson, et al., 1999).

The difference in uranium–oxygen distances in the equatorial oxygen shell for the samples at pH ~6 likely reflect a difference in the bonding of these oxygens with the sorption sites of the minerals. Hence, the split equatorial shells probably indicate discrete equatorial oxygens form chemical bonds at surface functional groups, as would be expected for an inner-sphere-type surface complex. In contrast, the single equatorial shell for samples at pH ~3 suggests a more uniform bonding environment for the oxygens as would be expected for an outer-sphere-type complex. Such an environment is consistent with ion exchange at cation-exchange sites of the sorbents. However, the experiments do not provide direct evidence that the uranyl ion is located in the interlayer exchange sites of montmorillonite or in the intracrystalline channels of clinoptilolite. The alternate x-ray absorption fine structure fit indicating equatorial splitting for clinoptilolite reacted at pH ~3 is consistent with distortion of the equatorial shell due to steric limitations imposed by the zeolite structure. Further investigations are needed to refine the zeolite sorption mechanisms. Additional work using polarized x-ray absorption fine structure could help in providing such evidence.

2.4.4 References (Section 2.3)

Andreeva, N.R. and N.B. Chernyavskaya. “Uranyl Ion Sorption by Mordenite and Clinoptilolite.” *Radiokhimiya*. Vol. 24. pp. 9–13. 1982.

Bertetti, F.P., R.T. Pabalan, and M.G. Almendarez. “Studies of Neptunium(V) Sorption on Quartz, Clinoptilolite, Montmorillonite, and α-alumina.” *Adsorption of Metals by Geomedia: Variables, Mechanisms, and Model Variations*. E. Jenne, ed. New York City, New York: Academic Press, Inc. pp. 131–148. 1998.

Hudson, E.A., L.J. Terminello, B.E. Viani, M. Denecke, T. Reich, P.G. Allen, J.J. Bucher, D.K. Shuh, and N.M. Edelstein. “The Structure of U6+ Sorption Complexes on Vermiculite and Hydrobiotite.” *Clays and Clay Minerals*. Vol. 47. pp. 439–457. 1999.

Pabalan, R.T., D.R. Turner, F.P. Bertetti, and J.D. Prikryl. "Uranium^{VI} Sorption Onto Selected Mineral Surfaces." *Adsorption of Metals by Geomedia*. E.A. Jenne, ed. New York City, New York: Academic Press, Inc. pp. 99–130. 1998.

Reeder, R.J., M. Nugent, and R.T. Pabalan. "Local Structure of Uranium(VI) Sorbed on Clinoptilolite and Montmorillonite." *Water-Rock Interaction.* R. Cidu, ed. Lisse, The Netherlands: A.A. Balkema Publishers. pp. 423–426. 2001.

Sylwester, E.R., E.A. Hudson, and P.G. Allen. "The Structure of Uranium(VI) Sorption Complexes on Silica, Alumina, and Montmorillonite." *Geochimica et Cosmochimica Acta*. Vol. 64. pp. 2,431–2,438. 2000.

Turner, G.D., J.M. Zachara, J.P. McKinley, and S.C. Smith. "Surface-Charge Properties and UO_2^{2+} Adsorption of a Surface Smectite." *Geochimica et Cosmochimica Acta*. Vol. 60 pp. 3,399–3,414. 1996.

Wanner, H., Y. Albinsson, O. Kml, E. Wieland, P. Wersin, and L.Charlet. "The Acid Base Chemistry of Montmorillonite. *Radiochimica Acta*. Vol. 66/67. pp. 733–738. 1994.

Zachara, J.M. and J.P. McKinley. "Influence of Hydrolysis on the Sorption of Metal Cations by Smectites: Importance of Edge Coordination Reactions." *Aquatic Sciences*. Vol. 55. pp. 250–261. 1993.

2.5 Key Geochemical Parameters Controlling Radionuclide Sorption

2.5.1 Effects of Aqueous Speciation

For actinides, sorption behavior typically varies as a function of its aqueous speciation, with a close correspondence between the pH dependence of sorption behavior, the predominance field of actinide-hydroxy complexes, and the presence of complexing ligands such as carbonate (Bertetti, et al., 1998; Pabalan, et al., 1998). Under low pH conditions, actinide sorption tends to be weak, except under low ionic strength conditions for cation exchangers such as montmorillonite and, to a lesser extent, clinoptilolite (e.g., Pabalan, et al., 1993; Turner, et al., 1996). With increasing pH, actinide sorption increases, with a maximum typically in the pH range where the hydroxy complexes are important. In carbonate-free laboratory systems, actinide sorption continues to increase with increasing pH and increasing hydrolysis (e.g., Bertetti, et al., 1998; Pabalan, et al., 1998; Turner, et al., 1998), but actinide sorption behavior is sensitive to the presence of carbonate or other ligands in solution that affect aqueous speciation. For example, in carbonate-bearing systems, actinide sorption tends to decrease with increasing pH and/or increasing carbonate concentration (Bertetti, et al., 1998; Pabalan, et al., 1998).

2.5.2 Physical Properties

In contrast to the relatively pronounced effects of aqueous speciation on actinide sorption, the similarity in the pH dependence of actinide sorption on a wide variety of minerals, such as quartz, alumina, clinoptilolite, montmorillonite, amorphous silica, kaolinite, and titanium oxide, suggests a relative insensitivity to surface charge characteristics of the sorbent as compared to the effect of changing the total number of available sites. For example, the CNWRA data demonstrate that U(VI) sorption on quartz, α-alumina, clinoptilolite, and montmorillonite in the presence of atmospheric CO_2 ($P_{CO2} = 10^{-3.5}$ atm) is strongly affected by solution pH

(Pabalan, et al., 1998). Although the minerals used in the experiments have different mineralogic and surface properties, U(VI) sorption on these minerals is similar with respect to dependence on pH. In all cases, U sorption is at a maximum at near-neutral pH (~6.0 to ~6.8) and decreases sharply toward more acidic or more alkaline conditions. In experiments, ionic strength effects up to about 1 M seem to be limited for actinide surface complexation reactions (Pabalan, et al., 1998). Elevated ionic strength may also stabilize aqueous complexes that can affect actinide sorption behavior. Similar behavior was observed for Np(V) sorption (Bertetti, et al., 1998), although the sorption maximum occurred at pH of around 8, reflecting the higher pH for the formation of Np(V)-hydroxy aqueous species.

2.5.3 Representing Actinide Sorption Data

Experimental sorption results are typically plotted in terms of percentage sorbed versus pH. In the U(VI)–H_2O–CO_2 system, the amount of U(VI) sorbed (in percent) relative to the initial amount of U(VI) in solution increases with increasing M/V ratio, giving a broader sorption "envelope." The apparent M/V effect, however, is mostly eliminated if the results are plotted in terms of K_d. As demonstrated in Pabalan, et al. (1998), U(VI) sorption on quartz, alumina, clinoptilolite, and montmorillonite is similar with respect to pH dependence. However, the K_d values for the different minerals vary over three orders of magnitude. This variation is an artifact of normalizing the data to the sorbent mass and representing sorption data in terms of K_d. Similar observations were reported for Np(V) sorption (Bertetti, et al., 1998).

Surface areas measured by gas adsorption (e.g., N_2-BET) methods are a relative index of the number of sorption sites on the mineral surface, and it may be more useful to represent sorption data normalized to the specific surface area of the mineral sorbent (Bertetti, et al., 1998; Pabalan, et al., 1998). Surface area normalized sorption data for clinoptilolite and montmorillonite are indistinguishable, whereas surface area normalized sorption data for quartz and alumina are almost coincident.

Surface areas determined by N_2-BET methods most likely overestimate the amount of sorption sites on layered silicates, such as montmorillonite, and zeolitic minerals, such as clinoptilolite. For example, it is believed that surface complex formation of U(VI) on montmorillonite occurs on the hydroxylated edge sites of the mineral (Turner, et al., 1996). Wanner, et al. (1994) estimated that only 10 percent of the N_2-BET specific surface area is accounted for by the crystallite edges of montmorillonite. Assuming that the "effective" surface area (A_{eff}) for montmorillonite and clinoptilolite is equivalent to about 10 percent of the measured surface area (A), sorption data for montmorillonite and clinoptilolite can be recast in terms of $K_{A,eff}$ where

$$K_{A,eff} = K_d / A_{eff} \qquad (2.5\text{-}1)$$

For nonlayered and nonporous minerals such as quartz and alumina, $K_A = K_{A,eff}$. K_A values for quartz, clinoptilolite, and montmorillonite, which have distinct mineralogic and surface properties, are essentially equivalent when recast in terms of $K_{A,eff}$. This suggests that at least for aluminosilicate minerals, expressing sorption in terms of $K_{A,eff}$ provides a generalized basis for performance assessment transport calculations. The K_d values for a given

hydrostratigraphic unit can then be backed out assuming an effective specific surface area and the relationship

$$K_d = K_{A,eff} \times A_{eff} \quad (2.5\text{-}2)$$

Similar results have been demonstrated for Np(V) (Bertetti, et al., 1998).

2.6 References (Section 2.4)

Bertetti, F.P., R.T. Pabalan, and M.G. Almendarez. "Studies of Neptunium^{V} Sorption on Quartz, Clinoptilolite, Montmorillonite, and -Alumina." *Adsorption of Metals by Geomedia*. E.A. Jenne, ed. New York City, New York: Academic Press. pp. 131–148. 1998.

Pabalan, R.T., J.D. Prikryl, P.M. Muller, and T.B. Dietrich. "Experimental Study of Uranium(6+) Sorption on the Zeolite Mineral Clinoptilolite." C. Interrante and R. Pabalan, eds. MRS Symposium Proceedings Volume 294: Scientific Basis for Nuclear Waste Management XVI. Pittsburgh, Pennsylvania: Material Research of Society. pp. 777–782. 1993.

Pabalan, R.T., D.R. Turner, F.P. Bertetti, and J.D. Prikryl. "Uranium^{VI} Sorption Onto Selected Mineral Surfaces." *Adsorption of Metals by Geomedia*. E.A. Jenne, ed. New York City, New York: Academic Press. 1998.

Turner, D.R., R.T. Pabalan, and F.P. Bertetti. "Neptunium(V) Sorption on Montmorillonite: An Experimental and Surface Complexation Modeling Study." *Clays and Clay Minerals*. Vol. 46. pp. 256–269. 1998.

Turner, G.D., J.M. Zachara, J.P. McKinley, and S.C. Smith. "Surface-Charge Properties and UO_2^{2+} Adsorption of a Surface Smectite." *Geochimica et Cosmochimica Acta*. Vol. 60. pp. 3,399–3,414. 1996.

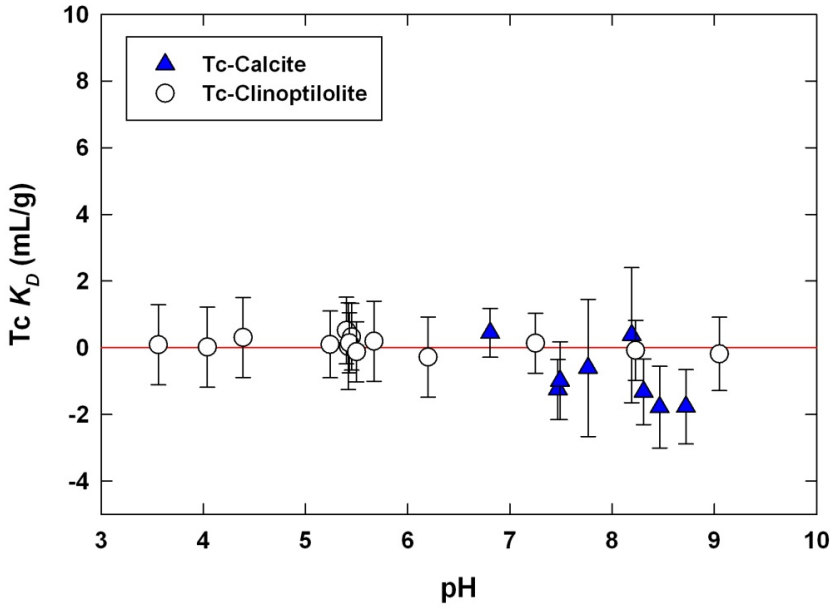

Figure 2.1-1. Results of Experiments Investigating Tc-99 Sorption on Calcite (Triangles) and Clinoptilolite (Circles). Estimates of the Minimum Uncertainty Associated With the Measurements Are Shown by the Error Bars. Data for Calcite Experiment Represent an Average of Four Separate Runs at Each pH. A Red Line Indicating K_d = 0 Is Shown as a Guide to the Reader.

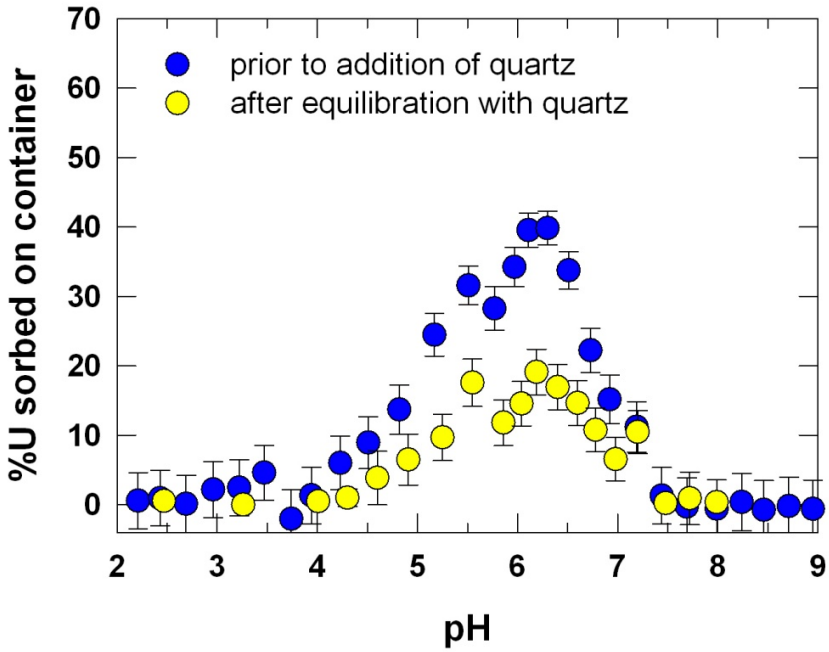

Figure 2.2-1. Plot of the Percentage U-233 Sorbed Onto Polycarbonate Experimental Containers Before (Blue) and After (Yellow) Addition of Quartz Substrate

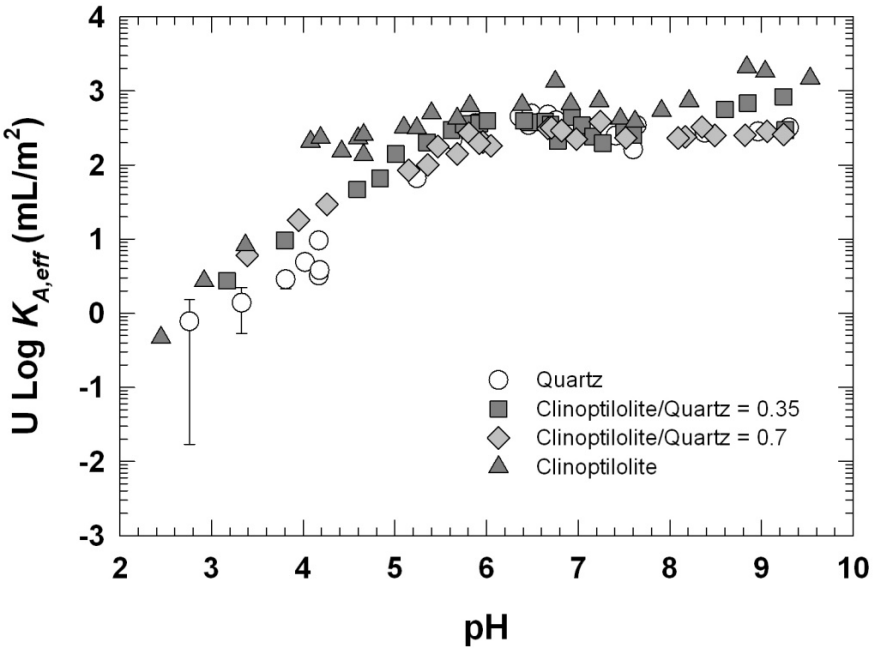

Figure 2.2-2. Plot of U-233 Sorption on Quartz in the Absence of CO_2(g) and Varying pH, Solid Mass to Solution Volume Ratios (M/V), and U-233 Concentrations. Error Bars Show the Calculated Total Uncertainty for Data.

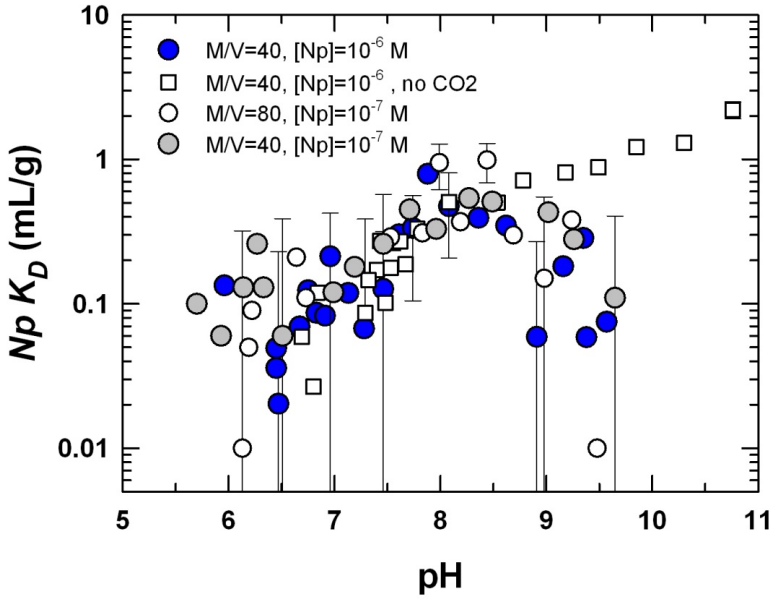

Figure 2.2-3. Plot of Np-237 Sorption on Quartz Under Varying pH, P_{CO2}, Solid Mass to Solution Volume Ratios (M/V), and Np-237 Concentrations. Error Bars Show Calculated Total Uncertainty for Selected Data.

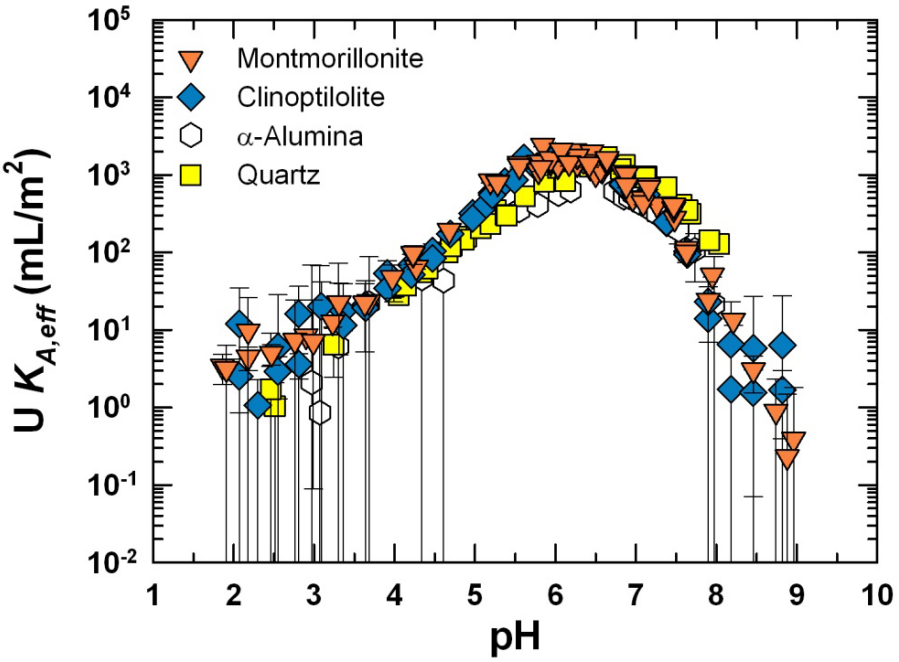

Figure 2.2-4. Plot of U-233 Sorption on α-Alumina, Clinoptilolite, Montmorillonite, and Quartz Under Atmospheric P_{CO2} Conditions and Normalized to Effective Surface Area ($K_{A,eff}$) of Each Mineral. Error Bars Show Calculated Total Uncertainty for Data.

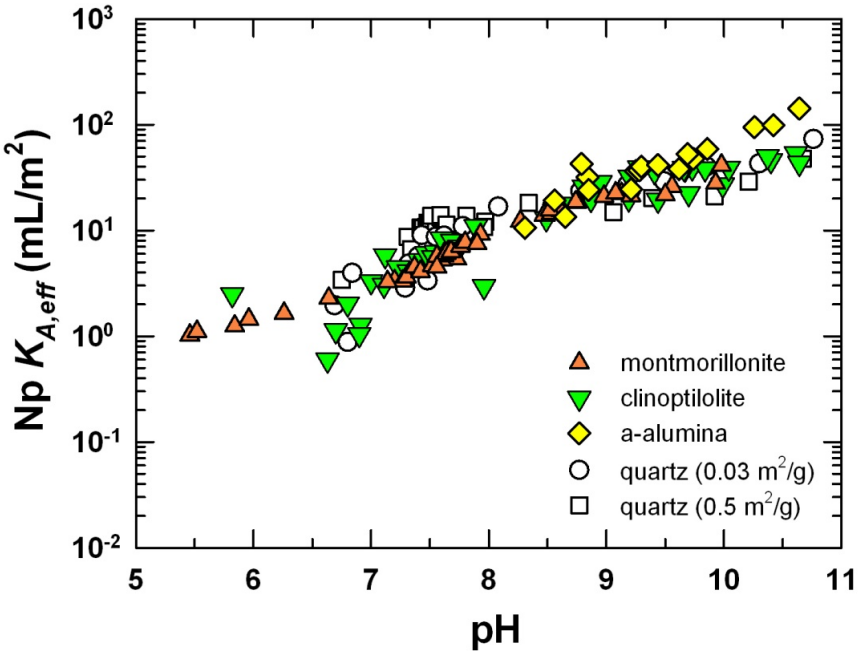

Figure 2.2-5. Plot of Np-237 Sorption on α-Alumina, Clinoptilolite, Montmorillonite, and Quartz in the Absence of CO_2(g) and Normalized to Effective Surface Area ($K_{A,eff}$) of Each Mineral

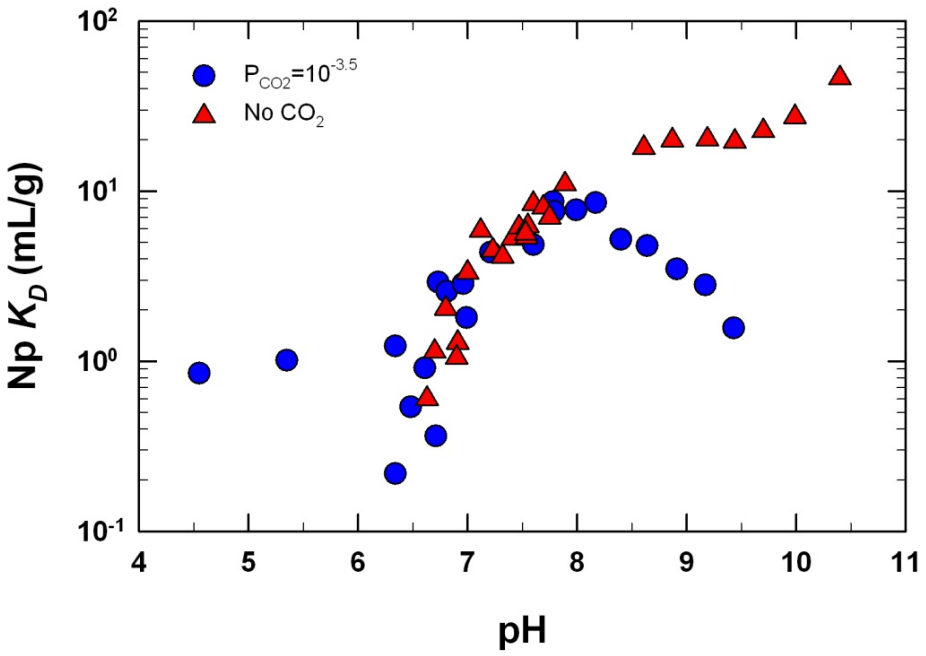

Figure 2.2-6. Plot of Np-237 Sorption on Clinoptilolite Under Varying P_{CO2} Conditions

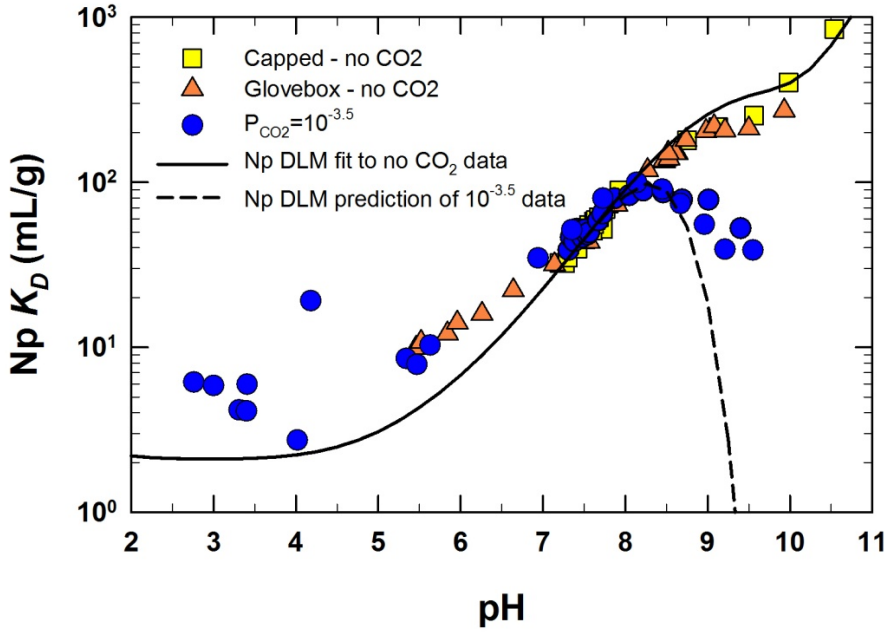

Figure 2.2-7. Plot of Np-237 Sorption on Montmorillonite Under Varying P_{CO2} Conditions. A Diffuse Layer Model Was Fit to the non-CO_2 Data and the Parameters Used To Predict Sorption at Atmospheric P_{CO2}.

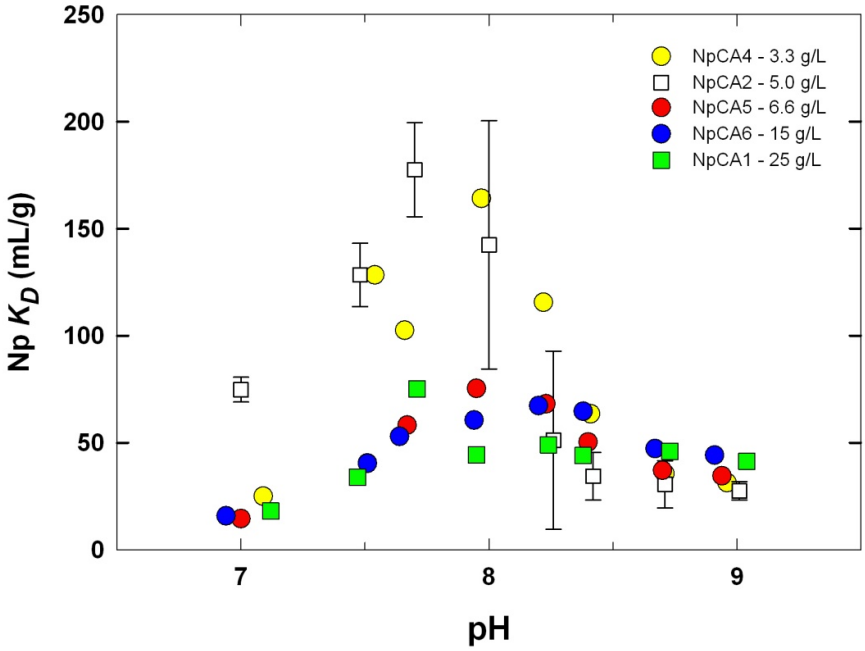

Figure 2.2-8. Plot of Np-237 Sorption on Calcite Under Atmospheric P_{CO2} and Varying Solid Mass to Solution Volume Ratios (M/V). Error Bars Show the Range of Values for Replicate Experiments in an Example Experimental Series (NpCA2).

Np K_D for Carbon Steel Corrosion Products and Calcite-Bearing Alluvium

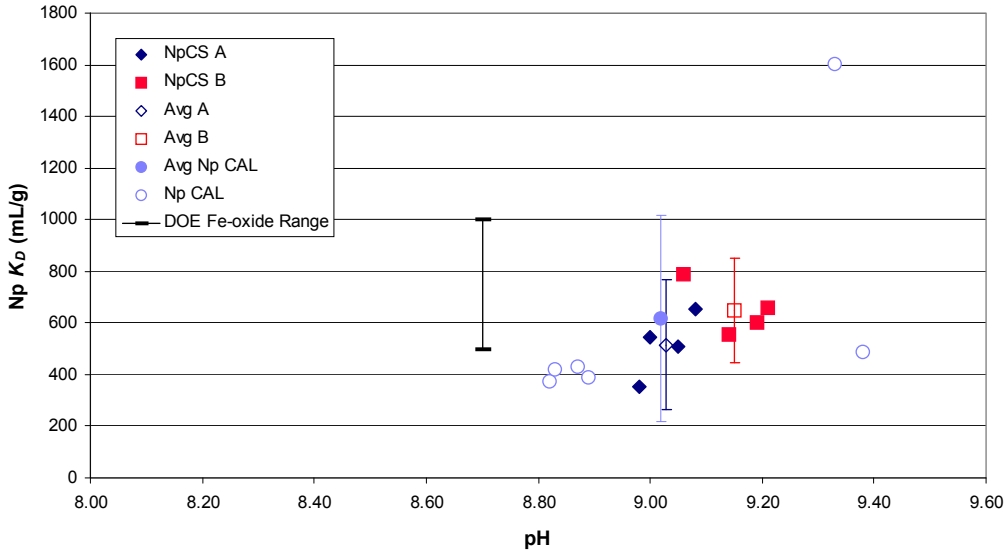

Figure 2.2-9. Plot of Measured Np-237 K_d Values for the Carbon Steel Corrosion Products, Calcite-Bearing Alluvium, and the Range of Values DOE Used (Bechtel SAIC Company, LLC, 2004) for Iron Oxides. The Solid Blue Circle Indicates the Average Measured Np-237 K_d for the Alluvium Samples at High pH; the Error Bars for the Alluvium Represent One Standard Deviation. The DOE Range for Np-237 Sorption Onto Iron Oxide Is Not Linked to Any Specific pH Value and Is Shown at pH of 8.7 as an Example Only.

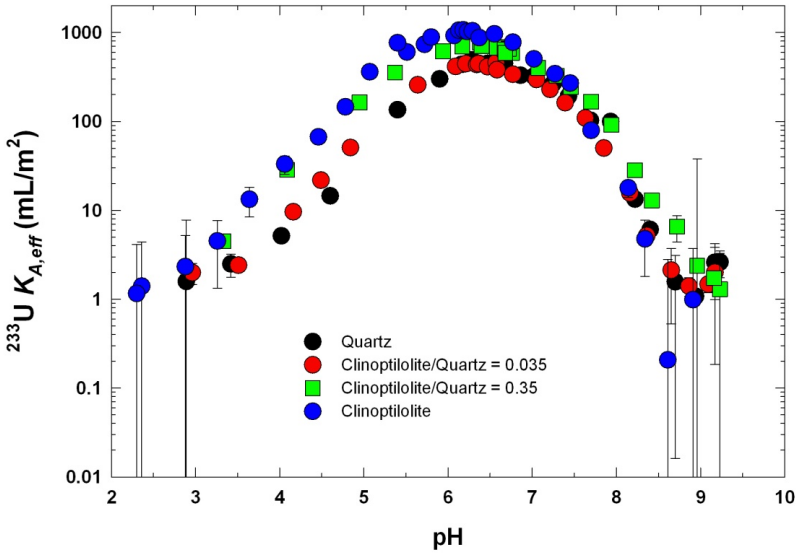

Figure 2.2-10. Plot of the Sorption of U-233 as a Function of Effective Surface Area for the Quartz–Clinoptilolite Mixed Mineral Experiments. Error Bars Show Calculated Uncertainty for Selected Samples.

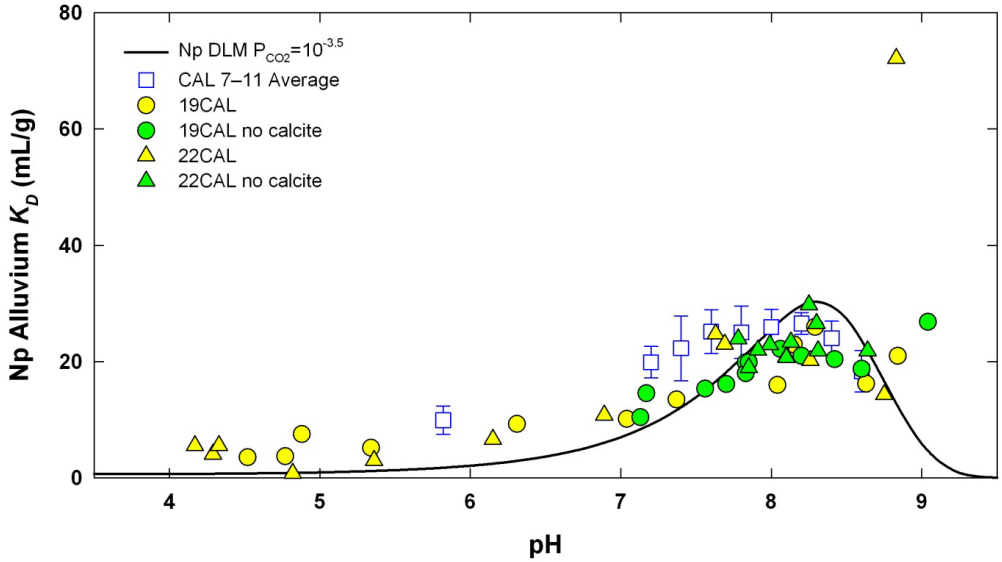

Figure 2.2-11. Plot of Np-237 Sorption on Alluvium Sample Composites (CAL) Collected From Fortymile Wash, Nevada. Experiments Were Conducted Under Atmospheric P_{CO2} Conditions. The White Squares (CAL 7–11) Represent the Average K_d Values on Well NC–EWDP–19PB-Composite Alluvium for Experiments CAL7 Through CAL11 (Bertetti and Werling, 2005). Results of Subsequent Experiments Using Composite Alluvium, Some of Which Was Pretreated to Remove Calcite, From Wells NC–EWDP–19PB and NC–EWDP–22PC Are Also Shown. The Solid Curve Represents a Model Prediction Based on the Diffuse-Layer Model Used for Np-237 Sorption on Montmorillonite (See Figure 2.2-7) and Scaled Using the Effective Surface Area for Montmorillonite and the Effective Surface Area for the Alluvium Composites (Bertetti, et al., 2004). Error Bars Represent ±1 Standard Deviation of the Averaged CAL 7 to CAL 11 Data at Each pH Value.

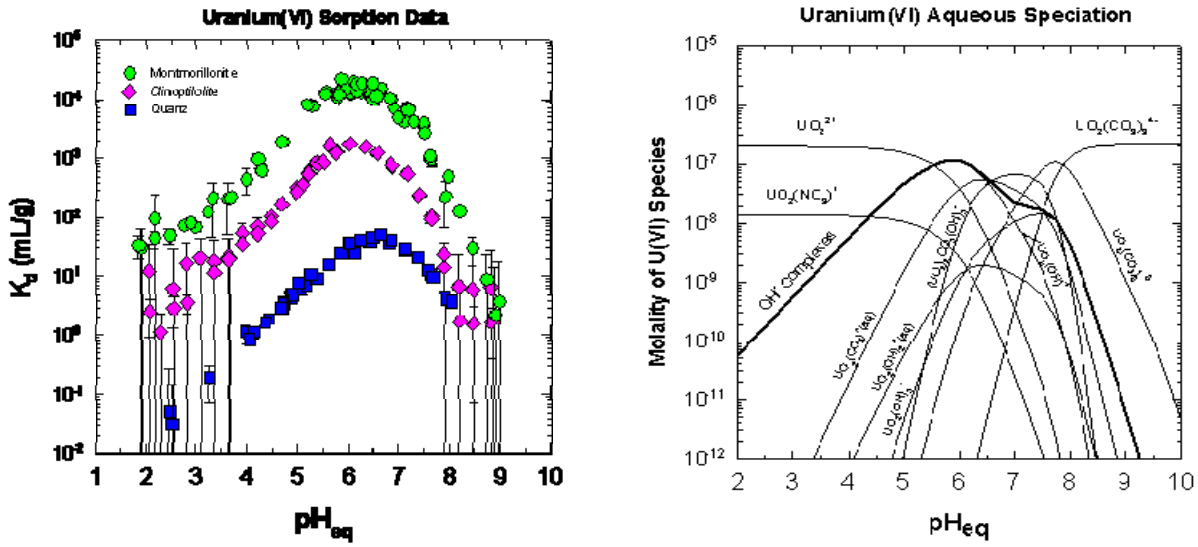

Figure 2.3-1. Comparison of (a) Uranyl Sorption on Na–Montmorillonite, Na–Clinoptilolite, and Quartz and (b) Uranyl Aqueous Speciation ($\Sigma U_i = 2.1 \times 10^{-7}$ M; $PCO_2 = 10^{-3.5}$ atm; 0.1 M $NaNO_3$ Matrix). Sorption Data From Pabalan, et al. (1998). The Thick Solid Curve in (b) Is the Total Molality of Uranyl Hydroxy Complexes. Potential Ion Exchange of UO_2^{2+} With Na^+ in Montmorillonite and Clinoptilolite at pH <4 Is Suppressed by the 0.1 M $NaNO_3$ Background Electrolyte of the Experiments.

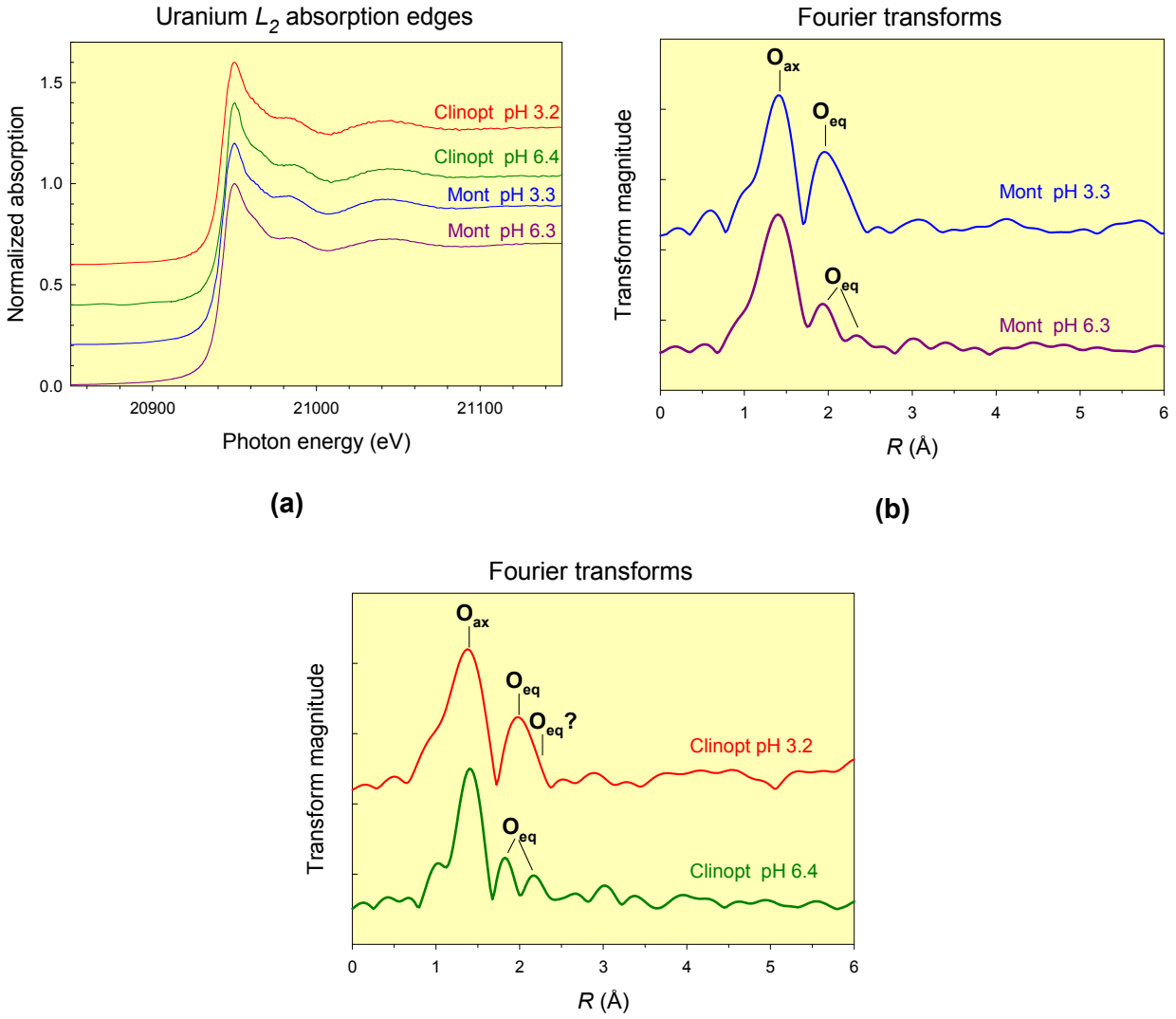

Figure 2.3-2. (a) Near-Edge Regions of Uranium L_2-Edge Absorption Spectra and Fourier Transform Magnitudes (k^3-Weighting; Uncorrected for Phase Shifts) for Uranyl Sorbed on (b) Montmorillonite and (c) Clinoptilolite at Different pH Values

Table 2.1-1. Summary of U(VI) Sorption Experiments on Various Minerals						
Experiment	**Mineral**	**M/V (g/L)**	**U conc. (M)**	**P_{CO2}**	**pH**	**Solution**
A1	α-alumina	2.88	5.00×10^{-7}	$10^{-3.5}$	2–9	0.1 M $NaNO_3$
A2	α-alumina	2.79	4.84×10^{-7}	$10^{-3.5}$	2–9	0.1 M $NaNO_3$
A3	α-alumina	2.81	4.90×10^{-7}	$10^{-3.5}$	2–9	0.1 M $NaNO_3$
C1	Na-clinoptilolite	2.04	2.17×10^{-7}	$10^{-3.5}$	2–9	0.1 M $NaNO_3$
C2	Na-clinoptilolite	2.09	2.22×10^{-6}	$10^{-3.5}$	2–9	0.1 M $NaNO_3$
C3	Na-clinoptilolite	2.05	1.90×10^{-8}	$10^{-3.5}$	2–9	0.1 M $NaNO_3$
C4	Na-clinoptilolite	2.07	2.17×10^{-7}	$10^{-3.5}$	2–9	0.1 M $NaNO_3$
C5	Na-clinoptilolite	20.28	2.10×10^{-7}	$10^{-3.5}$	2–9	0.1 M $NaNO_3$
C6	Na-clinoptilolite	2.43	2.10×10^{-7}	$10^{-2.0}$	2–9	0.1 M $NaNO_3$
M1	Na-montmorillonite	3.2	2.45×10^{-7}	$10^{-3.5}$	2–9	0.1 M $NaNO_3$
M2	Na-montmorillonite	0.27	2.06×10^{-7}	$10^{-3.5}$	2–9	0.1 M $NaNO_3$
M3	Na-montmorillonite	0.028	2.10×10^{-7}	$10^{-3.5}$	2–9	0.1 M $NaNO_3$
M4	Na-montmorillonite	0.28	2.16×10^{-6}	$10^{-3.5}$	2–9	0.1 M $NaNO_3$
Q1	quartz	2	2.14×10^{-7}	$10^{-3.5}$	2–9	0.1 M $NaNO_3$
Q2	quartz	20	2.11×10^{-7}	$10^{-3.5}$	2–9	0.1 M $NaNO_3$
Q3	quartz	50	2.06×10^{-7}	$10^{-3.5}$	2–9	0.1 M $NaNO_3$
Q4	quartz	20	2.00×10^{-8}	$10^{-3.5}$	2–9	0.1 M $NaNO_3$
Q5	quartz	50	2.15×10^{-6}	$10^{-3.5}$	2–9	0.1 M $NaNO_3$

Table 2.1.3-1. Summary of Np(V) Sorption Experiments on Various Minerals						
Experiment(s)	**Mineral**	**M/V (g/L)**	**Np conc. (M)**	**P_{CO2}**	**pH**	**Solution**
NpCA1, 1–3	calcite	25	2.5×10^{-6}	$10^{-3.5}$	7–9	0.1 M $NaClO_4$
NpCA2, 1–3	calcite	5	2.5×10^{-6}	$10^{-3.5}$	7–9	0.1 M $NaClO_4$
NpCA3, 1–2	calcite	10	2.5×10^{-6}	$10^{-3.5}$	7–9	0.1 M $NaClO_4$
NpCA4, 1–3	calcite	3.3	1.6×10^{-6}	$10^{-3.5}$	7–9	0.1 M $NaClO_4$
NpCA5, 1–3	calcite	6.6	1.6×10^{-6}	$10^{-3.5}$	7–9	0.1 M $NaClO_4$
NpCA6, 1–3	calcite	15	1.6×10^{-6}	$10^{-3.5}$	7–9	0.1 M $NaClO_4$
NpCA7, 1–4	calcite	3.3	1.6×10^{-6}	$10^{-3.5}$	7–9	0.1 M $NaClO_4$
NpCA8, 1–4	calcite	13.33	1.6×10^{-6}	$10^{-3.5}$	7–9	0.1 M $NaClO_4$
NpCA9, 1–4	calcite	3.33	8.2×10^{-7}	$10^{-3.5}$	7–9	0.1 M $NaClO_4$
NpCA10, 1–4	calcite	13.33	8.2×10^{-7}	$10^{-3.5}$	7–9	0.1 M $NaClO_4$
NpCA11, 1–3	calcite	5	2×10^{-6}	$10^{-3.5}$	7–9	0.1 M $NaClO_4$
NpCA12, 1–3	calcite	10	2×10^{-6}	$10^{-3.5}$	7–9	0.1 M $NaClO_4$
NpQ1	quartz	40	1×10^{-7}	$10^{-3.5}$	4–10	0.1 M $NaNO_3$
NpQ2	quartz	80	1×10^{-7}	$10^{-3.5}$	4–10	0.1 M $NaNO_3$
NpQ3	quartz	40	1×10^{-6}	$10^{-3.5}$	4–10	0.1 M $NaNO_3$
NpQ4	quartz	40	1×10^{-6}	capped	6–11	0.1 M $NaNO_3$
NpQ5	quartz	4	1×10^{-6}	capped	6–11	0.1 M $NaNO_3$
NpC1	Na-clinoptilolite	4	1×10^{-6}	$10^{-3.5}$	3–10	0.1 M $NaNO_3$
NpC2	Na-clinoptilolite	4	1×10^{-6}	capped	4–11	0.01 M $NaNO_3$
NpC3	Na-clinoptilolite	8	1×10^{-6}	$10^{-3.5}$	3–10	0.01 M $NaNO_3$
NpC4	Na-clinoptilolite	8	1×10^{-6}	no CO_2	4–11	0.1 M $NaNO_3$
NpM1	Na-montmorillonite	4	1×10^{-6}	capped	5–10	0.1 M $NaNO_3$
NpM2	Na-montmorillonite	4	1×10^{-6}	$10^{-3.5}$	3–10	0.1 M $NaNO_3$
NpM3	Na-montmorillonite	4	1×10^{-6}	no CO_2	5–10	0.1 M $NaNO_3$
NpA1	a-alumina	4	1×10^{-6}	capped	3–11	0.01 M $NaNO_3$
NpA2	a-alumina	4	1×10^{-6}	no CO_2	3–11	0.01 M $NaNO_3$

Table 2.2.7.1-1. Summary of U(VI) Sorption Experiments on Mixed Minerals							
Experiment	**Mineral(s)**	**M/V (g/L) Zeolite**	**M/V (g/L) Quartz**	**Zeolite/ Quartz Ratio**	**P_{CO2}**	**pH**	**U Conc. (M)**
C20	Na-clinoptilolite	20	–	–	$10^{-3.5}$	3–10	2.06×10^{-7}
CU20	Na-clinoptilolite	20	–	–	No CO2	3–10	2.09×10^{-7}
Q	quartz	–	28.6	–	$10^{-3.5}$	3–10	2.03×10^{-7}
QU	quartz	–	28.6	–	capped	3–10	2.04×10^{-7}
QC1	Na-clinoptilolite/quartz	1	28.6	0.035	$10^{-3.5}$	3–10	2.04×10^{-7}
QC10	Na-clinoptilolite/quartz	10	28.6	0.35	$10^{-3.5}$	3–10	1.92×10^{-7}
QC10U	Na-clinoptilolite/quartz	10	28.6	0.35	capped	3–10	2.04×10^{-7}
QC20	Na-clinoptilolite/quartz	20	28.6	0.7	$10^{-3.5}$	3–10	2.10×10^{-7}
QC20U	Na-clinoptilolite/quartz	20	28.6	0.7	No CO2	3–10	2.03×10^{-7}

Table 2.2.7.2-1. Summary of Np(V) Sorption Experiments on Alluvium and Related Minerals Using Actual or Simulated Groundwaters

Experiment	Substrate	M/V (g/L)	Np Conc. (M)	P_{CO2}	pH	Solution
AL1	alluvium, single depth*	16.7	7.9×10^{-7}	$10^{-3.5}$	single	19PB shallow string†
AL2	alluvium, single depth*	16.7	5.5×10^{6}	$10^{-3.5}$	single	19PB shallow string†
AL3	alluvium, single depth*	16.7	7.8×10^{-7}	$10^{-3.5}$	single	19PB shallow string†
AL4	alluvium, single depth*	3.3	7.7×10^{-7}	$10^{-3.5}$	6.5–9	19PB shallow string†
AL5	alluvium, single depth*	3.3	7.8×10^{-7}	$10^{-3.5}$	single	Simulated GW‡
AL6	alluvium, single depth*	3.3	7.8×10^{-7}	$10^{-3.5}$	single	Simulated GW‡ without calcium
C1	Na-clinoptilolite	3.3	8.0×10^{-7}	$10^{-3.5}$	single	19PB shallow string†
M1	Na-montmorillonite	3.3	8.0×10^{-7}	$10^{-3.5}$	single	19PB shallow string†
M2	Na-montmorillonite	3.3	7.8×10^{-7}	$10^{-3.5}$	6.5–9	19PB shallow string†
M3	Na-montmorillonite	3.3	7.8×10^{-7}	$10^{-3.5}$	single	Simulated GW‡
M4	Na-montmorillonite	3.3	7.8×10^{-7}	$10^{-3.5}$	single	Simulated GW‡ without calcium
M5	Na-montmorillonite	3.3	7.8×10^{-7}	$10^{-3.5}$	6.5–9	Simulated GW‡
M6	Na-montmorillonite	3.3	7.7×10^{-7}	$10^{-3.5}$	6.5–9	Simulated GW‡ without calcium
M7	Na-montmorillonite	3.3	8.5×10^{-7}	$10^{-3.5}$	6.5–9	Simulated GW‡
CAL1	composite alluvium§	3.3	7.8×10^{-7}	$10^{-3.5}$	single	Simulated GW‡
CAL2	composite alluvium	3.3	7.8×10^{-7}	$10^{-3.5}$	single	Simulated GW‡ without calcium
CAL3	composite alluvium	3.3	7.7×10^{-7}	$10^{-3.5}$	6.5–9	Simulated GW‡
CAL4	composite alluvium	3.3	7.6×10^{-7}	$10^{-3.5}$	6.5–9	Simulated GW‡ without calcium
CAL5	composite alluvium	3.3	8.3×10^{-7}	$10^{-3.5}$	6.5–9	Simulated GW‡
CAL6	composite alluvium	3.3	8.3×10^{-7}	$10^{-3.5}$	6.5–9	Simulated GW‡ without calcium
CAL7	composite alluvium	3.3	8.4×10^{-7}	$10^{-3.5}$	4–9	Simulated GW‡
CAL8	composite alluvium	3.3	8.4×10^{-7}	$10^{-3.5}$	6.5–9	Simulated GW‡ without calcium
CAL9	composite alluvium	3.3	8.2×10^{-7}	$10^{-3.5}$	4–9	Simulated GW‡
CAL10	composite alluvium	3.3	8.2×10^{-7}	$10^{-3.5}$	6.5–9	Simulated GW‡ without calcium
CAL11	composite alluvium	3.3	8.5×10^{-7}	$10^{-3.5}$	6.5–9	Simulated GW‡
	composite alluvium	3.3	8.7×10^{-7}	$10^{-3.5}$	4–9	Simulated GW‡
	composite alluvium	3.3	8.7×10^{-7}	$10^{-3.5}$	4–9	Simulated GW‡
	composite alluvium	3.3	8.7×10^{-7}	$10^{-3.5}$	4–9	Simulated GW‡
	composite alluvium	3.3	8.7×10^{-7}	$10^{-3.5}$	4–9	Simulated GW‡

*Alluvium from Borehole NC-EWDP-19PB interval 123.8 to 124.2 m
†Groundwater collected from NC-EWDP-19PB shallow string filtered through a 0.45 µm filter
‡Simulated GW = Simulated groundwater with 19PB composition
§Composite alluvium sample from 13 intervals listed in Table 3-1

Table 2.3-1. Best-Fit X-Ray Absorption Fine Structure Parameters for Uranyl Sorbed on Montmorillonite and Clinoptilolite

Montmorillonite pH 3.3				Montmorillonite pH 6.3			
Shell	CN	*R* (Å)	σ^2 (Å^2)	Shell	CN	*R* (Å)	σ^2 (Å^2)
$U\text{-}O_{ax}$	2	1.77	0.001	$U\text{-}O_{ax}$	2	1.79	0.002
$U\text{-}O_{eq1}$	5.5	2.41	0.007	$U\text{-}O_{eq1}$	3.5	2.28	0.010
—	—	—	—	$U\text{-}O_{eq2}$	3.4	2.44	0.010
MS‖	2.6	3.54	0.003	MS‖	2.4	3.59	0.002
ΔE_0	4.5			ΔE_0	4.4		
Clinoptilolite pH 3.2				**Clinoptilolite pH 6.4**			
Shell	CN*	*R* (Å)†	σ^2 (Å^2)‡	Shell	CN	*R* (Å)	σ^2 (Å^2)
$U\text{-}O_{ax}$	2§	1.78	0.001	$U\text{-}O_{ax}$	2	1.79	0.001
$U\text{-}O_{eq1}$	1.4	2.21	0.002	$U\text{-}O_{eq1}$	2.0	2.28	0.003
$U\text{-}O_{eq2}$	4.4	2.42	0.004	$U\text{-}O_{eq2}$	3.1	2.45	0.005
($U\text{-}O_{eq}$ (preliminary fit)	4.8	2.45	0.008				
MS‖	2.6	3.56	0.005	MS‖	2.3	3.57	0.004
ΔE_0¶	4.2			ΔE_0	5.1		

*Coordination numbers (CN) have errors of ± 20 percent
†Errors on interatomic distance, *R*, are ± 0.02 Å
‡Errors on Debye-Waller-type disorder parameters are ± 0.001 Å^2
§Fixed at two for most fits, but refined to a value near two for test fits
‖Four-legged multiple scattering path $O_{ax1}\text{-}U\text{-}O_{ax2}\text{-}U$
¶Global energy threshold varied during fitting

Table 2.3-2. Comparison of X-Ray Absorption Fine Structure Data From This Study With Literature Values					
Sorbent	**pH_{eq}**	**Shell**	**CN***	***R* (Å)†**	**σ^2 (Å^2)**
Montmorillonite	3.3	U-O_{ax}	2	1.77	0.001
(This study)		U-O_{eq}	5.5	2.41	0.007
Montmorillonite‡	3.2	U-O_{ax}	2	1.79	0.003
		U-O_{eq}	5.4	2.43	0.010
Vermiculite§	2.6	U-O_{ax}	2.1	1.78	0.002
		U-O_{eq}	4.6	2.43	0.008
Hydrobiotite§	2.6	U-O_{ax}	2.1	1.78	0.002
		U-O_{eq}	4.8	2.43	0.008
Montmorillonite	6.3	U-O_{ax}	2	1.79	0.002
(This study)		U-O_{eq1}	3.5	2.28	0.010
		U-O_{eq2}	3.4	2.44	0.010
Montmorillonite‡	6.4	U-O_{ax}	2	1.77	0.002
		U-O_{eq1}	2.97	2.30	0.003
		U-O_{eq2}	2.72	2.48	0.003
Vermiculite§	6.9	U-O_{ax}	2.23	1.80	0.003
		U-O_{eq1}	3.09	2.28	0.012
		U-O_{eq2}	1.02	2.48	0.002
Hydrobiotite§	7.1	U-O_{ax}	2.10	1.79	0.001
		U-O_{eq1}	1.27	2.24	0.008
		U-O_{eq2}	3.09	2.42	0.006

*Coordination number

†Interatomic distance

‡Sylwester, E.R., E.A. Hudson, and P.G. Allen. "The Structure of Uranium(VI) Sorption Complexes on Silica, Alumina, and Montmorillonite." *Geochimica et Cosmochimica Acta*. Vol. 64. pp. 2,431–2,438. 2000.

§Hudson, E.A., L.J. Terminello, B.E. Viani, M. Denecke, T. Reich, P.G. Allen, J.J. Bucher, D.K. Shuh, and N.M. Edelstein. "The Structure of U6+ Sorption Complexes on Vermiculite and Hydrobiotite." *Clays and Clay Minerals*. Vol. 47. pp. 439–457. 1999.

3 SORPTION MODELS

3.1 Empirical Models

Empirical equations relating dissolved radionuclide concentration to sorbed concentrations liquid phases can be generated for individual data sets through fitting curves and empirical coefficients to experimental sorption data. Because experimental sorption data are generally obtained at a single, constant temperature, these empirical equations are known as sorption "isotherms." Because of their general simplicity, empirical radionuclide sorption models are typically the method used to represent radionuclide sorption in performance assessment models. Empirical models, however, are lumped parameter models that cannot be used to discriminate between different processes that contribute to radionuclide sorption. For this reason, they are generally unsuited to simulating rapidly changing systems, and are limited to the conditions investigated in the experiments from which the model parameters (sorption coefficients) are derived. Therefore, to evaluate the adequacy of an empirical approach, it is critical to have an understanding of the magnitude of changes anticipated in the system of interest.

3.1.1 Linear Adsorption (K_d Approach) Isotherm

As described previously, the simplest type of adsorption isotherm is a linear sorption coefficient, K_d (in mL/g or m^3/kg)

$$K_d = \left(\frac{S}{C}\right)\left(\frac{V}{M}\right) \tag{3.1-1}$$

where S represents the amount of radionuclide sorbed {g/g [fl. oz]}, C represents the amount in solution (g/mL [oz/fl. oz]), V represents the solution volume (mL), and M represents the mass of solid {g [oz]}. The K_d is then used to represent the relative contaminant transport velocity through a retardation factor, R_f (unitless) (Freeze and Cherry, 1979), such that

$$R_f = \frac{\text{groundwater velocity}}{\text{contaminant velocity}} = 1 + \left(\frac{\rho_b}{\theta}\right)K_d \tag{3.1-2}$$

where ρ_b = bulk density and θ = porosity. The lower the value of K_d, the lower the retardation factor, and the faster a reactive species migrates through the subsurface. For a nonadsorbing species, $K_d = 0$, R_f reduces to 1 and the species migrates at the flow velocity.

The K_d is a lumped parameter and cannot be used by itself to discriminate the contributions of different sorption processes to contaminant retardation. An additional limiting characteristic of the K_d approach is the inability to recognize a maximum adsorption limit. In actuality, because there are a finite number of adsorption sites, adsorption will reach a practical upper limit. Additional uncertainty arises from the sensitivity of the parameter to aqueous chemical conditions, such as pH, alkalinity, or concentrations of complexing ligands, that may be encountered along a groundwater flow path (Kohler, et al., 1996; Davis, et al., 2004, 1998; Bethke and Brady, 2000). For example, the K_d for uranium(VI) adsorption on ferrihydrite at pH 8 decreases by four orders of magnitude as the partial pressure of carbon dioxide gas, P_{CO2}, increases from its value in air (0.032 percent) to 1 percent (Davis, et al., 2004). This is an important variation to understand, because the P_{CO2} in aquifers commonly reaches values of

1–5 percent, while most K_d values have been determined in laboratory experiments equilibrated with or exposed to air. Moreover, P_{CO2} often increases with transport after groundwater recharge, and this spatial/temporal trend in chemical conditions can greatly affect the retardation of contaminants. For these reasons, constant K_d models for adsorption do not adequately account for spatial variability in mineralogy and hydrochemistry along groundwater flow paths.

3.1.2 Freundlich Adsorption Isotherm

The Freundlich adsorption isotherm (Freundlich, 1926) is nonlinear and defined by the relationship

$$S = K_{Fr}C^n \tag{3.1-3}$$

where S and C are defined as for Eq. (3.1-1) and K_{Fr} and n are empirical coefficients. For the special case where n = 1, Eqs. (3.1-1) and (3.1-3) are identical. If adsorption/concentration data can be represented by a Freundlich isotherm, a plot of log S versus log C should result in a straight line with a slope equal to n and an intercept of log K_{Fr}. As is the case for a linear adsorption isotherm, no maximum is reached upon uptake through adsorption.

3.1.3 Langmuir Adsorption Isotherm

In adapting the Langmuir adsorption isotherm (Langmuir, 1918) to solution chemistry, the idea of an upper limit to surface adsorption was introduced. Assuming that all adsorption sites are homogeneous, the general form for the Langmuir isotherm is

$$S = \frac{K_{La}bC}{1+K_{La}C} \tag{3.1-4}$$

where b is the maximum adsorption capacity of the substrate (g solute/g adsorbent) and K_{La} is a constant representing the strength with which the solute is bound to the substrate (l/meq). Values of b and K_{La} can be determined by plotting a variety of possible linearizations or by nonlinear regression analysis (Kinniburgh, 1986).

The Langmuir isotherm accounts for the decrease in K_d values that occurs as an adsorbing surface becomes partially saturated with adsorbed species. The relationship is usually determined for a specific set of constant chemical and physical conditions while adsorbing ion concentration is varied.

3.1.4 Parameters for Empirical Equilibrium Adsorption Models

A variety of compilations of model-dependent adsorption parameters is available in the literature. Because of its simplicity, the largest number of adsorption parameter collections is available for the adsorption coefficient (K_d). In using different subsurface reactive transport computer codes, there are often default adsorption coefficients values in the input files. These values may or may not be linked to experimental data or site suitable conditions, and the user can subsequently revised them for a given simulation on a site-specific basis.

A number of computer codes developed to assess radiological dose have internal or default sorption coefficients that the user can choose to implement in the absence of detailed

site-specific information. For example, the DandD code (Kennedy and Strenge, 1992), developed to screen scenarios and exposure pathways for decommissioning and license termination, provides default K_d values derived from various sources or methods. For example, if the radionuclide of interest is assumed to be mobile, a K_d value of 0.0 is assigned to maximize the migration rate. As possible, the experimental values from the compilation of Sheppard and Thibault (1990) were used, with the smallest (most conservative) value selected from the four soil types considered in the compilation. For C-14 in soil, data from Sheppard, et al. (1991) were used. When experimental data were not available, a correlation between K_d values and soil-to-plant concentration ratios and measured soil-to-plant concentration ratios was used (Thibault, et al., 1990). Similarly, the RESRAD dose assessment software (Yu, et al., 1993a,b) uses default K_d values selected from several sources available (Baes and Sharp, 1983; Nuclear Safety Associates, 1980; Isherwood, 1981; NRC, 1980; Gee, et al., 1980; Staley, et al., 1979). The MEPAS environmental analysis and dose assessment code (Strenge and Peterson, 1989; Whelan, et al., 1996) uses a modified approach to consider the effects of solution chemistry and mineralogy on radionuclide sorption. A MEPAS user can enter a value for pH and the total percentage of clay, organic matter, and iron and aluminum oxides for the geologic media. The software then accesses a list of default K_d values that contains up to nine different values for each contaminant. The available K_d values are organized into three pH categories (pH 5, pH 5–9, and pH 9). Within each pH category, the K_d values are further organized into three soil categories: the combined total percentage of clay, organic matter, and iron and aluminum oxides in three ranges (<10 percent, 10–30 percent, and 30 percent).

A number of adsorption coefficient databases have been developed specifically to address radionuclide transport issues. Examples of K_d databases include the Sandia Sorption Data Management System (Siegel, et al., 1989), the Atomic Energy of Canada, Ltd. database (Thibault, et al., 1990), the SKI Project-90 database (Andersson, 1988), and the Nuclear Energy Agency adsorption database (Rüegger and Ticknor, 1992). Ames and Rai (1978) reviewed of available data and relevant chemistry for radionuclide interactions with soil and rock media. Based on literature review and onsite laboratory and field experiments, Looney, et al. (1987) have compiled estimates of K_d values applicable to the Savannah River Site at Aiken, South Carolina. A similar effort by Center for Nuclear Waste Regulatory Analyses (CNWRA®) staff developed K_d values to be used in evaluating U.S. Department of Energy (DOE) waste tank cleanup activities at the Savannah River Site and at Idaho National Laboratory (Prikryl and Pickett, 2007). Cantrell, et al., (2003) compiled K_d values and supporting data applicable to the DOE Hanford Site at Richland, Washington.

McKinley and Scholtis (1991) compiled and compared radionuclide adsorption coefficient databases used in performance assessment. Although developed for the purposes of radionuclide transport, the database reviewed in this work covers nearly half of the periodic table of elements and includes information on adsorption onto buffers and backfills (concrete, bentonite, clay/rock mixes), a wide range of host rocks (e.g., crystalline, sediments), and surface soils.

The U.S. Environmental Protection Agency (EPA) published a three-volume set of documents on understanding variation in K_d values (EPA, 2002; 1999a,b). Volume II (EPA, 1999b) contains a review of the geochemistry and K_d values for cadmium, cesium, chromium, lead, plutonium, radon, strontium, thorium, tritium (^3H), and uranium. Volume III (EPA, 2002) contains a review of the geochemistry and K_d values for americium, arsenic, curium, iodine, neptunium, radium, and technetium.

3.1.5 References (Section 3.1)

Ames, L.L. and D. Rai. "Radionuclide Interactions With Rock and Soil Media. Vol. I. EPA 520/6-78-007-a. Las Vegas, Nevada: EPA 1978.

Andersson, K. "SKI Project–90: Chemical Data." SKI Technical Report 91:21. Stockholm, Sweden: Swedish Nuclear Power Inspectorate. 1988.

Baes, C.F. and R.D. Sharp. "A Proposal For Estimation of Soil Leaching and Leaching Constants for Use in Assessment Models." *Journal of Environmental Quality.* Vol. 12. pp. 17–28. 1983.

Bethke, C.M. and P.V. Brady. "How the K_d Approach Undermines Ground Water Cleanup." *Ground Water*. Vol. 38. pp. 435–443. 2000.

Cantrell, K.J., R.J. Serne, and G.L. Last. "Hanford Contaminant Distribution Coefficient Database and Users Guide." PNNL–13895. Rev. 1. Richland, Washington: Pacific Northwest National Laboratory. 2003.

Davis, J.A., D.E. Meece, M. Kohler, and G.P. Curtis. "Approaches to Surface Complexation Modeling of Uranium(VI) Adsorption on Aquifer Sediments." *Geochimica et Cosmochimica Acta*. Vol. 68. pp. 3,621–341. 2004.

Davis, J.A., J.A. Coston, D.B. Kent, and C.C. Fuller. "Application of the Surface Complexation Concept to Complex Mineral Assemblages." *Environmental Science & Technology*. Vol. 32. pp. 2,820–2,828. 1998.

EPA. "Understanding Variation in Partition Coefficient, K_d, Values, Vol. III: Review of Geochemistry and Available K_d Values for Americium, Arsenic, Curium, Iodine, Neptunium, Radium, and Technetium." EPA 402–R–99–004C. Washington, DC: EPA. 2002.

EPA. "Understanding Variation in Partition Coefficient, K_d, Values, Vol. I: The K_d Model, Methods of Measurement, and Application of Chemical Reaction Codes." EPA 402–R–99–004A. Washington, DC: EPA 1999a.

EPA. "Understanding Variation in Partition Coefficient, K_d, Values, Vol. II: Review of Geochemistry and Available K_d Values for Cadmium, Cesium, Chromium, Lead, Plutonium, Radon, Strontium, Thorium, Tritium (^{3}H), and Uranium." EPA 402–R–99–004B. Washington, DC: EPA. 1999b.

Freeze, R.A. and J.A. Cherry. *Groundwater*. Englewood Cliffs, New Jersey: Prentice-Hall, Inc. 1979.

Freundlich, H. *Colloid and Capillary Chemistry*. London, England: Methuen. 1926.

Gee, G.W., A.C. Campbell, D.R. Sherwood, R.G. Strickert, and S.J. Phillips. NUREG/CR–1494, PNL–3381, "Interaction of Uranium Mill Tailings Leachate with Soils and Clay Liners." Washington, DC: Office of Nuclear Regulatory Research. NRC. 1980.

Isherwood, D. NUREG/CR–0912, "Geoscience Data Base Handbook for Modeling a Nuclear Waste Repository." Vols. 1 and 2. Washington, DC: NRC. 1981.

Kennedy, J.D. and D.L. Strenge. NUREG/CR–5512, PNL–7994, "Residual Radioactive Contamination from Decommissioning: Technical Basis for Translating Contamination Levels to Annual Total Effective Dose Equivalent." Washington, DC: NRC. <http://techconf.llnl.gov/radcri/java.html > 1992.

Kinniburgh, D.G. "General Purpose Adsorption Isotherms." *Environmental Science & Technology*. Vol. 20. pp. 895–904. 1986.

Kohler, M., G.P. Curtis, D.B. Kent, and J.A. Davis. "Experimental Investigation and Modeling of Uranium(VI) Transport Under Variable Chemical Conditions." *Water Resource Research*. Vol. 32. pp. 3,539–3,551. 1996.

Langmuir, D. "The Adsorption of Gases on Plane Surfaces of Glass, Mica, and Platinum." *Journal of the American Chemical Society*. Vol. 40. pp. 1,361–1,403. 1918.

Looney, B.B., M.W. Grant, and C.M. King. "Estimation of Geochemical Parameters for Assessing Subsurface Transport at the Savannah River Plant." DPST–85–904. Aiken, South Carolina: Savannah River Laboratory. 1987.

McKinley, I.G. and A. Scholtis. "Compilation and Comparison of Radionuclide Sorption Databases Used in Recent Performance Assessments." Radionuclide Sorption From the Safety Evaluation Perspective, Proceedings of an NEA Workshop, Interlaken, Switzerland, October 16–18, 1991. Paris, France: Nuclear Energy Agency. pp. 21–55. 1991.

NRC. NUREG–0706, "Final Generic Environmental Impact Statement on Uranium Milling—Vol. 1: Summary and Text; Vol. 2: Appendices A–F; Vol. 3: Appendices G–V Washington, DC: NRC, Office of Nuclear Material Safety and Safeguards. 1980.

Nuclear Safety Associates, Inc. "Comparison of Alternatives for Long-Term Management of High-Level Radioactive Waste at the Western New York Nuclear Service Center." Appendix IIIC. Bethesda, Maryland: Nuclear Safety Associates, Inc. 1980

Prikryl, J.D. and D.A. Pickett. "Recommended Site-Specific Sorption Coefficients for Reviewing Non-High-Level Waste Determinations at the Savannah River Site and Idaho National Laboratory." San Antonio, Texas: CNWRA. 2007.

Rüegger, B. and K.V. Ticknor. "The NEA Sorption Data Base (SDB): Radionuclide Sorption from the Safety Evaluation Perspective." Proceedings of a Nuclear Energy Agency Workshop. Interlaken, Switzerland, October 16–18, 1991. Paris, France: Organization for Economic Co-Operation and Development, Nuclear Energy Agency. pp. 57–78. 1992.

Sheppard, M.L., S.C. Sheppard, and B.D. Amiro. "Mobility and Plant Uptake of Inorganic ^{14}C and ^{14}C-Labeled PCB in Soils of High and Low Retention." *Health Physics*. Vol. 61. pp. 481–492. 1991

Sheppard, M.L. and D.H. Thibault. "Default Soil Solid/Liquid Partition Coefficients, K_ds, for Four Major Soil Types: A Compendium." *Health Physics*. Vol. 59. pp. 471–478. 1990.

Siegel, M.D., R. Rechard, K.L. Erickson, J.O. Leckie, D.B. Kent, D.A. Grover, S. Philips, R. Guzowski, and S. Faith. "Progress in Development of a Methodology for Geochemical Sensitivity Analysis for Performance Assessment—Volume 2: Speciation, Sorption, and Transport in Fractured Media." Project NRC FIN A1756. Albuquerque, New Mexico: Sandia National Laboratories. 1989.

Staley, G.B., G.P. Turi, and D.L. Schreiber. "Radionuclide Migration from Low-Level Waste: A Generic Overview." Management of Low-Level Radioactive Waste. M.W. Carter, et al., ed. New York City, New York: Pergamon Press. pp. 1,041–1,072. 1979.

Strenge, D.L. and S.R. Peterson. "Chemical Data Bases for Multimedia Environmental Pollutant Assessment System (MEPAS)." Version 1. PNL-7145. Richland, Washington: Pacific Northwest Laboratory. 1989.

Thibault, D.H., M.I. Sheppard, and P.A. Smith. "A Critical Compilation and Review of Default Soil Solid/Liquid Partition Coefficients, K_d, for Use in Environmental Assessments." AECL-100125. Atomic Energy of Canada Limited. Whiteshell Nuclear Research Establishment. Pinawa, Manitoba, Canada: 1990.

Whelan, G., J.P. McDonald, and C. Sato. "Multimedia Environmental Pollutant Assessment System (MEPAS): Groundwater Pathway Formulations." PNNL–10907. Richland, Washington: Pacific Northwest National Laboratory. 1996.

Yu, C., A.J. Zielen, J.-J. Cheng, Y.C. Yuan, L.G. Jones, D.J. LePoire, Y.Y. Wang, C. Loureiro, E. Gnanapragasam, E. Faillace, A. Wallo, W.A. Williams, and H. Peterson. "Manual for Implementing Residual Radioactive Material Guidelines Using RESRAD, Version 5.0." ANL/EAD/LD–2. Argonne, Illinois: Argonne National Laboratory. <http://web.ead.anl.gov/resrad/> 1993a.

Yu, C., C. Loureiro, J.-J. Cheng, L.G. Jones, Y.Y. Wang, Y.P. Cia, and E. Faillace. "Data Collection Handbook to Support Modeling the Impacts of Radioactive Material in Soil." ANL/EAIS–8. Argonne, Illinois: Argonne National Laboratory. 1993b.

3.2 Experimental and Modeling Study of Multicomponent Ion-Exchange Equilibria on Zeolite Minerals

3.2.1 Introduction

A major technical consideration in evaluating Yucca Mountain, Nevada, as a potential repository site for high-level wastes is the presence of thick lateral zones of diagenetically altered, zeolite-rich (clinoptilolite, heulandites, and mordenite) rhyolitic tuffs (Broxton, et al., 1987, 1986) that could serve as barriers to radionuclide migration to the accessible environment. Zeolites are crystalline, hydrated aluminosilicates of alkali and alkaline earth cations characterized by an ability to hydrate/dehydrate reversibly and to exchange some of their constituent cations with aqueous solutions, both without a major change in structure. Due to the favorable ion-exchange selectivity of zeolites for certain cations, such as Cs^+ and Sr^{2+}, naturally occurring zeolites have been studied for potential use in the treatment of nuclear wastewaters (Baxter and Berghauser, 1986; Howden and Pilot, 1984; Pansini, 1996; Robinson, et al., 1995) and in the remediation of sites contaminated with fission products such as Sr-90, Cs-135, and Cs-137 (Leppert, 1988; Valcke, et al., 1997a,b). Measured Yucca Mountain zeolite mineral compositions show lateral and vertical variations, [e.g., sodium-potassium-bearing and increasingly sodium-rich with depth

on the western side and calcium-potassium-bearing and increasingly calcium-rich with depth on the eastern side of Yucca Mountain (Broxton, et al., 1987, 1986)]. Because zeolite ion-exchange properties depend on factors including solid and aqueous phase compositions as well as aqueous solution concentrations, spatial variations in zeolite composition that have been observed at Yucca Mountain and natural or repository-induced changes in groundwater chemistry may influence the effectiveness of the zeolite minerals to retard radionuclide migration.

To provide a thermodynamic basis for understanding zeolite–water interactions at Yucca Mountain and other geochemical systems, ion-exchange experiments were conducted between aqueous solutions and the zeolite mineral clinoptilolite. Clinoptilolite was used in the experiments because it is the predominant zeolite mineral present in altered pyroclastic and volcaniclastic rocks (Mumpton, 1978; Mumpton and Ormsby, 1976), particularly those present at Yucca Mountain (Broxton, et al., 1987, 1986). The experiments were conducted using binary, ternary, and quaternary combinations of the cations Na^+, K^+, Cs^+, Sr^{2+}, or Ca^{2+}. In most cases, multiple solution concentrations were studied. A general thermodynamic model also was applied to enable predictions of ion-exchange equilibria in multicomponent systems typical of natural systems like Yucca Mountain.

The experiments and thermodynamic models are summarized in the following sections. More detailed descriptions are provided in Pabalan (1994, 1991), Pabalan and Bertetti (2001, 1999, 1994), and Bertetti and Pabalan (2003).

3.2.2 Ion-Exchange Experiments

Prior to the isotherm experiments, clinoptilolite material was prepared by crushing and purifying a sample of clinoptilolite-rich tuff from Death Valley Junction, California (Pabalan, 1994). The material was crushed using a mortar and pestle and then sieved to isolate and obtain size fractions (100–200 and 200–325 mesh, equivalent to 0.150–0.074 and 0.074–0.045 mm in diameter, respectively) suitable for use in the experiments. The 200–325 mesh fraction (indicating material that passed through the 200-mesh screen and was retained on the 325-mesh screen) was selected for use in this study because a greater mass of this size fraction was available following crushing. The clinoptilolite powder was cleaned of residual fines by ultrasonication and further purified following the methods described in Pabalan (1994).

Homoionic forms of Na^+, K^+, and Ca^{2+} clinoptilolite were prepared by reacting the purified zeolite with concentrated solutions (3 M) of Na^+, K^+, or Ca^{2+} (as chloride). The newly prepared sodium-form, potassium-form, and calcium-form clinoptilolite powders were dried at 65 °C [149 °F] overnight, then placed in a desiccator over a saturated NaCl solution and allowed to come to equilibrium with the water vapor in the desiccator prior to use.

The clinoptilolite powders used in the study (original material, purified form, and homoionic forms) were characterized for mineralogy using x-ray diffractometry and for chemistry using x-ray fluorescence spectrometry. The homoionic form chemical data were used to calculate the cation-exchange capacity of each form.

3.2.2.1 Binary Ion-Exchange Experiments

The binary ion-exchange experiments were conducted by reacting weighed amounts of homoionic clinoptilolite with known volumes of solution mixtures of the cations of interest. In general, a series of reference, or starting, solutions were prepared at various ratios of each

cation using chloride salts and doubly deionized, reagent-grade (>18MΩ) water. Total solution concentrations of the mixtures were held constant (e.g., 0.005, 0.05, or 0.5 N) while the ratio (equivalent cationic fraction) of each cation was varied according to the individual experimental design. Reference solutions were then dispensed and mixed with a mass of clinoptilolite powder to start each experiment. The zeolite mass to solution volume ratios and the aqueous mixture compositions used in the experiments were optimized in an attempt to yield (i) significant differences in the initial and final concentrations of the cations in solution and (ii) a relatively evenly spaced distribution of points along the ion-exchange isotherm. The experimental mixtures (clinoptilolite + salt solution) were contained in capped polypropylene bottles (of various volumes depending on the experiment) and were agitated on a gyratory shaker for at least 1 week. Experiments were maintained at 24 ± 1 °C [75.2 ± 1.8 °F].

At the end of each experiment, reference and experimental solution compositions were measured using one or multiple analytical techniques as required. The difference between initial experimental solution concentrations (determined by the reference solution values) and final equilibrium concentrations was used to calculate the changes in zeolite composition. Isotherms, representing the ion-exchange equilibrium of the system at the specified concentration and temperature, were plotted. The isotherm data were then used, in conjunction with the calculated cation exchange capacity and the thermodynamic model, to generate a thermodynamic description of the ion-exchange system. The binary systems studied are summarized in Table 3.2-1.

The Na^+, K^+, and Ca^{2+} concentrations in the reference and experimental solutions were measured using ion-selective electrodes, flame atomic absorption spectroscopy, or inductively coupled atomic emission spectrometry. Cs^+ and Sr^{2+} concentrations were determined indirectly using Sr-90 and Cs-137 as tracers. These radioisotopes provide a sensitive method of detection and can reduce the uncertainty in measured cation concentrations. In general, the radiotracers were used by adding aliquots to reference solutions, which were then used to mix the individual experimental solutions. The initial activity of the reference solutions and the final activity of the experimental solutions at equilibrium were used as surrogates for the concentration of the cation of interest (Sr^{2+} or Cs^+). The activity of the radioisotopes was measured using a liquid scintillation analyzer (Packard 3100TR) in beta counting mode.

3.2.2.2 Ternary Ion-Exchange Experiments

Ternary ion-exchange experiments were conducted following the general procedure Fletcher, et al. (1984) developed. This procedure was based on a systematic approach to the initial solution composition and distribution as plotted on a ternary diagram. The systematic approach provided a good statistical coverage of the entire range of conditions and thus a more robust examination of model performance.

Reference solutions were made using cation chloride salts and deionized water in the same manner as the binary experiments. The reference solutions were then mixed with a mass of homoionic zeolite and allowed to react for at least 1 week on a gyratory shaker. Reference (initial) and equilibrium experimental solutions (final) were then sampled for chemical analysis. Ternary system experiments are summarized in Table 3.2-2.

Solid zeolite samples from some of the $Na^+/K^+/Ca^{2+}$, $Na^+/K^+/Sr^{2+}$, $Na^+/K^+/Cs^+$, and $Na^+/K^+/Ca^{2+}/Sr^{2+}$ experimental systems were also taken and submitted for chemical analyses.

3.2.2.3 Quaternary Ion-Exchange Experiment

The quaternary ion-exchange experiment was conducted in the same manner as the ternary system experiments. A systematic experimental design was used, and a known mass of homoionic zeolite powder was reacted with solutions of varying cation composition, but at a constant ionic strength. Samples of the reference and experimental solutions as well as the equilibrium solid were taken for chemical analysis. The quaternary system experiment is summarized in Table 3.2-2.

3.2.3 Thermodynamic Model

The basic thermodynamic formulations for ion exchange are based on principles developed long ago by researchers on inorganic exchange materials, especially clays (Gaines, et al., 1953; Gapon, 1933; Kielland, 1935; Vanselow, 1932). These formulations are still widely used in current ion-exchange literature, irrespective of the nature of the exchanger under study.

3.2.3.1 Ion-Exchange Isotherm

For a binary ion exchange involving cations A^{z_A+} and B^{z_B+}, the basic reaction may be written as

$$z_B A^{z_A+} + z_A BL_{z_B} \Leftrightarrow z_A B^{z_B+} + z_B AL_{z_A} \qquad (3.2\text{-}1)$$

where z_A+ and z_B+ are the valences of the respective cations and L is defined as a portion of zeolite framework holding unit negative charge. Anions are also present in the aqueous solution and maintain electroneutrality in that phase.

The binary exchange equilibrium can be described conveniently by an ion-exchange isotherm, which is a plot of the equilibrium concentration of an exchanging ion in solution against the equilibrium concentration of that same ion in the zeolite at constant temperature and solution concentration. The isotherm is usually plotted in terms of the equivalent cation fraction of the ion in solution against that in the solid (Dyer, et al., 1981). The equivalent cationic fractions of A^{z_A+} and B^{z_B+} ($\bar{E}_A$ and $\bar{E}_B$, respectively) in the zeolite phase are defined as

$$\bar{E}_A = \frac{z_A \bar{n}_A}{z_A \bar{n}_A + z_B \bar{n}_B}; \; \bar{E}_B = \frac{z_B \bar{n}_B}{z_A \bar{n}_A + z_B \bar{n}_B} \qquad (3.2\text{-}2)$$

where $\bar{n}_A$ and $\bar{n}_B$ are the number of moles of ions A^{z_A+} and B^{z_B+}, respectively, in the zeolite. Equivalent cationic fractions in the aqueous solution can be defined similarly as

$$E_A = \frac{z_A n_A}{z_A n_A + z_B n_B}; \; E_B = \frac{z_B n_B}{z_A n_A + z_B n_B} \qquad (3.2\text{-}3)$$

where n_A and n_B are the number of moles of A^{z_A+} and B^{z_B+}, respectively, in the aqueous phase.

The ion-exchange isotherm can then be plotted from the equilibrium values of $\bar{E}_A$ and E_A (or $\bar{E}_B$ and E_B). For the binary exchange reaction shown in Eq. (3.2-1)

$$E_B = 1 - E_A; \quad \bar{E}_B = 1 - \bar{E}_A \tag{3.2-4}$$

Thus, the isotherm fully defines the equilibrium at a specified temperature and solution concentration.

3.2.3.2 Thermodynamic Equilibrium Constant

The thermodynamic equilibrium constant, $K_{(A,B)}$, for Eq. (3-1) is given by

$$K_{(A,B)} = \frac{(\bar{a}_A)^{z_B}(a_B)^{z_A}}{(a_A)^{z_B}(\bar{a}_B)^{z_A}} \tag{3.2-5}$$

where a represents activities of the aqueous species and $\bar{a}$ represents activities of the zeolite components. The equilibrium constant is a measure of the relative affinity between the zeolite and the two cations involved in the exchange. The zeolite may be considered as a solid solution of two components AL_{z_A} and BL_{z_B} (Barrer and Klinowski, 1977; Ekedahl, et al., 1950; Freeman, 1961), where L_{z_A} is the amount of anionic framework associated with an A^{z_A+} ion and carrying anionic charge z_A- and L_{z_B} is the amount of framework associated with B^{z_B+} and carrying anionic charge z_B-. The number of moles of AL_{z_A} and BL_{z_B} are then respectively equal to the total number of moles n_A and n_B of ions A^{z_A+} and B^{z_B+} in the zeolite, and solid phase compositions can be described in terms of cationic mole fractions of A^{z_A+} and B^{z_B+} in the zeolite

$$\bar{X}_A = \frac{\bar{n}_A}{\bar{n}_A + \bar{n}_B}; \quad \bar{X}_B = \frac{\bar{n}_B}{\bar{n}_A + \bar{n}_B} \tag{3.2-6}$$

Eq. (3.2-5) may be expanded to give

$$K_{(A,B)} = \frac{(\bar{X}_A)^{z_B}(M_B)^{z_A}}{(\bar{X}_B)^{z_A}(M_A)^{z_B}} \times \frac{(f_A)^{z_B}}{(f_B)^{z_A}} \times \frac{(\gamma_B)^{z_A}}{(\gamma_A)^{z_B}} \tag{3.2-7}$$

or,

$$K_{(A,B)} = K_{v(A,B)} \times \frac{(f_A)^{z_B}}{(f_B)^{z_A}} \tag{3.2-8}$$

where $K_{v(A,B)}$ is the Vanselow corrected selectivity coefficient (Townsend, 1986; Vanselow, 1932) defined by

$$K_{v(A,B)} = \frac{(\bar{X}_A)^{z_B}(M_B)^{z_A}}{(\bar{X}_B)^{z_A}(M_A)^{z_B}} \times \frac{(\gamma_B)^{z_A}}{(\gamma_A)^{z_B}} \quad (3.2\text{-}9)$$

and M_A and M_B are the molarities of A^{z_A+} and B^{z_B+} in the aqueous phase. The quantities γ_A and γ_B are single-ion activity coefficients for the aqueous cations and account for nonideal behavior in the aqueous phase. The quantities f_A and f_B are rational (i.e., in terms of mole fractions) activity coefficients for the zeolite components and account for nonideality in the zeolite phase.

It is necessary to define the standard states of the various components to allow the evaluation of $K_{(A,B)}$, f_A, and f_B from experimental data using the Gibbs-Duhem relation. For the aqueous electrolyte solution external to the zeolite phase, the usual standard state is that of a hypothetical, one molar solution referenced to infinite dilution. For the exchanger phase, it has been normal practice to make the standard state for each exchanging cation the appropriate homoionic form of the zeolite in equilibrium with an infinitely dilute solution of the same cation (Gaines and Thomas, 1953; Sposito, 1981). With that standard state, the criterion for ideal behavior in the zeolite solid solution is that $\bar{a}_i = \bar{X}_i$ for all $\bar{X}_i$.

3.2.3.3 Activity Coefficients of Aqueous Ions

An evaluation of equilibrium constants and zeolite phase activity coefficients from experimental data involves activity correction for the aqueous phase. Ion-exchange studies (Fletcher and Townsend, 1985) demonstrated the importance of correctly evaluating aqueous solution activity coefficients for accurate interpretation of exchange equilibria, particularly on systems with mixed background anions. In previous CNWRA studies (Pabalan, 1994; Pabalan and Bertetti, 1999, 1994, 2001), the ion-interaction model Pitzer developed (1991, 1987, and 1973) was used to calculate the activity coefficients of aqueous ions. However, other aqueous activity coefficient models are equally useful. In the work summarized in this report, activity coefficients of aqueous ions were calculated using the B-dot equation of Helgeson (1969). The model is valid to an ionic strength of about 1 molal, which covers the range of most ion-exchange studies, and has been developed to span a wide range of temperatures {up to 300 °C [572 °F]}. The B-dot equation was used in this study to permit future use of the ion-exchange model with geochemical codes such as EQ3/6 (Wolery, 1992) and Geochemist's Workbench (Bethke, 1996).

3.2.3.4 Activity Coefficients of Zeolite Components

Various models have been proposed to represent the activity coefficients of exchangeable ions or solid solutions (Chu and Sposito, 1981; Elprince and Babcock, 1975; Elprince, et al., 1980; Grant and Sparks, 1989; Mehablia, et al., 1996; Morgan, et al., 1995; Pabalan, 1994). Two models that have been used in ion-exchange studies are the Margules and Wilson equations. These equations have been widely applied to describe nonideal behavior in both solid and liquid solutions (Pitzer, 1995).

Margules Model

The Margules model has been used successfully in studies of ion-exchange equilibria involving zeolite minerals (Pabalan, 1994; Shibue, 1998). In this model, the molar excess Gibbs energy

of mixing, $\overline{G}^E$, for a zeolite solid solution with two-components, AL_{z_A} and BL_{z_B}, is represented by the equation

$$\frac{\overline{G}^E}{RT} = \overline{X}_A \overline{X}_B (\overline{X}_B W_A + \overline{X}_A W_B) \tag{3.2-10}$$

where W_A and W_B are empirical parameters that are functions only of temperature and pressure. From Eq. (3-9) and the Gibbs-Duhem relation, the zeolite activity coefficients, f_A and f_B, can be expressed in terms of W_A and W_B as

$$\ln f_A = \overline{X}_B^2 [W_A + 2\overline{X}_A (W_B - W_A)]; \ln f_B = \overline{X}_A^2 [W_B + 2\overline{X}_B (W_A - W_B)] \tag{3.2-11}$$

For solid solutions with three or more components, analogous expressions can be derived (Grant and Sparks, 1989; Mukhopadhyay, et al., 1993).

The Vanselow selectivity coefficient, $K_{v(A,B)}$, can then be represented by

$$\ln K_{v(A,B)} = \ln K_{(A,B)} + z_A \overline{X}_A^2 [W_B + 2\overline{X}_B (W_A - W_B)] - z_B \overline{X}_B^2 [W_A + 2\overline{X}_A (W_B - W_A)] \tag{3.2-12}$$

Values of $K_{(A,B)}$, W_A, and W_B can be derived by nonlinear regression of Eq. (3-12) to isotherm data. If the zeolite phase behaves ideally, $f_A = f_B = 1$ and $g^{ex} = 0$ for all values of $\overline{X}_A$ and $\overline{X}_B$, and $K_{(A,B)} = K_{v(A,B)}$. Values of W_A and W_B are zero for ideal solid solutions.

Wilson Model

The Wilson model also has been applied successfully to studies of ion-exchange equilibria (e.g., de Lucas, et al., 1992; Elprince and Babcock, 1975; Ioannidis, et al., 2000; Mehablia, et al., 1996; Shallcross, et al., 1988; Shibue, 1999). For a two-component zeolite solid solution, the molar excess Gibbs energy is taken to be

$$\frac{\overline{G}^E}{RT} = -\overline{X}_A \ln (\overline{X}_A + \Lambda_{AB} \overline{X}_B) - \overline{X}_B \ln (\overline{X}_B + \Lambda_{BA} \overline{X}_A) \tag{3.2-13}$$

where Λ_{AB} and Λ_{BA} are empirical parameters. In this model, the measure of nonideality is the departure of the parameters from 1.0. For a solid solution that behaves ideally, $\Lambda_{AB} = \Lambda_{BA} = 1.0$. The corresponding activity coefficients for the binary solid solution are

$$\ln f_A = -\ln (\overline{X}_A + \Lambda_{AB} \overline{X}_B) + \overline{X}_B \left(\frac{\Lambda_{AB}}{\overline{X}_A + \Lambda_{AB} \overline{X}_B} - \frac{\Lambda_{BA}}{\Lambda_{BA} \overline{X}_A + \overline{X}_B} \right) \tag{3.2-14}$$

and

$$\ln f_B = -\ln (\overline{X}_B + \Lambda_{BA} \overline{X}_A) + \overline{X}_A \left(\frac{\Lambda_{BA}}{\overline{X}_B + \Lambda_{BA} \overline{X}_A} - \frac{\Lambda_{AB}}{\Lambda_{AB} \overline{X}_B + \overline{X}_A} \right) \tag{3.2-15}$$

In a manner similar to the Margules model, the Vanselow selectivity coefficient, $K_{V(A,B)}$, can then be represented by

$$\ln K_{v(A,B)} = \ln K_{(A,B)} + z_A \ln f_B - z_B \ln f_A \tag{3.2-16}$$

Eqs (3.2-14) and (3.2-15) can be substituted for $\ln f_A$ and $\ln f_B$, respectively, in Eq. (3.2-16) to create an expression analogous to Eq. (3.2-12), where $\ln K_{V(A,B)}$, Λ_{AB}, and Λ_{BA} can be derived by nonlinear regression to isotherm data. For multicomponent systems, the Wilson equation can be generalized to

$$\frac{\overline{G}^E}{RT} = -\sum_{i=1}^{m} \overline{X}_i \ln\left(\sum_{j=1}^{m} \Lambda_{ij} \overline{X}_j\right) \tag{3.2-17}$$

and

$$\ln f_k = 1 - \ln\left(\sum_{j=1}^{m} \Lambda_{kj} \overline{X}_j\right) - \sum_{i=1}^{m}\left(\frac{\overline{X}_i \Lambda_{ik}}{\sum_{j=1}^{m} \Lambda_{ij} \overline{X}_j}\right) \tag{3.2-18}$$

where Λ_{ii}, Λ_{jj}, Λ_{kk}, and so on are equal to 1.0 and the other Λ_{ij} are just the binary parameters. The absence of parameters beyond the binary terms makes the Wilson model attractive for application to ternary or more complex mixtures. However, Pitzer (1995) points out that interactions of three different species in a mixture do occur, and a provision for their representation is needed when they are significant.

3.2.3.5 Modeling

To develop a more uniform approach to modeling ion-exchange reactions in zeolite, the two thermodynamic models described in the preceding section used to represent activity coefficients of exchangeable ions in solid solutions were evaluated for use in interpreting and predicting experimental results. Both equations have been used successfully in studies of ion-exchange equilibria, and both rely on empirical parameters to represent aspects of the solid solution behavior. The Margules model has been exclusively used in previous CNWRA ion-exchange studies. However, a limitation of the Margules approach is the need to derive parameters to represent ternary ion-interactions, in addition to those derived from binary ion-exchange experiments. The Wilson approach, on the other hand, is formulated such that parameters developed for binary systems can be used to represent ternary system behavior, without the need for additional parameters.

Initially, an algebraic expression representing the binary form of Wilson model [Eq. (3.2-16)] was derived for incorporation into a curve-fitting algorithm using the software TableCurve Version 3.0 (Jandel Scientific). Confirmatory testing of the curve-fitting algorithm was conducted to test for consistency and for capability of the algorithm to reproduce thermodynamic parameters from previous experimental data. Three parameters can be directly obtained from the nonlinear fit the equilibrium constant [$K_{(A,B)}$] of the reaction {often expressed as $\ln [K_{(A,B)}]$} and the two empirical parameters, Λ_{AB} and Λ_{BA}. The empirical parameters represent nonideality of the

exchange and interaction of the exchanging cations. Interestingly, the obtained fit parameters are highly sensitive to the weighting used for each data set. Following testing, a rather extensive literature search was performed to gather appropriate ion-exchange data for systems of interest, including those not directly included in the experimental plan of this study. The Wilson model was applied to several experimental data sets in several binary ion-exchange systems, and the model was compared to Margules model results from the same systems.

3.2.4 Results And Discussion

3.2.4.1 Binary Ion-exchange Results

Several important binary ion-exchange experiments were conducted. These experiments were designed to confirm results obtained from the literature and to provide additional data for development of thermodynamic parameters. The experimental systems studied included Na^+/Cs^+, K^+/Na^+, K^+/Cs^+, K^+/Sr^{2+}, K^+/Ca^{2+}, and Ca^{2+}/Sr^{2+}, and the data are plotted in Figure 3.2-1. The error bars shown in each figure were calculated using the equations presented in Pabalan (1994). For each binary system, isotherm points were calculated from the initial and final concentrations of both cations participating in the ion-exchange reaction. In general, the isotherm points calculated independently from the concentrations of the two cations agree very well. The disagreements for some isotherm points shown in Figure 3.2-1(f) for the Sr^{2+}/Ca^{2+} system are probably related to analytical problems.

3.2.4.2 Comparison of Margules and Wilson Models

The derived parameters for the Margules and Wilson models are provided in Table 3.2-3. Isotherms calculated using the derived Wilson parameters for each system are shown in Figures 3.2-2 to 3.2-5, which also plot ion-exchange data from this study and from the literature.[1] The regression results indicate that (i) the equilibrium constants (listed in the Table 3.2-3 as ln K values) derived from the same set of data using either model are very close (exceptions are found where the isotherm points do not cover a wide range of solution equivalent mole fraction), (ii) the ln Ks derived from experimental data at different solution concentrations (i.e., from previous experiments conducted at CNWRA) vary slightly, (iii) the Margules and Wilson empirical parameters can vary widely depending on the data used in the regression, and (iv) the Wilson model "behaves" better than the Margules model (i.e., the Wilson model is not as sensitive to the lack of data at the extreme ends of the isotherm) (the Margules model tends to become unstable where limited data are available).

3.2.4.3 Results of Ternary and Quaternary Ion-Exchange Experiments

Ternary ion-exchange experiments were conducted on three systems: $Na^+/K^+/Cs^+$, $Na^+/Ca^{2+}/K^+$, and $Na^+/K^+/Sr^{2+}$. The first system involves monovalent cations only, whereas the latter two involve heterovalent exchange reactions. All three systems were studied at concentrations of 0.05 N and 0.005 N. A quaternary ion-exchange experiment studying the $Na^+/K^+/Ca^{2+}/Sr^{2+}$ (0.05 N) system was also conducted and completed. Not all systems were analyzed for the equilibrium zeolite compositions. The systems in which solid phase samples were separated after equilibration with the aqueous solution and analyzed are the 0.005 N

[1]Isotherms calculated using the Wilson and Margules models are similar. For clarity, only isotherms calculated using the Wilson models are plotted.

$Na^+/K^+/Ca^{2+}$, 0.05 N $Na^+/K^+/Ca^{2+}$, 0.05 N $Na^+/K^+/Sr^{2+}$, and 0.05 N $Na^+/K^+/Ca^{2+}/Sr^{2+}$ systems. Solid samples from the 0.005 N $Na^+/K^+/Cs^+$ system were also taken and analyzed using inductively coupled plasma atomic emission spectrometry, but due to an error in specifying the required analytical protocol, the Cs^+ concentration in the zeolite samples was not analyzed—only the Na^+ and K^+ concentrations were analyzed.

$Na^+/K^+/Ca^{2+}$ (0.005 N)

The initial and equilibrium solution compositions in the 0.005 N $Na^+/K^+/Ca^{2+}$ system are shown in Figure 3.2-6(a). The high selectivity of clinoptilolite for K^+ relative to Na^+ and for Ca^{2+} relative to Na^+ is reflected in the enrichment of Na^+ in the aqueous phase. The preference of clinoptilolite for K^+ and Ca^{2+} relative to Na^+ is also demonstrated in Figure 3.2-6(b), which compares the equilibrium zeolite composition with the equilibrium solution composition. Note that the experiments used a homoionic Na form of clinoptilolite, which would plot at the E_{Na} corner of the diagram.

Figure 3.2-6(b) also compares the measured equilibrium solution composition (red circles) and the solution compositions (yellow circles) predicted from the thermodynamic model, using as input values the measured zeolite composition. Considering the uncertainties in analytical data, the agreement between measured and predicted values is very good.

$Na^+/K^+/Ca^{2+}$ (0.05 N)

The initial and equilibrium solution compositions in the 0.05 N $Na^+/K^+/Ca^{2+}$ system are shown in Figure 3.2-7(a). The results also indicate enrichment of Na^+ in the aqueous phase, although it was not as strong as that observed at 0.005 N [Figure 3.2-6(a)]. On the other hand, Figure 3.2-7(b) illustrates the much stronger selectivity of clinoptilolite for K^+ relative to both Na^+ and Ca^{2+}. The equilibrium zeolite compositions plot mostly toward the E_K, indicating that the initially homoionic Na-clinoptilolite has become mostly K-rich.

Figure 3.2-7(b) also compares the measured equilibrium solution composition (red circles) and the solution compositions (yellow circles) predicted from the thermodynamic model, using as input values the measured zeolite composition. The agreement between measured and predicted values is good considering the uncertainties in analytical data.

$Na^+/K^+/Sr^{2+}$ (0.005 N)

The initial and equilibrium solution compositions in the 0.005 N $Na^+/K^+/Sr^{2+}$ system are shown in Figure 3.2-8(a). The high selectivity of clinoptilolite for the K^+ relative to Na^+ and for Sr^{2+} relative to Na^+ is reflected in the enrichment of Na^+ in the aqueous phase. No zeolite samples were taken for measurement of equilibrium composition. The zeolite compositions plotted in Figure 3.2-8(b) were estimated based on the initial and final concentrations of Na^+, K+, and Sr^{2+} in the aqueous phase. Figure 3.2-8(b) illustrates the preference of clinoptilolite for K^+ and Sr^{2+} relative to Na^+. Note that the experiment used a homoionic Na form of clinoptilolite, which would plot at the E_{Na} corner of the diagram.

$Na^+/K^+/Sr^{2+}$ (0.05 N)

The initial and equilibrium solution compositions in the 0.05 N $Na^+/K^+/Sr^{2+}$ system are shown in Figure 3.2-9(a). The results also indicate enrichment of Na^+ in the aqueous phase, although it was not as strong as that observed at 0.005 N (Figure 3.2-8a). On the other hand,

Figure 3.2-9(b) illustrates the stronger selectivity of clinoptilolite for K^+ relative to both Na^+ and Sr^{2+}. The initially Na form of clinoptilolite became K-rich after reaction with $Na^+/K^+/Sr^{2+}$ solutions.

Figure 3.2-9(b) also compares the measured equilibrium solution composition (red circles) and the solution compositions (yellow circles) predicted from the thermodynamic model, using as input values the measured zeolite composition. The agreement between measured and predicted values is very good considering the uncertainties in analytical data.

$Na^+/K^+/Cs^+$ (0.005 N)

The initial and equilibrium solution compositions in the 0.005 N $Na^+/K^+/Cs^+$ system are shown in Figure 3.2-10(a). The high selectivity of clinoptilolite for the K^+ relative to Na^+ and for Cs^+ relative to Na^+ is reflected in the enrichment of Na^+ in the aqueous phase. Zeolite samples were taken for measurement of equilibrium composition, but due to an error in specifying the analytical protocol for the zeolite samples, only Na and K analyses were done. The zeolite compositions plotted in Figure 3.2-10(b) were estimated based only on the measured Na and K concentrations of the zeolite. Figure 3.2-10(b) illustrates the preference of clinoptilolite for K^+ and Cs^+ relative to Na^+. Note that the experiment used a homoionic Na form of clinoptilolite, which would plot at the E_{Na} corner of the diagram.

Figure 3.2-10(b) also compares the measured equilibrium solution composition (red circles) and the solution compositions (yellow circles) predicted from the thermodynamic model, using as input values the estimated zeolite composition. Considering that the input values used for the thermodynamic model calculations are only estimated values, the agreement between measured and predicted values is relatively good.

$Na^+/K^+/Cs^+$ (0.005 N)

The initial and equilibrium solution compositions in the 0.05 N $Na^+/K^+/Cs^+$ system are shown in Figure 3.2-11(a). Note that this system was the first ternary system studied and the initial solutions had different cationic ratios from those used in later experiments. Only 6 different initial solution compositions were used to generate the 18 isotherm points. One of those six compositions is a pure Cs^+ solution, four were Na^+/Cs^+ mixtures, and one is a $Na^+/K^+/Cs^+$ mixture. Also, in this experiment only, the K form of clinoptilolite was used, as opposed to the Na form used in later experiments. The data shown in Figure 3.2-11(a) show enrichment of K^+ in the aqueous phase, resulting from replacement of the K^+ initially in the zeolite by the Cs^+ and Na^+ initially in the aqueous phase.

No zeolite samples were taken for measurement of equilibrium composition. The zeolite compositions plotted in Figure 3.2-11(b) (green squares) were estimated based on the initial and final concentrations of Na^+, K+, and Cs^+ in the aqueous phase. Figure 3.2-11(b) shows that the zeolite composition, which was initially the K form and would plot in the E_K corner of the triangle, became Na^+ and Cs^+ rich after ion-exchange with the aqueous solutions.

Figure 3.2-11(b) also compares the measured equilibrium solution composition (red circles) and the solution compositions (yellow circles) predicted from the thermodynamic model, using as input values the estimated zeolite composition. The agreement between measured and predicted values is fair to poor and likely reflects both analytical uncertainty and the imprecision of the method used to estimate the equilibrium zeolite composition.

Quaternary System $Na^+/K^+/Ca^{2+}/Sr^{2+}$ (0.05 N)

The results for the quaternary $Na^+/K^+/Ca^{2+}/Sr^{2+}$ system at 0.05 N are shown in Figure 3.2-12(a–d) as a series of ternary diagrams. In the figures, tie lines connect the equilibrium compositions of the zeolite and aqueous phases. Most of the equilibrium zeolite compositions plot toward the E_K corner of the ternary plots, illustrating the high selectivity of clinoptilolite for K^+. No comparison is made between predicted and measured values because time constraints did not permit modifying the thermodynamic model to permit calculations of ion-exchange equilibria for quaternary systems.

3.2.5 Summary and Conclusions

Ion-exchange experiments were conducted involving the zeolite mineral clinoptilolite and binary, ternary, and quaternary aqueous mixtures of Na^+, K^+, Cs^+, Ca^{2+}, and Sr^{2+}. The results of experiments involving binary cation mixtures, supplemented by data from published literature, were used to derive parameters for a thermodynamic model for zeolite component activity coefficients based on the Wilson equation. To help constrain the range of fitted model parameters and reduce the variance in derived parameter values, a correlation method that has been used in the literature to predict the formation constants of hydroxo-metal complexes was applied. Excellent agreement is obtained between values calculated with the model and experimental data on binary mixtures. The predictive capability of the thermodynamic model, which uses parameters derived from binary mixtures only, was tested by comparing calculated values and experimental data from experiments involving ternary cation mixtures. In general, the agreement between measured and calculated values is very good. Although further work is needed to compare the model predictions with the experimental data involving quaternary cation mixtures, the results for the ternary systems suggest that the thermodynamic model based on the Wilson equation can successfully predict ion-exchange equilibria in multicomponent systems of interest in geochemistry and chemical engineering. Although these models apply to short-lived fission products, and have not been incorporated into the performance assessment models for Yucca Mountain, they do provide insights in different sorption mechanisms that may be important in other waste management issues.

3.2.6 References (Section 3.2)

Ames, L.L., Jr. "Cation Exchange Properties of Heulandite-Clinoptilolite Series Members." Volume II. *Physical Sciences.* D.W. Pearce and M.R. Compton, eds. BNWL–481–3. Richland, Washington: Pacific Northwest Laboratory. pp. 54–59. 1968.

Ames, L.L., Jr. "Some Zeolite Equilibria With Alkali Metal Cations." *American Mineral.* Vol. 49. pp. 127–145. 1964a.

Ames, L.L., Jr. "Some Zeolite Equilibria With Alkaline Earth Metal Cations." *American Mineral.* Vol. 49. pp. 1,099–1,110. 1964b.

Barrer R.M. and J. Klinowski. "Theory of Isomorphous Replacement in Aluminosilicates." *Philosophical Transaction of the Royal Society of London.* Vol. A285. pp. 637–676. 1977.

Baxter S.G. and D.C. Berghauser. "The Selection and Performance of the Natural Zeolite Clinoptilolite in British Nuclear Fuel's Site Ion Exchange Effluent Plant, SIXEP." Waste Management `86: Proceedings of the Symposium on Waste Management. pp. 347–356. 1986.

Bethke, C.M. *Geochemical Reaction Modeling*. Oxford, England: Oxford University Press. 1996.

Bertetti, F.P. and R.T. Pabalan. "Experimental and Modeling Study of Multicomponent Ion-Exchange Equilibria on Zeolite Minerals." Project 20-9211—Final Report. San Antonio, Texas: CNWRA. 2003.

Broxton D.E., D.L. Bish, and R.G. Warren. "Distribution and Chemistry of Diagenetic Minerals at Yucca Mountain, Nye County, Nevada." *Clays and Clay Minerals.* Vol. 35, No. 2. pp. 89–110. 1987.

Broxton D.E., R.G. Warren, R.C. Hagan, and G. Luedemann. "Chemistry of Diagnetically-Altered Tuffs at a Potential Nuclear Waste Repository, Yucca Mountain, Nye County, Nevada." Los Alamos, New Mexico: Los Alamos National Laboratory. 1986.

Chelishchev, N.F., B.G. Berenshtein, T.A. Berenshtein, N.K. Gribanova, and N.S. Martynova. "Ion-Exchange Properties of Clinoptilolites." *Doklady Akademii Nauk SSSR.* Vol. 210. pp. 1,110–1,112. 1973.

Chu S.-Y. and G. Sposito. "The Thermodynamics of Ternary Cation Exchange Systems and the Subregular Model." *Soil Science Society of America Journal.* Vol. 45. pp. 1,084–1,089. 1981.

de Lucas A., J. Zarca, and P. Canizares. "Ion-Exchange Equilibrium of Ca^{2+} ions, Mg^{2+} ions, K^{+} Ions, Na^{+} ions, and H^{+} Ions on Amberlite IR-120—Experimental Determination and Theoretical Prediction of the Ternary and Quaternary Equilibrium Data." *Separation Science and Technology.* Vol. 27, No. 6. pp. 823–841. 1992.

Dyer, A., H. Enamy, and R.P. Townsend. "The Plotting and Interpretation of Ion-Exchange Isotherms in Zeolite Systems." *Separation Science and Technology.* Vol. 16, No. 2. pp. 173–183. 1981.

Ekedahl, E., E. Hogfeldt, and L.G. Sillen. "Activities of the Components in Ion Exchangers." *Acta Chemica Scandinavica.* Vol. 4. pp. 556–558. 1950.

Elprince, A.M. and K.L. Babcock. "Prediction of Ion-Exchange Equilibria in Aqueous Systems With More Than Two Counter-Ions." *Soil Science.* Vol. 120, No. 5. pp. 332–338. 1975.

Elprince, A.M., A.P. Vanselow, and G. Sposito. "Heterovalent, Ternary Cation Exchange Equilibria: NH_4+-Ba^{2+}-La^{3+} Exchange on Montmorillonite." *Soil Science Society of America Journal.* Vol. 44. pp. 964–969. 1980.

Fletcher, P., K.R. Franklin, and R.P. Townsend. "Thermodynamics of Binary and Ternary Ion Exchange in Zeolites: The Exchange of Sodium, Ammonium, and Potassium ions in Mordenite." *Philosophical Transactions of the Royal Society of London.* Vol. A312. pp. 141–178. 1984.

Fletcher, P. and R.P. Townsend. "Ion Exchange in Zeolites: The Exchange of Cadmium and Calcium in Sodium X Using Different Anionic Backgrounds." *Journal of the Chemical Society Faraday Transactions: 1.*" Vol. 81. pp. 1,731–1,744. 1985.

Freeman, D.H. "Thermodynamics of Binary Ion-Exchange Systems." *Journal of Chemical Physics.* Vol. 35, No. 1. pp. 189–191. 1961.

Gaines, J., L. George, and H.C. Thomas. "Adsorption Studies on Clay Minerals—II: A Formulation of the Thermodynamics of Exchange Adsorption." *Journal of Chemical Physics.* Vol. 21, No. 4. pp. 714–718. 1953.

Gapon, Y.N. "Theory of Exchange Adsorption in Soils." *Journal of General Chemistry USSR* 3. pp. 144–163. 1933.

Grant, S.A. and D.L. Sparks. "Method for Evaluating Exchangeable-Ion Excess Gibbs Energy Models in Systems With Many Species." *Journal of Physical Chemistry.* Vol. 93. pp. 6,265–6,267. 1989.

Helgeson, H.C. "Thermodynamics of Hydrothermal Systems at Elevated Temperatures and Pressures." *American Journal of Science*. Vol 267. pp. 724–804. 1969.

Howden, M. and J. Pilot. "The Choice of Ion Exchanger for British Nuclear Fuels Ltd.'s Site Ion Exchange Effluent Plant." *Ion Exchange Technology.* D. Naden and M. Streat, eds. Chichester, West Sussex, United Kingdom: Ellis Horwood Limited. pp. 66–73. 1984.

Howery, D.G. and H.C. Thomas. "Ion Exchange on the Mineral Clinoptilolite." *The Journal of Physical Chemistry.* Vol. 69. pp. 531–537. 1965.

Ioannidis, S.A., A. Anderko, and S.J. Sanders. "Internally Consistent Representation of Binary Ion Exchange Equilibria." *Chemical Engineering Science.* Vol. 55, No. 14. pp. 2,687–2,698. 2000.

Jama, M.A. and H. Yucel. "Equilibrium Studies of Sodium-Ammonium, Potassium-Ammonium, and Calcium-Ammonium Exchanges on Clinoptilolite Zeolite." *Separation Science and Technology*. Vol. 24. pp. 1,393–1,416. 1990.

Kielland, J. "Thermodynamics of Base-Exchange of Some Different Kinds of Clays." *Journal Society of Chemical Industry, London Transactions*. Vol. 54. pp. 232–234. 1935.

Leppert, D.E. "An Oregon Cure for Bikini Island? First Results From the Zeolite Immobilization Experiment." *Oregon Geology.* Vol. 50. pp. 140–141. 1988.

Mehablia, M.A., D.C. Shallcross, and G.W. Stevens. "Ternary and Quaternary Ion Exchange Equilibria." *Solvent Extraction and Ion Exchange.* Vol. 14, No. 2. pp. 309–322. 1996.

Morgan, J.D., D.H. Napper, and G.G. Warr. "Thermodynamics of Ion Exchange Selectivity at Interfaces." *Journal of Physical Chemistry.* Vol. 99, No. 23. pp. 9,458–9,465. 1995.

Mukhopadhyay, B., S. Basu, and M.J. Holdaway. "A Discussion of Margules-Type Formulations for Multicomponent Solutions With a Generalized Approach." *Geochimica et Cosmochimica Acta.* Vol. 57. pp. 277–283. 1993.

Mumpton, F.A. "Natural Zeolites: A New Industrial Mineral Commodity." *Natural Zeolites: Occurrence, Properties, Use.* L.B. Sand and F.A. Mumpton, eds. Elmsford, New York: Pergamon Press. pp. 3-27. 1978.

Mumpton, F.A. "Development of Uses for Natural Zeolites: A Critical Commentary." *Occurrence, Properties, and Utilization of Natural Zeolites.* D. Kallo and H.S. Sherry, eds. Budapest, Hungary: Akademiai Kiado. pp. 333–366. 1988.

Mumpton, F. A. and W.C. Ormsby. "Morphology of Zeolites in Sedimentary Rocks by Scanning Electron Microscopy." *Clays and Clay Minerals*. Vol. 24. pp. 1–23. 1976.

Pabalan, R.T. "Nonideality Effects on the Ion Exchange Behavior of the Zeolite Mineral Clinoptilolite." *Scientific Basis for Nuclear Waste Management XIV.* T. Abrajano and L. Johnson, eds. MRS Symposium Proceedings 212. Pittsburgh, Pennsylvania: Materials Research Society. pp. 559–567. 1991.

Pabalan, R.T. "Thermodynamics of Ion-Exchange Between Clinoptilolite and Aqueous Solutions of Na^+/K^+ and Na^+/Ca^{2+}." *Geochimica et Cosmochimica Acta*. Vol. 58. pp. 4,573–4,590. 1994.

Pabalan, R.T. and F.P. Bertetti. "Thermodynamics of Ion-Exchange Between Na^+/Sr^{2+} Solutions and the Zeolite Mineral Clinoptilolite." *Scientific Basis for Nuclear Waste Management XVI.* A. Barkatt and R. Van Konynenberg, eds. MRS Symposium Proceedings 333. Pittsburgh, Pennsylvania: Materials Research Society. pp. 731–738. 1994.

Pabalan, R.T. and F.P. Bertetti. "Experimental and Modeling Study of Ion Exchange Between Aqueous Solutions and the Zeolite Mineral Clinoptilolite." *Journal of Solution Chemistry.* Vol. 28, No. 4. pp. 367–393. 1999.

Pabalan, R.T. and F.P. Bertetti. "Cation-Exchange Properties of Natural Zeolites." *Reviews in Geochemistry and Mineralogy.* D.L. Bish and D.W. Ming, eds. pp. 453–518. Washington, DC: Mineralogical Society of America. 2001.

Pabalan, R.T., V. Jain, R.F. Vance, S. Ioannidis, D.A. Pickett, C.S. Brazel, J.T. Persyn, E.J. Taylor, and M.E. Inman. "Hanford Tank Waste Remediation System Pretreatment Chemistry and Technology." San Antonio, Texas: CNWRA. 1999.

Pansini, M. "Natural Zeolites as Cation Exchangers for Environmental Protection." *Mineralium Deposita.* Vol. 31, No. 6. pp. 563–575. 1996.

Pitzer, K.S. "Thermodynamics of Electrolytes, 1—Theoretical Basis and General Equations." *Journal of Physical Chemistry.* Vol. 77. pp. 268–277. 1973.

Pitzer, K.S. "A Thermodynamic Model for Aqueous Solutions of Liquid-Like Density." *Reviews in Mineralogy.* Vol. 17. pp. 97–142. 1987.

Pitzer, K.S. "Ion Interaction Approach: Theory and Data Correlation." *Activity Coefficients in Electrolyte Solutions.* K.S. Pitzer, ed. Boca Raton, Florida: CRC Press. pp. 75–153. 1991.

Pitzer, K.S. *Thermodynamics*. New York City, New York: McGraw-Hill, Inc. 1995.

Robinson, S.M., W.D. Arnold, and C.H. Byers. "Multicomponent Ion Exchange Equilibria in Chabazite Zeolite." *Emerging Technologies in Hazardous Waste Treatment II.* Vol. 468. D.W. Tedder and F.G. Pohland, eds. Washington, DC: American Chemical Society. pp. 133–152. 1991.

Robinson, S.M., T.E. Kent, and W.D. Arnold. "Treatment of Contaminated Wastewater at Oak Ridge National Laboratory by Zeolites and Other Ion Exchangers." *Natural Zeolites '93: Occurrence, Properties, Use.* D.W. Ming and F.A. Mumpton, eds. Brookport, New York: International Committee on Natural Zeolites. pp. 579–586. 1995.

Shallcross, C.D., C.C. Hermann, and J.B. McCoy. "An Improved Model for the Prediction of Multicomponent ion Exchange Equilibria." *Chemical Engineering Science.* Vol. 43. pp. 279–288. 1988.

Sherry, H.S. "Cation Exchange on Zeolites." *Molecular Sieve Zeolites-I Advances in Chemistry Series 101.* E.M. Flanigen and L.B. Sand, eds. American Chemical Society. pp. 350–379. 1971.

Shibue, Y. "Cation-Exchange Properties of Phillipsite (a Zeolite Mineral): The Differences Between Si-Rich and Si-Poor Phillipsites." *Separation Science and Technology.* Vol. 33, No. 3. pp. 333–355. 1998.

Shibue, Y. "Calculations of Fluid-Ternary Solid Solution Equilibria: An Application of the Wilson Equation to Fluid-(Fe,Mn,Mg)TiO_3 Equilibria at 600 °C and 1 kbar." *American Mineralogist.* Vol. 84, No. 9. pp. 1,375–1,384. 1999.

Sposito, G. *The Thermodynamics of Soil Solutions*. New York City, New York: Oxford University Press. 1981.

Townsend, R.P. "Ion Exchange in Zeolites: Some Recent Developments in Theory and Practice." *Pure and Applied Chemistry.* Vol. 58, No. 10. pp. 1,359–1,366. 1986.

Townsend, R.P. and M. Loizidou. "Ion-Exchange Properties of Natural Clinoptilolite, Ferrierite, and Mordenite—I: Sodium-Ammonium Equilibria." *Zeolites.* Vol. 4. pp. 191–195. 1984.

Valcke, E., B. Engels, and A. Cremers. "The Use of Zeolites as Amendments in Radiocaesium– and Radiostrontium-Contaminated Soils: A Soil-Chemical Approach—1: Cs-K Exchange in Clinoptilolite and Mordenite." *Zeolites.* Vol. 18, Nos. 2–3. pp. 205–211. 1997a.

Valcke, E., B. Engels, and A. Cremers. "The Use of Zeolites as Amendments in Radiocaesium– and Radiostrontium–Contaminated Soils: A Soil-Chemical Approach—2: Sr-Ca Exchange in Clinoptilolite, Mordenite, and Zeolite A." *Zeolites.* Vol. 18, Nos. 2–3. pp. 212–217. 1997b.

Vanselow, A.P. "Equilibria of the Base-Exchange Reactions of Bentonites, Permutite, Soil Colloids, and Zeolites." *Soil Science.* Vol. 33. pp. 95–113. 1932.

Wolery, T.J. "EQ3NR, A Computer Program for Geochemical Aqueous Speciation-Solubility Calculations: Theoretical Manual, User's Guide, and Related Documentation (Version 7.0)." UCRL–MA–110662, Part III. Livermore, California: Lawrence Livermore National Laboratory. 1992.

3.3 General Features of a Surface Complexation Modeling Approach

3.3.1 Introduction to Surface Complexation Modeling

The surface charge of many minerals varies as a function of pH (Kent, et al., 1988; Davis and Kent, 1990; Turner and Sassman, 1996; Sverjensky and Sahai, 1996; Sahai and Sverjensky, 1997a,b). Surface complexation models address this pH dependence assuming an amphoteric surface composed of hydroxyl groups ($>SOH^0$). By adding a hydrogen ion (protonation), a positively charged surface site ($>SOH_2^+$) is developed. Conversely, losing a proton (deprotonation) leads to the development of a negatively charged surface ($>SO^-$). At low pH, the $>SOH_2^+$ sites outnumber the $>SO^-$ sites and the net surface charge is positive. At higher pH, the $>SO^-$ sites are more numerous and the net surface charge is negative. At some intermediate pH, referred to as the zero point of charge (pH_{ZPC}), the sites will balance and the surface will not exhibit any net charge. Depending on pH, therefore, the electrostatic attraction from these sites can lead to the specific adsorption of cations or anions from solution.

In most surface complexation models, the acid-base behavior of a mineral surface is simulated using equilibrium protonation/deprotonation reactions in the form

$$> SOH^0 + H^+ => SOH_2^+ \qquad (3.3\text{-}1)$$

$$> SOH^0 => SO^- + H^+ \qquad (3.3\text{-}2)$$

where $>SOH^0$ represents a neutral surface site. The equilibrium constants for these protonation and deprotonation reactions, K_+ and K_-, defined by mass action as

$$K_+ = \frac{[> SOH_2^+]}{[> SOH^0][H^+]} \qquad (3.3\text{-}3)$$

$$K_- = \frac{[> SO^-][H^+]}{[> SOH^0]} \qquad (3.3\text{-}4)$$

are referred to as intrinsic surface acidity constants. Eqs. (3.3-3) and (3.3-4) show the pH dependence of surface charge development.

By assuming an analogy to aqueous speciation reactions, surface adsorption can be described using a combination of equilibrium protonation/deprotonation and complexation reactions (Davis and Leckie, 1978; Hayes, et al., 1990; Davis and Kent, 1990; Dzombak and Morel, 1990; Langmuir, 1997; Gunnarsson, 2002; Payne, et al., 2004). Mass balance and mass action relations are then used in a manner analogous to that employed by geochemical aqueous speciation codes to determine the distribution of the elements between those dissolved in the bulk solution and those specifically sorbed onto the solid. For example, the sorption of cation M^{m+} at the mineral–water interface can be written as

$$> SOH^0 + M^{m+} = > SOM^{(m-1)} + H^+ \qquad (3.3\text{-}5)$$

The corresponding equilibrium constant for the reaction is defined such that

$$K_{\text{Rxn 3.3-5}} = \frac{\left[>\text{SOM}^{(m-1)}\right]\left[\text{H}^{+}\right]}{\left[>\text{SOH}^{0}\right]\left[\text{M}^{m+}\right]} \qquad (3.3\text{-}6)$$

and is used to constrain the mass action of the geochemical equilibrium model of the mineral–water interface.

Depending on the specific surface complexation models approach used, additional parameters may be needed to include the electrostatic effects of a charged mineral surface. Electrical work performed in moving ions across the zone of charge influence adjacent to the interface will affect the activity of aqueous species near the charged surface relative to the bulk solution. In the surface complexation models approach, the change in activity of species (e.g., H^+ and M^{m+}) near the surface due to electrostatic forces is assumed to be governed by the Boltzmann relation such that

$$\left\{\text{M}^{m+}\right\}_{\text{surface}} = \left\{\text{M}^{m+}\right\}_{\text{bulk}}\left[\exp\left(-\text{F}\psi_{\text{j}}/\text{RT}\right)\right]^{m} \qquad (3.3\text{-}7)$$

where $\exp[-F\Psi_j/RT]$ is the Boltzmann factor; Ψ_j is the model-dependent electrostatic potential of the j^{th} layer; m is the valence of the ion F and R are the Faraday ($J\cdot volt\ equiv^{-1}$) and ideal gas ($J\cdot K^{-1}\cdot mole^{-1}$) constants, respectively; and T is absolute temperature (K). This correction is incorporated into the mass action expressions for surface reactions.

Mass balance for the total concentration of available surface sites ($T_{>SOH}$ in mol sites$\cdot$L^{-1}) is

$$\text{TOT}_{>\text{SOH}} = \frac{(\text{N}_{\text{s}})\ (\text{A}_{\text{SP}})\ (\text{M}/\text{V})\cdot 10^{18}}{6.023\times 10^{23}} \qquad (3.3\text{-}8)$$

where N_S is site density (sites/nm^2), A_{SP} (m^2/g) is the specific surface area of the mineral, M/V is the solid mass to solution volume ratio (g/L), 10^{18} is the conversion from nm^2 to m^2, and 6.023×10^{23} is Avogadro's number.

Another consideration for surface complexation models is developed in the two-site conceptual model Dzombak and Morel (1990) introduced to account for surface loading effects observed for cation sorption. In this conceptual model, it is assumed that the surface consists of a low density of high-affinity surface functional groups [Type 1 or "strong" sites (>SOH$_s^0$)] and a much greater density of low-affinity groups [Type 2 or "weak" sites (>SOH$_w^0$)]. The strong sites are assumed to saturate first and are used to explain the change from a linear proportionality between the amount sorbed and the amount dissolved to a more asymptotic relationship that is typically observed in cation adsorption. The weak sites are assumed to be present in sufficient concentration to account for the observed sorption maxima. This two-site conceptual approach can successfully represent macroscopic sorption behavior, but in practice it introduces the potential for an increase in the number of model parameters that must be developed.

3.3.2 Model-Specific Features

Although general features for establishing surface complexation formation are shared by all SCM approaches, the models differ in how the mineral–water interface is divided between the

charged surface and the bulk solution, and in the charge/potential relationships used to describe the interface layers (Figure 3.3-1). Model-specific aspects are detailed elsewhere (Kent, et al., 1988; Westall and Hohl, 1980; Davis and Kent, 1990; Dzombak and Morel, 1990; Brendler, et al., 2004). Each is summarized here.

3.3.2.1 Diffuse Layer Model

The diffuse layer model assumes that protonation/deprotonation and ion adsorption only occur in one plane at the mineral–water interface and that only those ions specifically adsorbed in this "o plane" contribute to the total surface charge density [Figure 3.3-1(a)]. In the diffuse layer model, the Stern-Grahame extension of the Gouy-Chapman relationship for symmetrical electrolytes is used to describe the interdependence between ionic strength (I), charge ($\sigma_d = -\sigma_o = -\sigma_s$ at the boundary with the o plane), and electrostatic potential ($\Psi_d = \Psi_o$).

The diffuse layer model is the simplest surface complexation model with the fewest adjustable parameters. Because of its simplicity, while retaining the thermodynamic aspects of the surface complexation model approach, the diffuse layer model is the sorption model that was used for most of the CNWRA process model abstractions for performance assessment.

3.3.2.2 Constant Capacitance Model

Like the diffuse layer model, the constant capacitance model also assumes a one-layer interface, and the reactions, mass balance, and mass action used to describe surface phenomena are the same as those presented for the diffuse layer model. In contrast to the diffuse layer model, the constant capacitance model assumes that the charged surface is separated from the bulk solution by a layer of constant capacitance [Figure 3.3-1(b)]. Based on this assumption, surface charge ($\sigma_d = -\sigma_o = -\sigma_S$) is related to surface potential ($\Psi_o = \Psi_d$) through a linear potential gradient from the charged substrate to the bulk solution. The constant capacitance model is limited, however, to a specified ionic strength. In a strict sense, changes in ionic strength require recalculation of a linear capacitance, C_1. Generally, the capacitance term is not provided as a characteristic property of a given system, but instead is applied as an empirical parameter fit to the data (Westall and Hohl, 1980; Hayes, et al., 1991; 1990). This adjustment has the advantage of providing a better fit to a given data set, but at the expense of the theoretical basis of the model.

3.3.2.3 Triple-Layer Model

As the name suggests, the triple-layer model employs three layers to represent the mineral–water interface [Figure 3.3-1(c)]. In the original construction of the triple-layer model (Davis, et al., 1978), protonation/deprotonation of surface sites (K_- and K_+) was restricted to an innermost o plane, while specifically adsorbed ions were assigned to the β plane (i.e., outer-sphere complexes). Subsequent modifications (Hayes and Leckie, 1987) provided for inner-sphere complexes to describe strongly bound metals. The outermost diffuse layer, the d plane, is made up of a diffuse region of counter ions extending into the bulk solution. This conceptual model leads to the introduction of an additional set of reactions for sorption of outer-sphere complexes. Surface charges in the triple-layer model are divided between the three layers σ_o, σ_β, and σ_d for the o, β, and d layers, respectively. At the boundary between the intermediate β layer and the outermost d layer, the diffuse layer charge (σ_d) is defined such that $\sigma_o + \sigma_\beta + \sigma_d = 0$. A linear relationship is used to describe the charge/potential relationships for the inner two layers using constant capacitances C_1 and C_2 associated with the areas between

the o and β planes and β and d planes, respectively. The charge/potential relationship for the outermost diffuse layer is the same as that used for the diffuse layer model.

3.3.2.4 Nonelectrostatic Surface Complexation Model

In contrast to traditional surface complexation models that include charge/potential relationships and incorporate electrostatic corrections into the mass action expressions for surface equilibria (e.g., Eq. 3.3-7), nonelectrostatic surface complexation models (Koß, 1988; Davis, et al., 1998; Del Nero, et al., 1998; Zavarin and Bruton, 1999; Emren and Jacobsson, 2004; Koheler, et al., 2004) treat adsorption strictly as a chemical reaction phenomenon. In this approach, there are no explicit terms in the mass action expression to represent coulombic energy effects and the activity coefficient of the surface specie(s) is assumed to be 1. In a fashion similar to parameter estimation for more traditional surface complexation models, nonelectrostatic model parameters are determined by fitting a suite of one or more surface reactions to sorption data gathered over a range in chemical conditions. In effect, a nonelectrostatic approach acknowledges the difficulty in representing the surface charge accurately at the submicroscopic scale for complex, multimineral assemblages found in nature.

3.3.2.5 Generalized Composite and Component Additivity Modeling Approaches

Ultimately, performance assessment studies are concerned with the potential transport of radionuclides through the geosphere. In contrast, surface complexation model approaches were initially developed to simulate sorption onto simple (hydr)oxides under well-controlled laboratory conditions. While (hydr)oxides, such as ferrihydrite, goethite, and MnO_2, are common in nature, aluminosilicate minerals (e.g., clays and zeolites) also may contribute significantly to radionuclide sorption. In addition, many natural materials of interest are a complex mixture of minerals and mineral coatings. This makes the representation of the charge-potential relationship at the mineral–water interface uncertain and difficult to quantify under *in-situ* conditions.

There are typically two approaches to address sorption on mineral mixtures (Payne, et al., 2004; Waite, et al., 2000). The component additivity approach assumes that the mixture is represented by proportions of one or more pure mineral phases with generic surface functional groups, such as silanol ($>SiOH^0$), aluminol ($>AlOH^0$), or ferrinol ($>FeOH^0$). The individual surface properties for these phases are determined from experimental sorption data obtained for simple (hydr)oxides, such as SiO_2 and ferrihydrite (Altmann, 1984; Honeyman, 1984; Turner, et al., 1996; Pabalan, et al., 1998; Pabalan and Turner, 1997; Turner, et al., 1998; Waite, et al., 2000; Arnold, et al., 2001; Prikryl, et al., 2001; Brendler, et al., 2004; Hayes, et al., 1990; Payne, et al., 2004). The component additivity approach relies on combining the results of sorption modeling for each of these mineral phases to predict sorption behavior for the mineral mixture. Payne, et al. (2004) refer to this as a “bottom-up” approach.

In contrast, a generalized composite model is a “top-down” approach (Payne, et al., 2004) that assumes the surface properties of natural materials are not well known, and contributions of individual site types to sorption behavior cannot be characterized with certainty. In the generalized composite approach, one or more generic site types (Wanner, et al., 1994; Davis, et al., 1998; Waite, et al., 2000; Payne, et al., 2004) are assumed and sorption data are described using a set of plausible surface reactions. Although electrostatics can be included, the generalized composite approach is more commonly developed as a nonelectrostatic model because of the uncertainty in selecting an appropriate charge-potential relationship for the mineral surface (Bradbury and Baeyens, 1997; Del Nero, et al., 1998; Davis, et al., 2002, 1998;

Zavarin and Bruton, 1999; Davis, 2001; Davis and Curtis, 2003; Kohler, et al., 2004; Payne, et al., 2004). While extrapolation beyond the experimental conditions used to determine the generalized composite model parameters is uncertain, the use of apparent binding constants and surface equilibria incorporates the aqueous chemistry aspects of the system to simulate complex sorption behavior (Davis, et al., 1998).

3.3.3 References (Section 3.3)

Altmann, S.A. "Copper Binding in Heterogeneous, Multicomponent Aqueous Systems: Mathematical and Experimental Modeling Study." Ph.D. dissertation. Stanford University, Stanford, California. 1984.

Arnold, T., T. Zorn, H. Zänker, G. Bernhard and H. Nitsche. "Sorption Behavior of U(VI) on Phyllite: Experiments and Modeling. *Journal of Contaminant Hydrology.* Vol. 47. pp. 219–231. 2001.

Bradbury, M.H. and B. Baeyens. "A Mechanistic Description of Ni and Zn Sorption on Na-Montmorillonite, Part II: Modeling." *Journal of Contaminant Hydrology*. Vol. 27. pp. 223–248. 1997.

Brendler, V., A. Richter, C. Nebelung and A. Vahle,. "Development of a Mineral-Specific Sorption Database for Surface Complexation Modeling, Part I: Final Report." Project PtWt+E 02E9471. Dresden, Germany: Forschungszentrum Rossendorf. 2004.

Davis, J.A. and G.P. Curtis. NUREG/CR–6820, "Application of Surface Complexation Modeling to Describe Uranium(vi) Adsorption and Retardation at the Uranium Mill Tailings Site at Naturita, Colorado." Washington, DC: NRC. 2003.

Davis, J.A. NUREG/CR–6708, "Surface Complexation Modeling of Uranium(VI) Adsorption on Natural Mineral Assemblages." Washington, DC: NRC. 2001.

Davis, J.A. and D.B. Kent. "Surface Complexation Modeling in Aqueous Geochemistry, Reviews in Mineralogy, Volume 23." *Mineral-Water Interface Geochemistry*. M.F. Hochella, Jr. and A.F. White, eds. Washington, DC: Mineralogical Society of America. pp. 177–260. 1990.

Davis, J.A. and J.O. Leckie. "Surface Ionization and Complexation at the Oxide/Water Interface 2, Surface Properties of Amorphous Iron Oxyhydroxide and Adsorption of Metal Ions." *Journal of Colloid and Interface Science*. Vol. 67. pp. 90–107. 1978.

Davis, J.A., T.E. Payne, and T.D. Waite. "Simulating the pH and pCO_2 Dependence of Uranium(VI) Adsorption by a Weathered Schist with Surface Complexation Models." *Geochemistry of Soil Radionuclides*. P.-C. Zhang and P.V. Brady, eds. Soil Science Society of Madison, Wisconsin: America Special Publication 59. pp. 61–86. 2002.

Davis, J.A., J.A. Coston, D.B. Kent, and C.C. Fuller. "Application of the Surface Complexation Concept to Complex Mineral Assemblages." *Environmental Science and Technology*. Vol. 32. pp. 2,820–2,828. 1998.

Davis, J.A., R.O. James and J.O. Leckie. "Surface Ionization and Complexation at the Oxide/Water Interface 1, Computation of Electrical Double Layer Properties in Simple Electrolytes." *Journal of Colloid and Interface Science*. Vol. 63. pp. 480–499. 1978.

Del Nero, K. Ben Said, B. Madè, A. Clément, and G. Bontems. "Effect of pH and Carbonate Concentration in Solution on the Sorption of Neptunium(V) by Hydrargilite: Application of the Non-Electrostatic Model." *Radiochimica Acta*. Vol. 81. pp. 133–141. 1998.

Dzombak, D.A. and F.M.M. Morel. *Surface Complexation Modeling: Hydrous Ferric Oxide.*" New York City, New York: John Wiley and Sons. 1990.

Emren, A.T. and A-M. Jacobsson. "Comparison of a Non-Electrostatic Surface Complexation Model and Surface Phase Theories for Prediction of Future Sorption Properties." Materials Research Society Symposium Proceedings: Scientific Basis for Nuclear Waste Management—XXVIII. J.M. Hanchar, S. Stroes-Gascoyne, and L. Browning, eds. Pittsburgh, Pennsylvania: Materials Research Society. pp. 365–371. 2004.

Gunnarsson, M. "Surface Complexation at the Iron Oxide/Water Interface—Experimental Investigations and Theoretical Developments." ISBN 91–628–5431–3. Göteborg , Sweden: Chalmers Reproservice. 2002.

Hayes, K.F. and J.O. Leckie. "Mechanism of Lead Ion Adsorption at the Goethite-Water Interface." Geochemical Processes at Mineral Surfaces: ACS Symposium Series 323. J.A. Davis and K.F. Hayes, eds. Washington, DC: American Chemical Society. pp. 114–141. 1987.

Hayes, K.F., G. Redden, W. Ela and J.O. Leckie. "Surface Complexation Models: An Evaluation of Model Parameter Estimation Using FITEQL and Oxide Mineral Titration Data." *Journal of Colloid and Interface Science*. Vol. 142. pp. 448–469. 1991.

Hayes, K.F., G. Redden, W. Ela, and J.O. Leckie. NUREG/CR–5547, "Application of Surface Complexation Models for Radionuclide Adsorption: Sensitivity Analysis of Model Input Parameters." Washington, DC: NRC. 1990.

Honeyman B.E. "Cation and Anion Adsorption at the Oxide/Solution Interface in Systems Containing Binary Mixtures of Adsorbents: An Investigation of the Concept of Additivity." Ph.D. dissertation. Stanford University. Stanford, California. 1984.

Kent, D.B., V.S. Tripathi, N.B. Ball, J.O. Leckie and M.D. Siegel. NUREG/CR–4807, "Surface-Complexation Modeling of Radionuclide Adsorption in Subsurface Environments." Washington, DC: NRC. 1988.

Kohler, M., G.P. Curtis, D.E. Meece, and J.A. Davis. "Methods for Estimating Adsorbed Uranium(VI) and Distribution Coefficients of Contaminated Sediments." *Environmental Science and Technology*. Vol. 38. pp. 240–247. 2004.

Koß, V. "Modeling of U(VI) Sorption and Speciation in a Natural Sediment–Groundwater System. *Radiochimica Acta*. Vols. 44 and 45. pp. 403–406. 1988.

Langmuir, D. *Aqueous Environmental Geochemistry*. Englewood Cliffs, New Jersey: Prentice-Hall. 1997.

Pabalan, R.T., D.R. Turner, F.P. Bertetti, and J.D. Prikryl. "Uranium^{VI} Sorption Onto Selected Mineral Surfaces." *Adsorption of Metals by Geomedia*. E.A. Jenne, ed. New York, City, New York: Academic Press, Inc. pp. 99–130. 1998.

Pabalan, R.T. and D.R. Turner. "Uranium(6+) Sorption on Montmorillonite: Experimental and Surface Complexation Modeling Study." *Aqueous Geochemistry*. Vol. 2. pp. 203–226. 1997.

Payne, T.E., J.A. Davis, M. Ochs, M. Olin, and C.J. Tweed. "Uranium Adsorption on Weathered Schist–Intercomparison of Modelling Approaches." *Radiochimica Acta*. Vol. 92. pp. 651–661. 2004.

Prikryl, J.D., A. Jain, D.R. Turner, and R.T. Pabalan. "UraniumVI Sorption Behavior on Silicate Mineral Mixtures. *Journal of Contaminant Hydrology*. Vol. 47. pp. 241–253. 2001.

Sahai, N. and D.A. Sverjensky. "Estimation of Internally-Consistent Parameters for the Triple-Layer Model by the Systematic Analysis of Oxide Surface Titration Data." *Geochimica et Cosmochimica Acta*. Vol. 61. pp. 2,801–2,826. 1997a.

Sahai, N. and D.A. Sverjensky. "Solvation and Electrostatic Model for Specific Electrolyte Adsorption." *Geochimica et Cosmochimica Acta*. Vol. 61. pp. 2,827–2,848. 1997b.

Sverjensky, D.A. and N. Sahai. "Theoretical Prediction of Single-Site Surface-Protonation Equilibrium Constants for Oxides and Silicates in Water." *Geochimica et Cosmochimica Acta*. Vol. 60. pp. 3,773–3,797. 1996.

Turner, D.R., R.T. Pabalan and F.P. Bertetti. "Neptunium(V) Sorption on Montmorillonite: An Experimental and Surface Complexation Modeling Study." *Clays and Clay Minerals*. Vol. 46. pp. 256–269. 1998.

Turner, D.R. and S.A. Sassman. "Approaches to Sorption Modeling for High-Level Waste Performance Assessment." *Journal of Contaminant Hydrology*. Vol. 21. pp. 311–332. 1996.

Turner G.D., J.M. Zachara, J.P. McKinley, and S.C. Smith. "Surface-Charge Properties and UO_2^{2+} Adsorption on a Surface Smectite." *Geochimica et Cosmochimica Acta*. Vol. 60. pp. 3,399–3,414. 1996.

Waite, T.D., J.A. Davis, B.R. Fenton, and T.E. Payne. "Approaches to Modelling Uranium(VI) Adsorption on Natural Mineral Assemblages." *Radiochimica Acta*. Vol. 88. pp. 687–693. 2000.

Wanner, H., Y. Albinsson, O. Karnl, E. Wieland, P. Wersin, and L. Charlet. "The Acid/Base Chemistry of Montmorillonite." *Radiochimica Acta*. Vols. 66 and 67. pp. 733–738. 1994.

Westall, J.C. and H. Hohl. "A Comparison of Electrostatic Models for the Oxide/Solution Interface." *Advances in Colloid and Interface Science*. Vol. 12. pp. 265–294. 1980.

Zavarin, M. and C.J. Bruton. "A Non-Electrostatic Surface Complexation Approach to Modeling Radionuclide Migration: The Role of Iron Oxides and Carbonate. UCRL–JC–133474. Livermore, California: Lawrence Livermore National Laboratory. 1999.

3.4 Molecular Dynamics Simulation of Uranium(VI) Sorption

Sorption experiments, such as those described in Section 2, provide useful information on the effects of solution chemistry and mineral sorbent properties on uranyl sorption behavior. However, these experiments study only the macroscopic aspects of the interaction of uranium

with the mineral surface and give no direct information on the structure and local chemical environment of the sorbed species. X-ray absorption spectroscopy, which includes x-ray absorption near-edge structure and extended x-ray absorption fine structure spectroscopy, is useful in directly probing the structure and oxidation state of sorbed metals. Some x-ray absorption spectroscopy results are presented in Section 2.3. Although x-ray absorption fine structure provides information on the number of oxygen atoms coordinated to the uranium atom and on uranium–oxygen interatomic distances, it does not determine directly whether the coordinating oxygen atom is contributed by a solvating water, by a hydroxide or carbonate ligand, or by a surface hydroxyl group. Also, because of the low solubility of uranium, particularly at near-neutral to alkaline pH, x-ray absorption fine structure analysis can be complicated by formation of oligomeric uranyl species or precipitation of a uranium solid when relatively high uranyl concentrations are used to enhance the x-ray signal.

Molecular simulation techniques can serve as a useful complement to sorption experiments and spectroscopic methods. The sorption behavior of specific uranyl species on different minerals can be studied directly through simulations of realistic models of molecular complexes and mineral surfaces. The complicating effects of oligomeric species formation and precipitation can be avoided by using a suitable number of molecular species in the simulation. This section describes the use of molecular simulations in a preliminary study of the sorption of uranyl species on a quartz surface. Quartz was selected as the sorbent for this study because it is a major rock-forming mineral in many geologic environments, it has a relatively simple composition, and experimental data are available on uranyl sorption on this mineral over wide ranges of uranium concentration, pH, and solid-mass to solution volume ratio.

The molecular simulation approach is detailed in Greathouse, et al. (2002). It comprised a comprehensive series of molecular dynamics simulations of aqueous uranyl complexes with OH^- and CO_3^{2-} in bulk water and near the quartz (010) surface. The OH^- and CO_3^{2-} anions are common components in natural waters, and CO_3^{2-} is likely a dominant anionic species in the groundwaters of Yucca Mountain, Nevada. The quartz (010) surface was chosen in this preliminary study with the goal of examining the effects of surface protonation and coordinating ligands on surface complexation and energy.

3.4.1 Computational Methods

The simulations were performed using the Open Force Field module of Cerius2 4.0 from Accelrys, Inc. (formerly Molecular Simulations, Inc.). The Crystal Builder module was used to create a 32-unit cell slab of α-quartz, and the Surface Builder module was used to create the (010) surface. The simulation supercell had *x* and *y* dimensions of 19.68 and 21.65 Å, respectively, corresponding to four unit cells of quartz in each direction. The quartz slab was approximately 2 unit cells (ca. 8 Å) in depth and consisted of 80 silicon atoms and 160 oxygen atoms. The quartz slab was terminated with hydrogen atoms (upper surface) and hydroxyl groups (lower surface), resulting in two singly protonated surfaces (336 atoms). The *z* dimension of the supercell was fixed at 32.00 Å to allow room for water molecules and aqueous species (UO_2^{2+}, CO_3^{2-}, and OH^-).

To examine uranyl adsorption near deprotonated surface oxygen atoms, a partially deprotonated surface was created by moving protons from a cluster of six surface hydroxyl groups to distant hydroxyl groups. Potential parameters for aqueous species were based on the Consistent-Valence Forcefield, which employs the flexible version of the Simple Point Charge water model. Intramolecular motion (bond stretching and angle bending) was allowed for all aqueous species and for hydroxyl groups at the upper quartz surface. The remainder of the

quartz surface was held rigid throughout the simulations. The potential energy component for nonbonded interactions consisted of Coulombic and van der Waals terms between atoms *i* and *j* at a separation of *r*. The potential energy term for bonded interactions consisted of angle-bending and bond-stretching terms. Other than the quartz slab, which was treated as a rigid body, no species contained more than three atoms bonded in a chain; hence, a torsional term was not used.

For simulations in bulk solution, a cubic supercell with an 18.2-Å edge length containing 200 water molecules and the necessary ionic species was used. All hydrated slab simulations were conducted with 300 water molecules. Three-dimensional periodic boundary conditions were applied to the supercell in all simulations, resulting in either a bulk solution or macroscopic quartz–water system.

Before beginning a molecular dynamics simulation, the local water structure around the ions and the quartz surface was optimized for at least 500 steps using the OFF Minimizer module of Cerius2. After minimization, the uranyl ion had already formed its primary coordination shell. Molecular dynamics simulations were performed using the OFF Dynamics module of Cerius2 in the constant (*NVT*) ensemble with the Nosé-Hoover thermostat. Temperature was set to 300 K with a 0.1-ps relaxation time, although an average temperature of approximately 298 K was achieved in most simulations. A cutoff of 9 Å was used for short-range interactions, and Coulombic interactions were treated using the three-dimensional Ewald sum. Total simulation times were 100 ps with a timestep of 0.0005 ps.

Equilibration was achieved after 10–20 ps, as determined by monitoring running averages and fluctuations in the potential energy and temperature. Equilibrium average values for potential energy and temperature were obtained, and the (*x*, *y*, *z*) trajectories of water molecules and aqueous species were plotted. Radial distribution functions were obtained in the usual manner (Allen and Tildesley, 1987) and were itemized according to either forcefield atom types (uranium–oxygen$_w$) or by element type (uranium–oxygen). This approach allowed the components of the uranium–oxygen radial distribution functions peaks due to water oxygen atoms, surface oxygen atoms, or anion oxygen atoms to be distinguished.

3.4.2 Results and Discussion

Results for simulations in bulk solution are presented in Table 3.4-1. The equilibrium coordination shell for $[UO_2(H_2O)_5]^{2+}$ consisted of five water molecules in a pentagonal bipyramidal geometry, with uranyl oxygen atoms in the axial positions. Figure 3.4-1 shows the uranium–oxygen and uranium–hydrogen radial distribution functions averaged over the equilibrium portion of the simulation. The uranium–oxygen radial distribution functions contain two peaks, one corresponding to the primary solvation shell at 2.49 Å and a second broader peak at 4.85 Å. This average uranium–oxygen$_w$ distance of 2.49 Å agrees well with the experimental value of 2.42 Å, obtained from proton nuclear magnetic resonance and x-ray diffraction experiments (Aberg, et al., 1983).

Averaged uranium–oxygen radial distribution functions for simulations of hydroxide and carbonate complexes (OH^- or CO_3^{2-}) are shown in Figure 3.4-2(a), with peak distances tabulated in Table 3.4-1. The presence of OH^- or CO_3^{2-} in the uranyl complex results in a split equatorial shell about the uranium atom, with oxygen atoms from OH^- or CO_3^{2-} occupying positions closer than water oxygen atoms. For the uranyl hydroxy complexes, the calculated uranium–oxygen–hydrogen distances are consistent with gas-phase *ab initio* calculations of the complex $[UO_2(H_2O)(OH)_4]^{2-}$, which gave U–OH and U–O$_w$ distances of 2.43–2.47 Å and 2.65 Å,

respectively (Wahlgren, et al., 1999). The equatorial uranium–oxygen–hydrogen distances are also in agreement with recent extended x-ray absorption fine structure experiments of UO_2^{2+} in aqueous tetramethylammonium hydroxide solution, in which the uranium–oxygen–hydrogen distance was measured to be 2.22 Å and 2.24 Å (Clark, et al., 1999; Wahlgren, et al., 1999).

Carbonate ions formed bidentate complexes with uranium, and a similar equatorial splitting was seen [Figure 3.4-2(a) and Table 3.4-1]. No experimental or *ab initio* results for the aqueous carbonate complexes studied here were available for comparison. However, the tricarbonato complex, $[UO_2(CO_3)_3]^{4-}$, has been studied. Recent extended x-ray absorption fine structure experiments show the uranium–oxygen(carbonate) distance to be 2.42 Å for $[UO_2(CO_3)_3]^{4-}$ in the solid phase and 2.46 Å for the trimeric form, $[(UO_2)_3(CO_3)_6]^{6-}$, in aqueous solution (Allen, et al., 1995). Gas-phase calculations on $[UO_2(CO_3)_3]^{4-}$ show this length to be 2.58 Å. For both the hydroxy and carbonato complexes, the simulation results show equatorial uranium–oxygen distances in much better agreement with experiments than gas-phase quantum mechanical calculations, indicating that perhaps the presence of surrounding solvent molecules is key when performing calculations of aqueous uranyl complexes.

Singly Protonated Surface. Simulations performed with the singly protonated quartz (010) surface are summarized in Figure 3.4-2(b) and Table 3.4-2. A model of the quartz–water interface initially was tested with a simulation supercell constructed with 300 water molecules. An equilibrium snapshot of this supercell is shown in Figure 3.4-3. To investigate uranyl adsorption onto the quartz (010) surface, a single uranyl ion was added to the 300-water supercell, at an initial uranium-surface distance of 6 Å. The equilibrated structure [Figure 3.4-4(a)] indicates that the uranyl ion maintained its five fold water solvation shell while forming an outer-sphere surface complex with quartz. As seen in Figure 3.4-4(b), the uranyl oxygen–uranium–oxygen axis maintained an angle of approximately 45 °C [113 °F] to the surface normal. The average uranium–$oxygen_w$ distance of 2.51 Å (Table 3.4-2) indicates that the first coordination shell geometry of UO_2^{2+} is the same near the quartz surface as in bulk water.

Simulations in the presence of carbonate and hydroxide ions also were performed, with the carbonate or hydroxide ions initially placed in close proximity to the uranyl ion. For the hydroxide ion, separate simulations were performed with a single UO_2^{2+} ion with one, two, or three OH^- in the aqueous layer. In all cases, the uranyl ion maintained a fivefold coordination shell, thus forming outer-sphere complexes with the singly protonated quartz surface. As with simulations in the bulk, the presence of OH^- or CO_3^{2-} is indicated by a split in the equatorial shell [Figure 3.4-2(b) and Table 3.4-2]. The averaged uranium–oxygen distances are nearly identical to those in bulk solution, indicating that the singly protonated surface has little effect on the uranyl coordination geometry.

Deprotonated Surface. Results for simulations of UO_2^{2+} sorption near a partially deprotonated quartz surface are summarized in Figure 3.4-2(c) and Table 3.4-3. In the initial simulation of water near this surface, the oxygen–oxygen and oxygen–hydrogen radial distribution function peaks were identical to those values from the singly protonated surface. Next, a uranyl ion was placed near the partially deprotonated surface (at 4.0 or 2.50 Å distance). The uranyl ion maintained its fivefold water solvation shell and never formed an inner-sphere surface complex. The radial distribution function data showed an average uranium–oxygen distance of 2.50 Å with five water oxygen atoms occupying the first solvation shell. Only when the uranyl ion was initially placed at a distance of 2.0 Å from the quartz surface did an inner-sphere surface complex form. As Table 3.4-3 indicates, the resulting surface complex, $\{UO_2(H_2O)_4[O]^{2+}\}$, had an average uranium–oxygen distance of 2.50 Å. Here the notation [O] is used to indicate the

presence of surface oxygen atoms in the equatorial shell of uranium. The availability of deprotonated surface oxygen atoms appears to be a prerequisite for the formation of inner-sphere uranyl surface complexes. However, the results indicate that such surface complexes form only when the initial uranium–surface distance was less than 2.0 Å. In addition, the results show only a single equatorial shell for this adsorbed species, in contrast to the split equatorial shell suggested by extended x-ray absorption fine structure results of the uranyl ion adsorbed to silica surfaces (Reich, et al., 1996; Sylwester, et al., 2000). Again, such a split equatorial shell is observed in our simulations only when another ligand (OH^- or CO_3^{2-}) is present in the equatorial shell of UO_2^{2+}.

With one or two hydroxide ions coordinated to the uranium atom, inner-sphere surface complexes also formed, but only when the uranyl species was placed within 2.0 Å of the surface, with no water molecules in between. Figure 3.4-5(a) shows an equilibrium snapshot of the $[(UO_2)(H_2O)(OH)_2\{O\}_2]$ surface complex.

With carbonate ions in the simulation supercell, an inner-sphere surface complex formed when only one ion was coordinated to UO_2^{2+}, and only with monodentate surface coordination. Such a surface complex is shown in Figure 3.4-5(b), with CO_3^{2-} oriented such that hydrogen bonding occurs between one carbonate oxygen atom and surface protons. Table 3.4-3 indicates the presence of a split equatorial shell, consisting of an inner peak of carbonate oxygen atoms and an outer peak of water and surface oxygen atoms. The dicarbonato complex $[UO_2(H_2O)(CO_3)_2]^{2-}$, with each carbonate ion acting as a bidentate ligand, never formed an inner-sphere surface complex but remained anchored to the surface via hydrogen bonding between the coordinating water molecule and the surface. For the dicarbonato complex, average uranium–$oxygen_L$ and uranium–$oxygen_w$ distances are similar to those for the singly protonated surface.

3.4.3 Conclusions

The range of possible uranyl orientations and motion relative to the quartz surface is summarized in Figure 3.4-6, which shows the trajectory of the *z* coordinate of a uranium atom from three simulations. Near the partially deprotonated surface, the uranyl ion forms an inner-sphere complex involving one or two surface oxygen atoms. The uranium atom is fastened to the surface, as evidenced by the limited motion in the *z* direction. Near the singly protonated surface, the uranyl ion forms an outer-sphere complex with hydrogen bonding between a coordinated water molecule and the surface [Figure 3.4-4(a)]. As a result, the fully solvated ion hovers approximately 5 Å above the surface. Finally, a layer of nonsolvating water molecules can be interposed between a uranyl complex and the surface, resulting in a diffuse species. A diffuse uranyl complex is characterized by increased mobility relative to the surface, as seen in Figure 3.4-6. Two mechanisms exist for the formation of stable uranyl surface complexes. First, a uranyl ion coordinated by water molecules and/or anion ligands can form an outer-sphere surface complex, in which a solvating water molecule is hydrogen bonded to a surface oxygen atom. This arrangement results in a uranium–silicon distance of approximately 6 Å (Table 3.4-2). Second, a uranyl ion can form an inner-sphere surface complex, via either monodentate or bidentate coordination to surface oxygen atom(s). The average uranium–silicon distance in this case is approximately 4 Å (Table 3.4-3). The combination of inner-sphere surface complexation between the uranium and surface oxygen atoms and additional hydrogen bonding between solvating oxygen atoms and surface protons results in an immobile surface complex. However, due to difficulties in adequate phase space sampling, inner-sphere surface complexes were not seen in the simulations unless the uranyl ion was initially placed less than 2.0 Å from the surface with no interposing water molecules.

3.4.4 References (Section 3.4)

Aberg, M., D. Ferri, J. Glaser, and I. Grenthe. "Structure of the Hydrated Eioxouranium(VI) Ion in Aqueous Solution. An X-ray Diffraction and ^{1}H NMR Study." *Inorganic Chemistry*. Vol. 22. pp. 3,986–3,989. 1983.

Allen, M. P. and D.J. Tildesley. *Computer Simulation of Liquids*. Oxford, England: Clarendon Press. 1987.

Allen, P.G., J.J. Bucher, D.L. Clark, N.M. Edelstein, S.A. Ekberg, J.W. Gohdes, E.A. Hudson, N. Kaltsoyannis, W.W. Lukens, M.P. Neu, P.D. Palmer, T. Reich, D.K. Shuh, C.D. Tait, and B.D. Zwick. "Multinuclear NMR, Raman, EXAFS, and X-ray Diffraction Studies of Uranyl Carbonate Complexes in Near-Neutral Aqueous Solution: X-ray Structure of $[C(NH_2)_3]_6[(UO_2)_3(CO_3)_6]\cdot 6.5H_2O$." *Inorganic Chemistry*. Vol. 34. pp. 4,797–4,807. 1995.

Clark, D.L., S.D. Conradson, R.J. Donohoe, D.W. Keogh, D.E. Morris, P.D. Palmer, R.D. Rogers, and C.D. Tait. "Chemical Speciation of the Uranyl ion Under Highly Alkaline Conditions: Synthesis, Structures, and Oxo Ligand Exchange Dynamics." *Inorganic Chemistry*. Vol. 38. pp. 1,456–1,466. 1999.

Greathouse, J.A., R.J. O'Brien, G. Bemis, and R.T. Pabalan. "Molecular Dynamics Study of Aqueous Uranyl Interactions With Quartz (010)." *Journal of Physical Chemistry B*. Vol. 106. pp. 1,646–1,655. 2002.

Reich, T., H. Moll, M.A. Denecke, G. Geipel, G. Bernhard, and H. Nitsche. "Characterization of Hydrous Uranyl Silicate by EXAFS." *Radiochimica Acta*. Vol. 74. pp. 219–223. 1996.

Sylwester, E. R., E. A. Hudson, and P.G. Allen. "The Structure of Uranium(VI) Sorption Complexes on Silica, Alumina, and Montmorillonite." *Geochimica et Cosmochimica Acta*. Vol. 64. pp. 2,431–2,438. 2000.

Wahlgren, U., H. Moll, I. Grenthe, B. Schimmelpfennig, L. Maron, V. Vallet, and O. Gropen. "Structure of Uranium(VI) in Strong Alkaline Solutions: A Combined Theoretical and Experimental Investigation." *Journal of Physical Chemistry A*. Vol. 103. pp. 8,257–8,264. 1999.

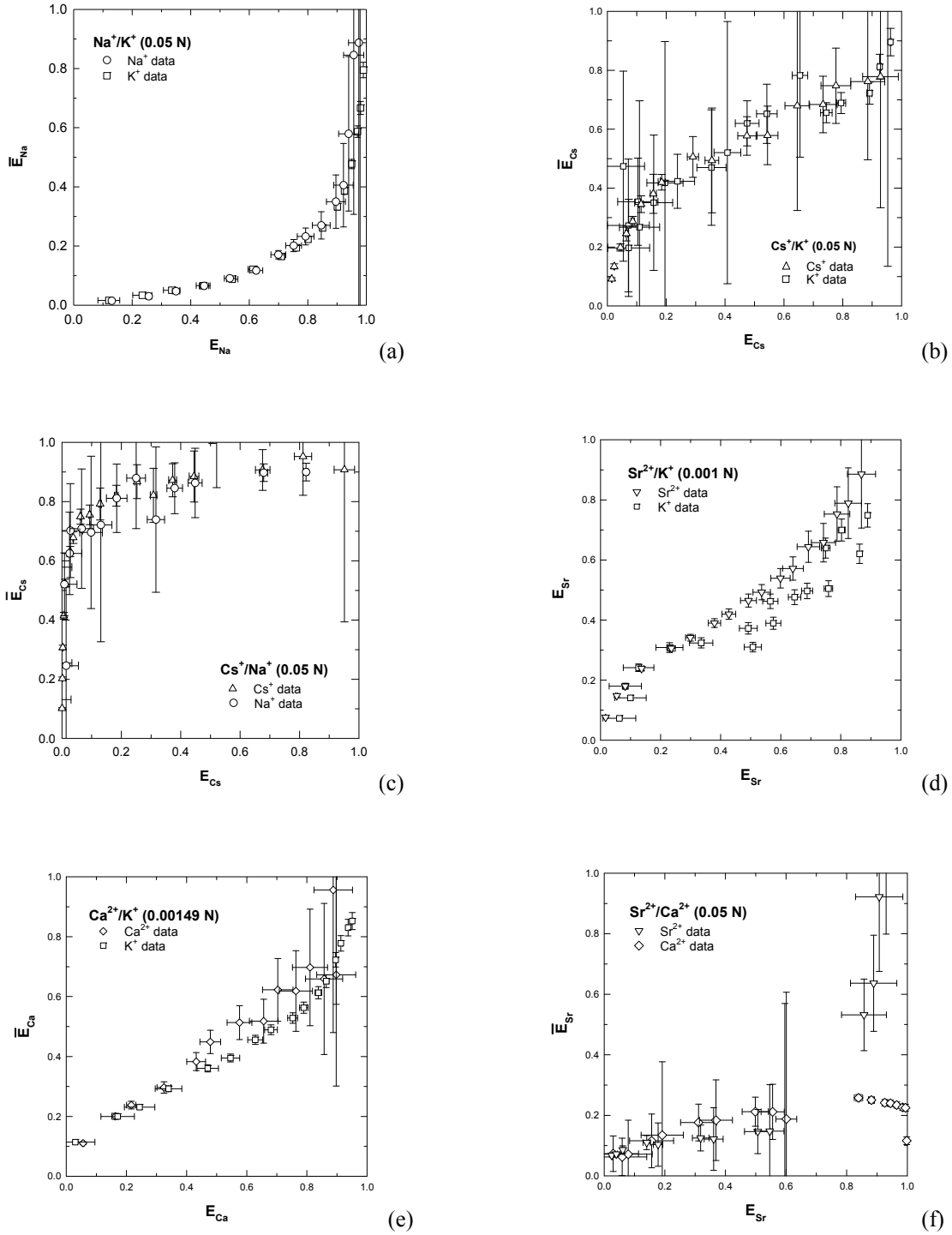

Figure 3.2-1. Experimental Data for Ion Exchange Between Clinoptilolite and Aqueous Solutions of (a) Na^++K^+, (b) Cs^++K^+, (c) Cs^++Na^+, (d) Sr^{2+}+K^+, (e) Ca^{2+}+K^+, and (f) Sr^{2+}+Ca^{2+}

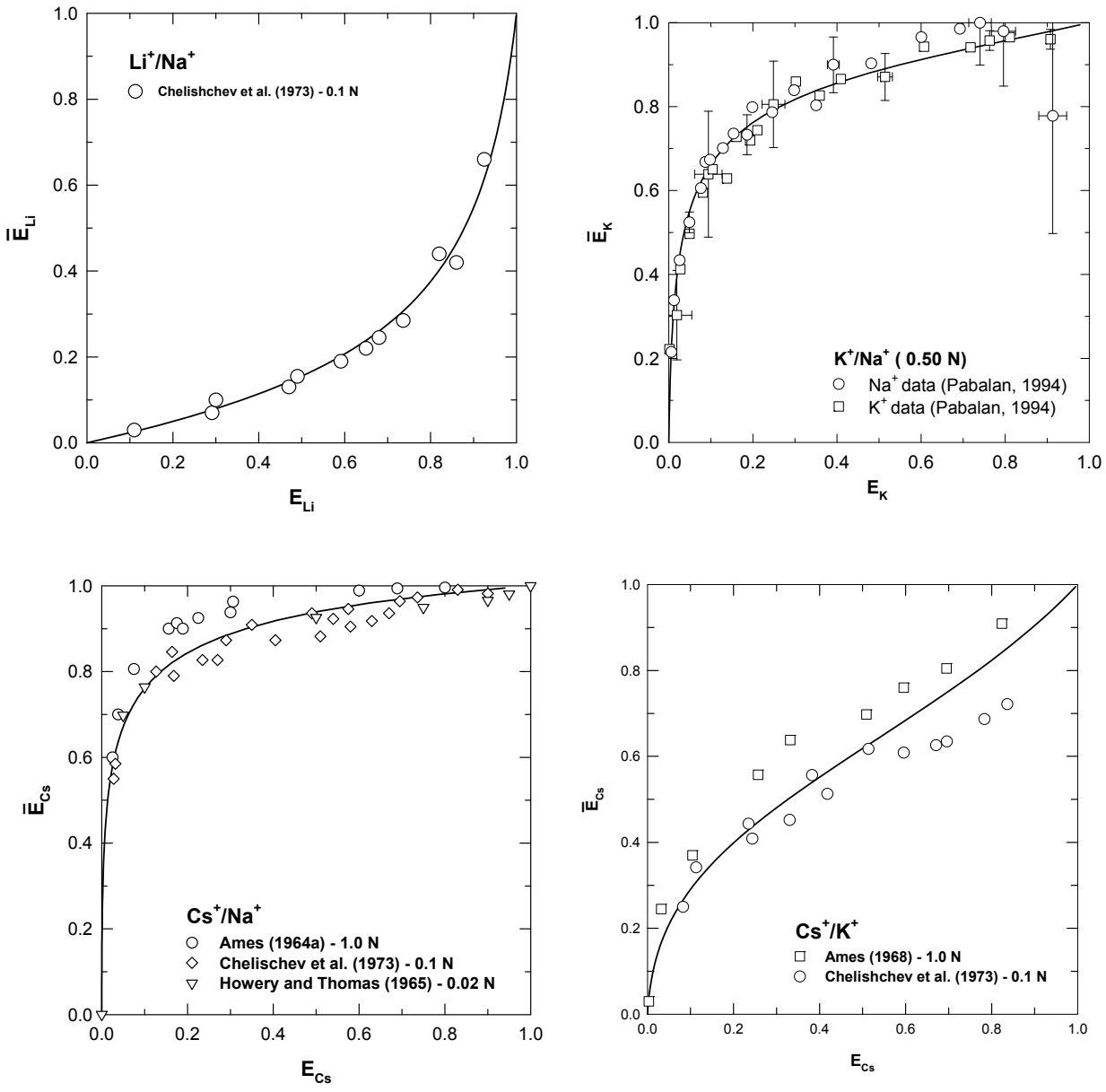

Figure 3.2-2. Comparison of Experimental Data on Ion Exchange Involving Clinoptilolite and Aqueous Solutions of Li^+/Na^+, K^+/Na^+, Cs^+/Na^+, and Cs^+/K^+ With Isotherms (Solid Curve) Calculated Using the Wilson Model. The Model Used Parameters Derived From Regressing the Vanselow Selectivity Coefficients Calculated From the Ion-Exchange Data to Eqs. (3.2-14) to (3.2-16). R^2 Values Derived From Fitting Vanselow Selectivity Coefficients for the Systems Li^+/Na^+, K^+/Na^+, Cs^+/Na^+, and Cs^+/K^+ Are 0.45, 0.92, 0.15, and 0.49, Respectively.

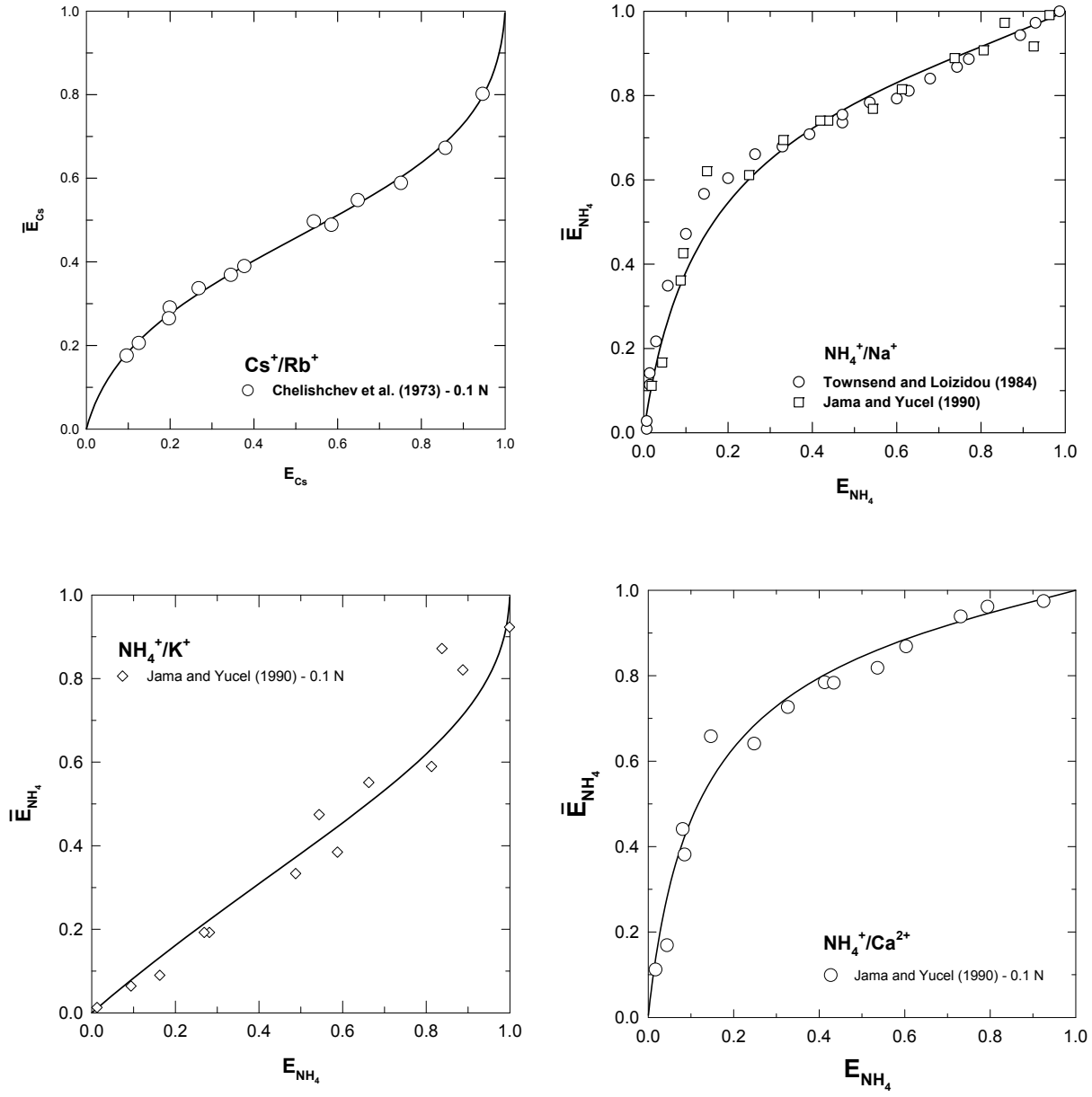

Figure 3.2-3. Comparison of Experimental Data on Ion Exchange Involving Clinoptilolite and Aqueous Solutions of Cs^+/Rb^+, NH_4^+/Na^+, NH_4^+/K^+, and NH_4^+/Ca^{2+} With Isotherms (Solid Curve) Calculated Using the Wilson Model. The Model Used Parameters Derived From Regressing the Vanselow Selectivity Coefficients Calculated From the Ion-Exchange Data to Eqs. (3.2-14) to (3.2-16). R^2 Values Derived From Fitting Vanselow Selectivity Coefficients for the Systems Cs^+/Rb^+, NH_4^+/Na^+, NH_4^+/K^+, and NH_4^+/Ca^{2+} Are 0.98, 0.32, 0.29, and 0.78, Respectively.

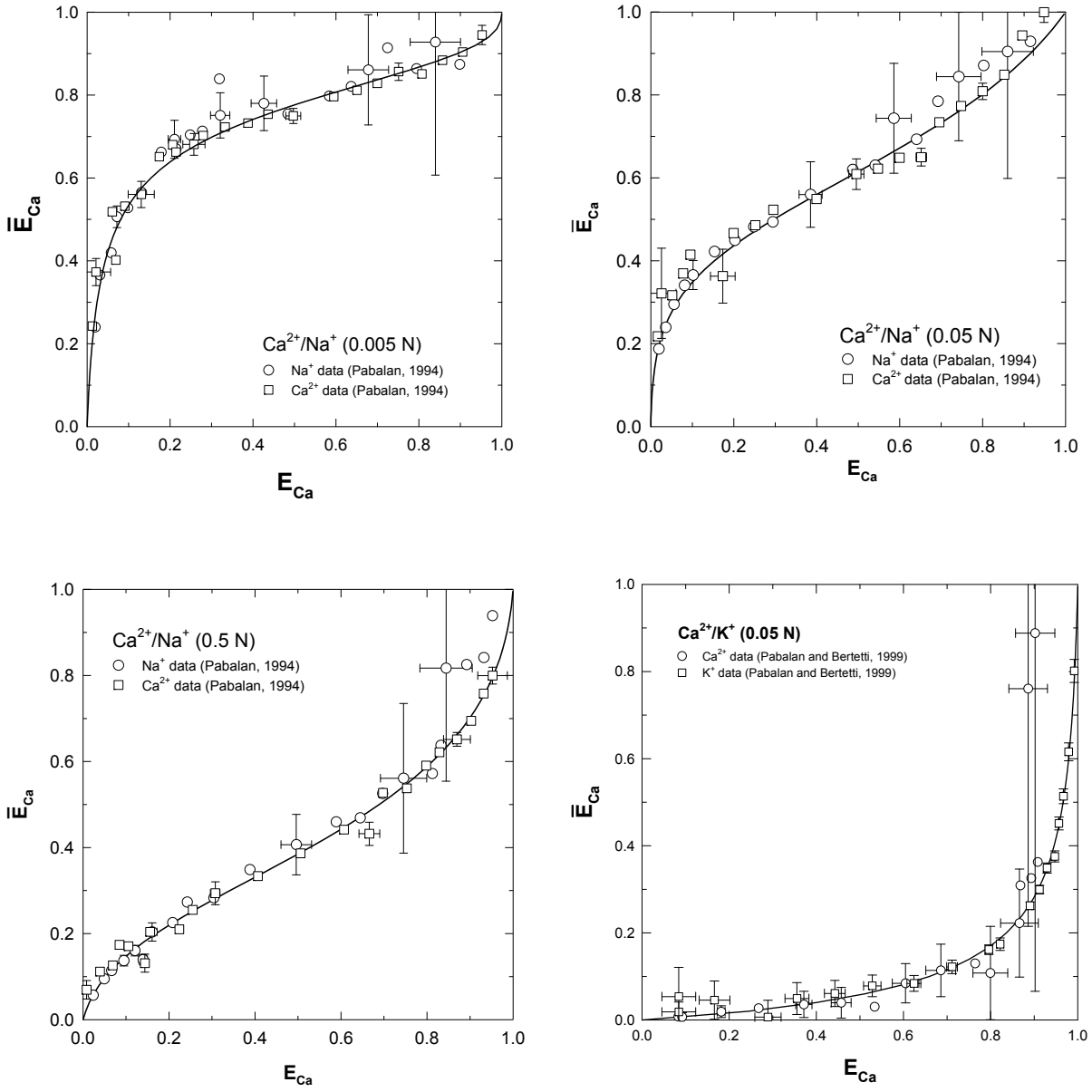

Figure 3.2-4. Comparison of Experimental Data on Ion Exchange Involving Clinoptilolite and Aqueous Solutions of 0.005 N Ca^{2+}/Na^{+}, 0.05 N Ca^{2+}/Na^{+}, 0.5 N Ca^{2+}/Na^{+}, and 0.05 N Ca^{2+}/K^{+} With Isotherms (Solid Curve) Calculated Using the Wilson Model. The Model Used Parameters Derived From Regressing the Vanselow Selectivity Coefficients Calculated From the Ion-Exchange Data to Eqs. (3.2-14) to (3.2-16). R^2 Values Derived From Fitting Vanselow Selectivity Coefficients for the Systems 0.005 N Ca^{2+}/Na^{+}, 0.05 N Ca^{2+}/Na^{+}, 0.5 N Ca^{2+}/Na^{+}, And 0.05 N Ca^{2+}/K^{+} Are 0.68, 0.95, 0.98, and 0.95, Respectively.

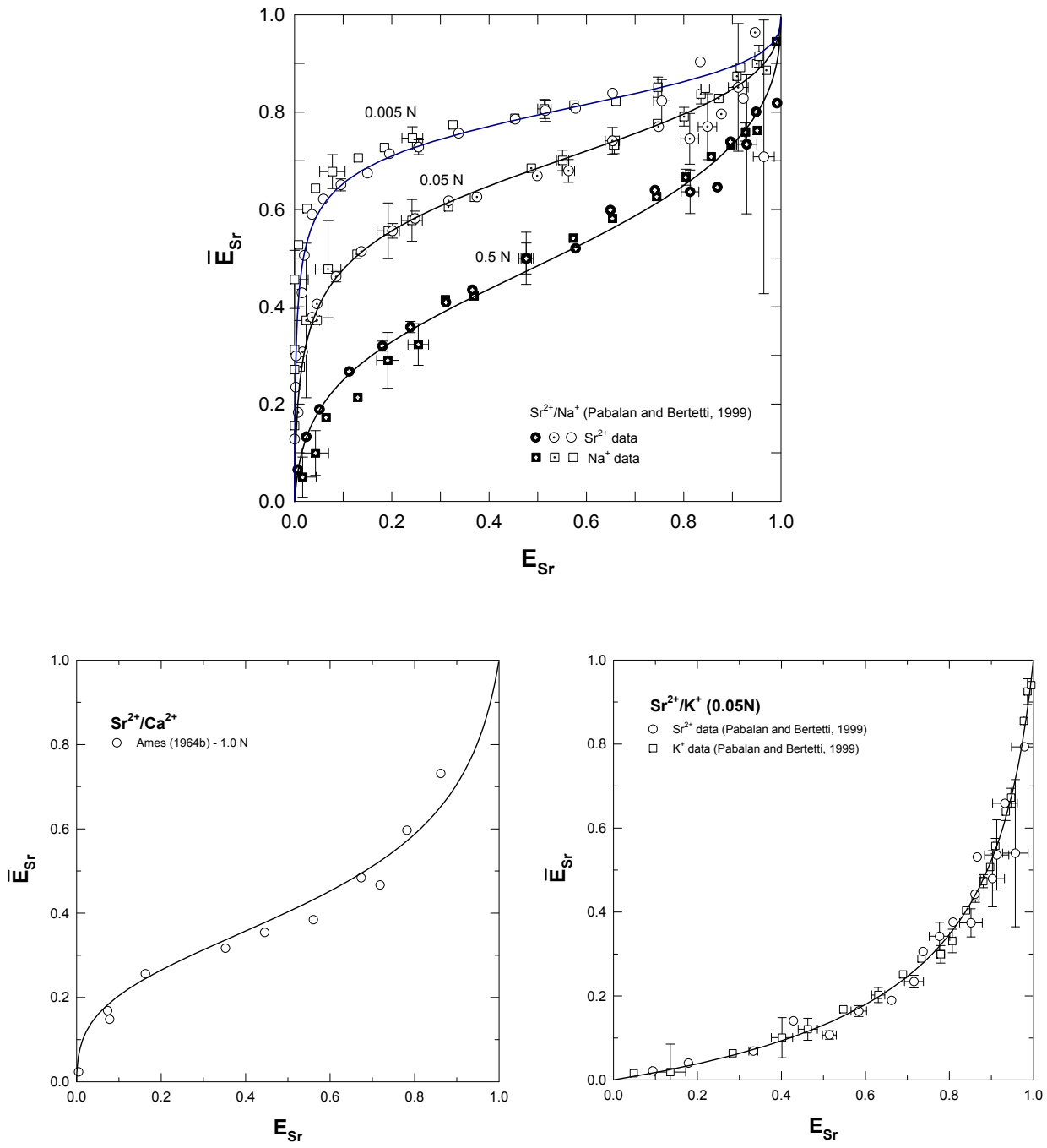

Figure 3.2-5. Comparison of Experimental Data on Ion Exchange Involving Clinoptilolite and Aqueous Solutions of 0.005 N Sr^{2+}/Na^{+}, 0.05 N Sr^{2+}/Na^{+}, 0.5 N Sr^{2+}/Na^{+}, 1.0 N Sr^{2+}/Ca^{2+}, and 0.05 N Sr^{2+}/K^{+} With Isotherms (Solid Curve) Calculated Using the Wilson Model. The Model Used Parameters Derived From Regressing the Vanselow Selectivity Coefficients Calculated From the Ion-Exchange Data to Eqs (3.2-14) to (3.2-16). R^2 Values Derived From Fitting Vanselow Selectivity Coefficients for the Systems Sr^{2+}/Na^{+} (0.005, 0.05, and 0.05 N), 1.0 N Sr^{2+}/Ca^{2+}, and 0.05 N Sr^{2+}/K^{+} Are 0.68, 90, and 0.88, Respectively.

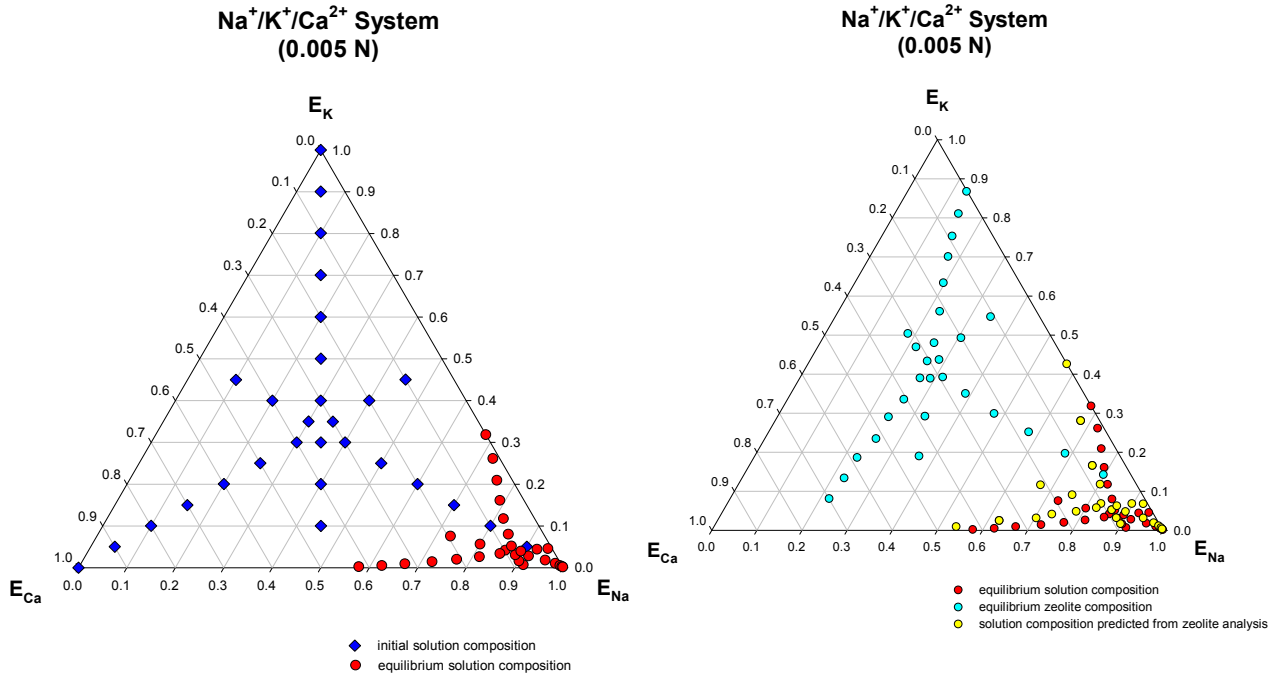

(a) (b)

Figure 3.2-6. (a) Initial and Equilibrium Solution Compositions in the 0.005 N $Na^+/K^+/Ca^{2+}$ System. (b) Solution and Zeolite Compositions at Equilibrium in the 0.005 N $Na^+/K^+/Ca^{2+}$ System. Also Shown in (b) Are the Solution Compositions Predicted From the Thermodynamic Model, Using As Input Values the Measured Equilibrium Zeolite Compositions.

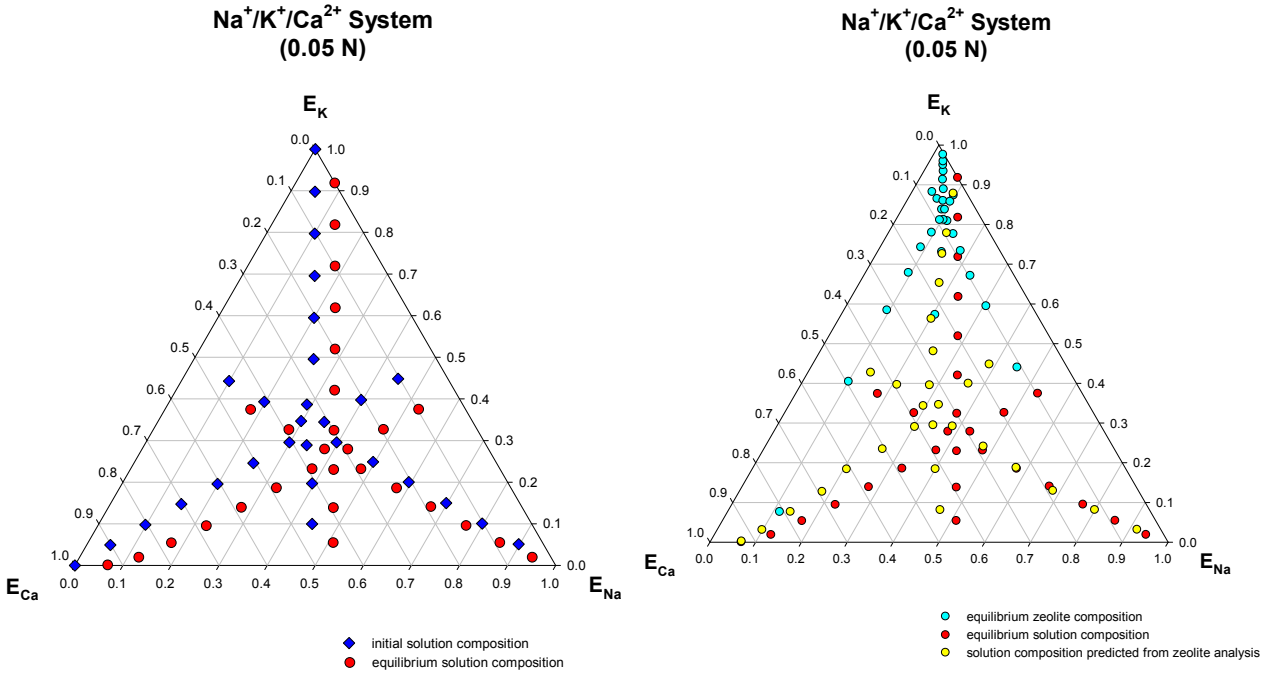

Figure 3.2-7. (a) Initial and Equilibrium Solution Compositions in the 0.05 N $Na^+/K^+/Ca^{2+}$ System. (b) Solution and Zeolite Compositions at Equilibrium in the 0.05 N $Na^+/K^+/Ca^{2+}$ System. Also Shown in (b) Are the Solution Compositions Predicted From the Thermodynamic Model, Using as Input Values the Measured Equilibrium Zeolite Compositions.

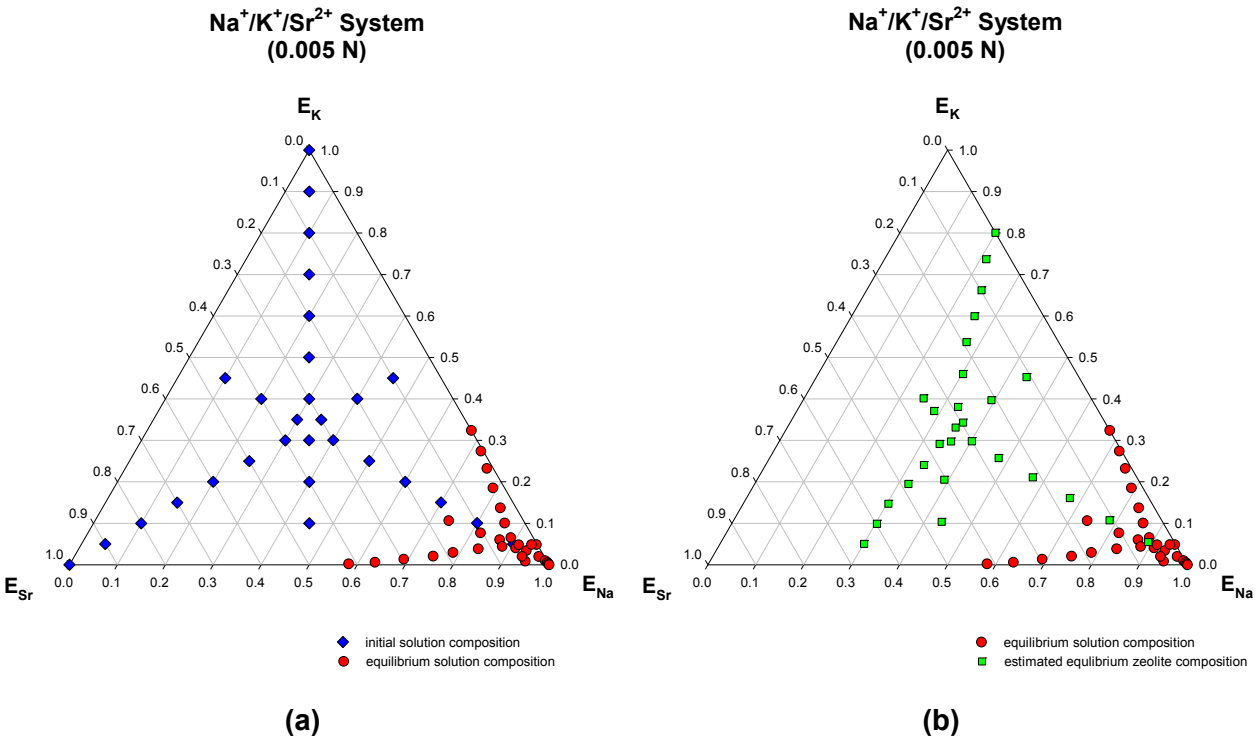

Figure 3.2-8. (a) Initial and Equilibrium Solution Compositions in the 0.005 N $Na^+/K^+/Sr^{2+}$ System. (b) Equilibrium Solution Compositions (Red Circles) in the 0.005 N $Na^+/K^+/Sr^{2+}$ System. No Zeolite Samples That Equilibrated With the Aqueous Phase Were Analyzed. The Estimated Zeolite Compositions at Equilibrium Plotted as Green Squares Were Calculated From the Initial and Final Concentrations of Na^+, K^+, and Sr^{2+} in the Aqueous Phase.

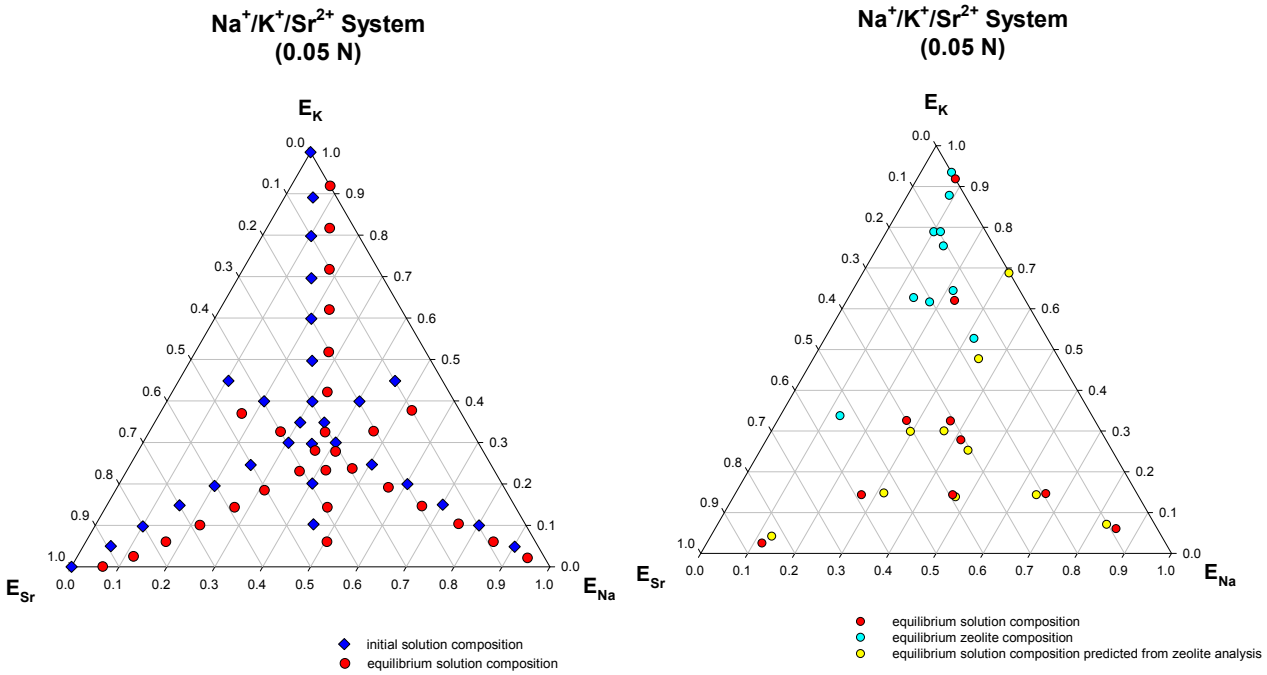

Figure 3.2-9. (a) Initial and Equilibrium Solution Compositions in the 0.05 N $Na^+/K^+/Sr^{2+}$ System. (b) Solution and Zeolite Compositions at Equilibrium in the 0.05 N $Na^+/K^+/Sr^{2+}$ System. Also Shown in (b) Are the Solution Compositions Predicted From the Thermodynamic Model, Using As Input Values the Measured Equilibrium Zeolite Compositions. Only Selected Zeolite Samples Were Analyzed, Thus the Data Points for Equilibrium Zeolite Compositions Are Fewer Than the Data Points for Initial and Equilibrium Solution Compositions Shown in Figure 3.2-9(a).

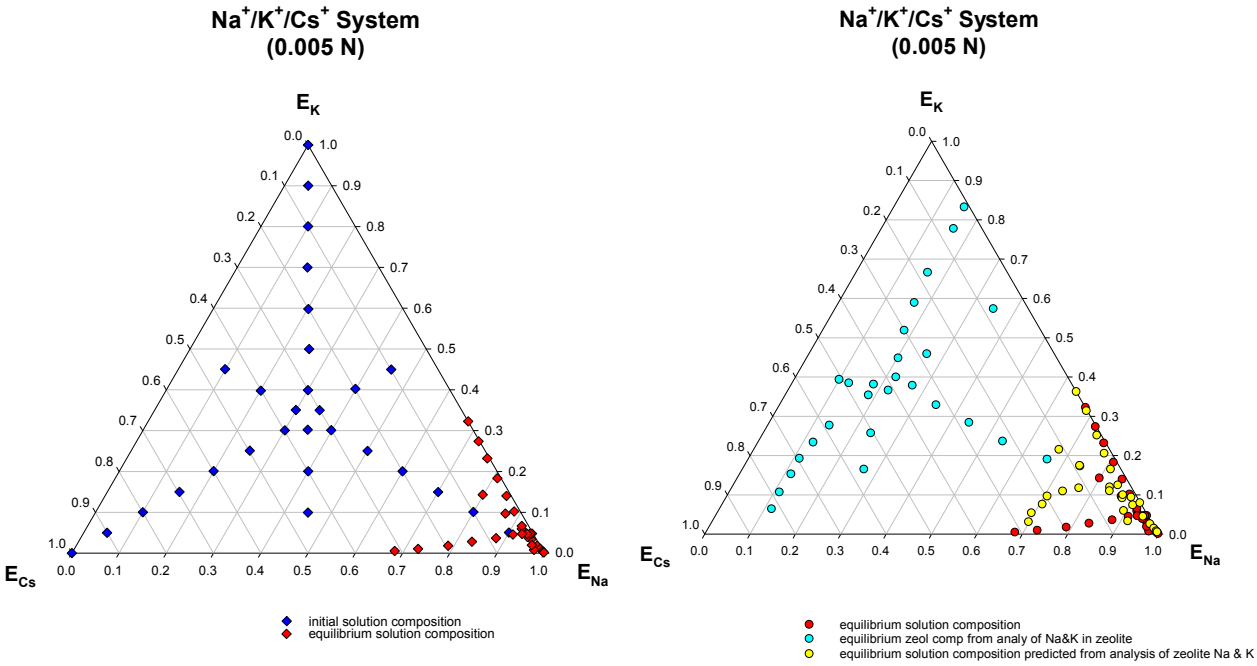

(a) (b)

Figure 3.2-10. (a) Initial and Equilibrium Solution Compositions in the 0.005 N $Na^+/K^+/Cs^+$ System. (b) Solution and Zeolite Compositions at Equilibrium in the 0.005 N $Na^+/K^+/Cs^+$ System. Also Shown in (b) Are the Solution Compositions Predicted From the Thermodynamic Model, Using as Input Values the Estimated Equilibrium Zeolite Compositions.

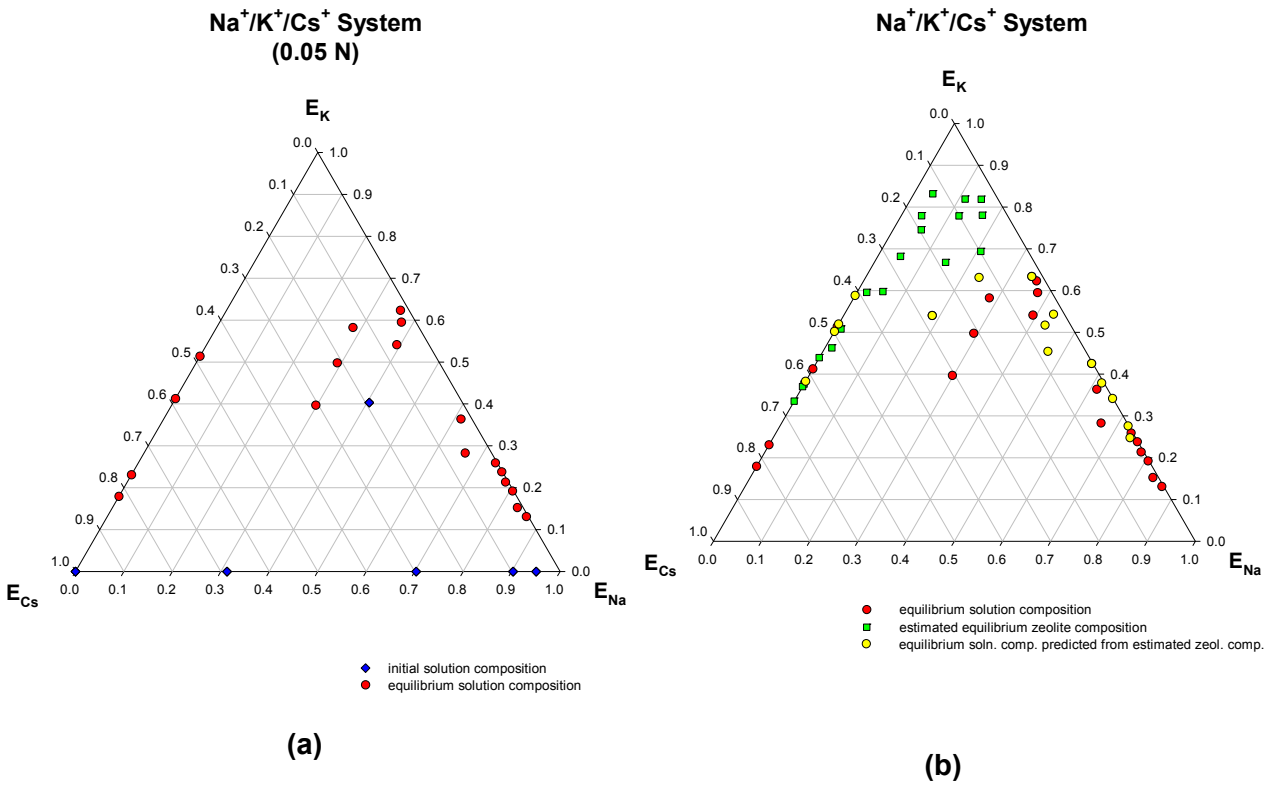

Figure 3.2-11. (a) Initial and Equilibrium Solution Compositions in the 0.05 N $Na^+/K^+/Cs^+$ System. (b) Solution and Zeolite Compositions at Equilibrium in the 0.05 N $Na^+/K^+/Cs^+$ System. Also Shown in (b) Are the Solution Compositions Predicted From the Thermodynamic Model, Using as Input Values the Estimated Equilibrium Zeolite Compositions.

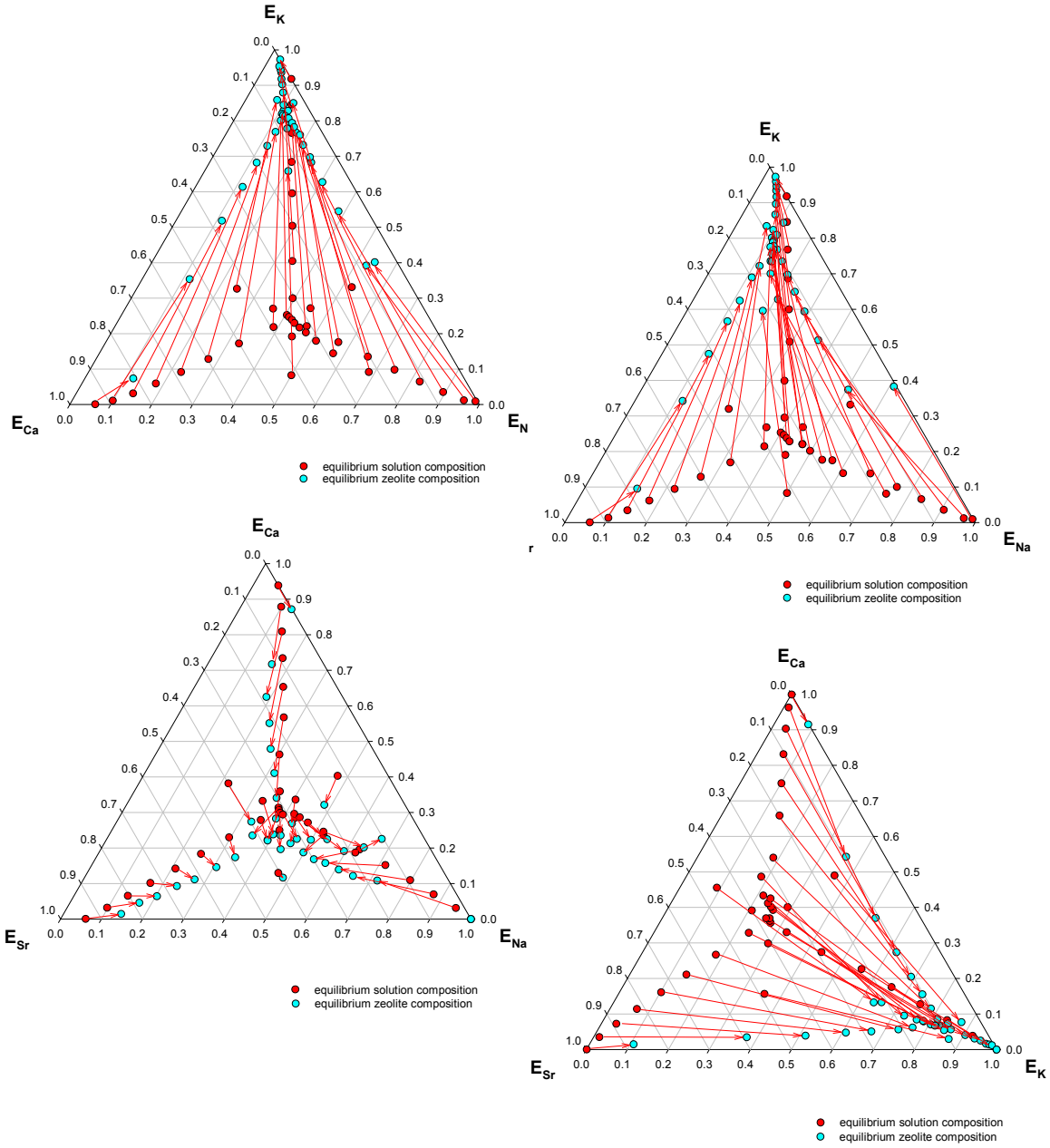

Figure 3.2-12. Solution and Zeolite Compositions at Equilibrium in the Quaternary $Na^{+}/K^{+}/Ca^{2+}/Sr^{2+}$ System at 0.05 N. Tie-Lines Connect Corresponding Zeolite and Aqueous Samples.

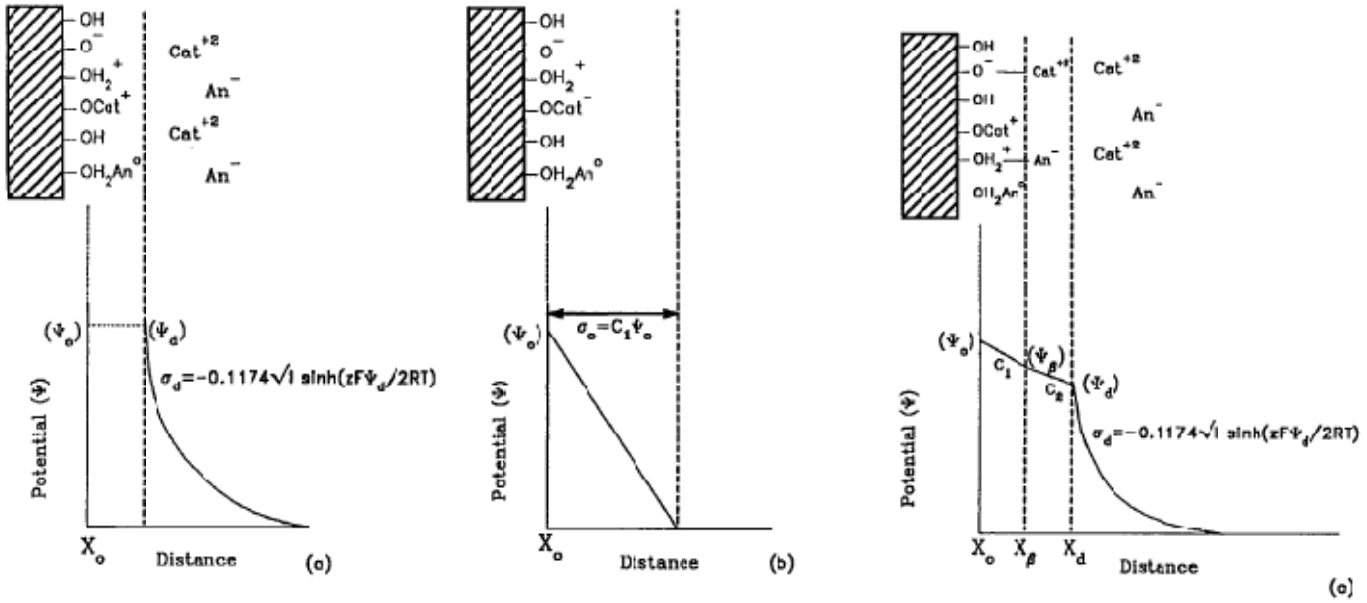

Figure 3.3-1 Schematic Diagram of the Mineral-Water Interface as Represented in Different Surface Complexation Modeling Approaches. (a) Diffuse-Layer Model, (b) Constant Capacitance Model, and (c) Triple Layer Model. (Modified from Hayes, et al., 1991).

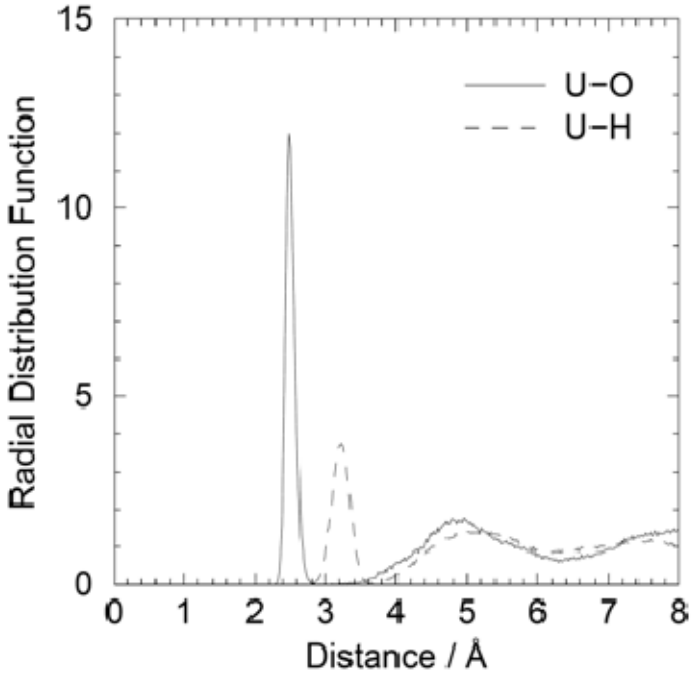

Figure 3.4-1. Plots of the U–O (Solid Line) and U–H (Dashed Line) Radial Distribution Functions From a Simulation of UO_2^{2+} in a Box of 200 Water Molecules. The Peak Due To Axial Oxygen Atoms in UO_2^{2+} Is Not Shown. Reproduced With Permission From Greathouse, J.A., R.J. O'Brien, G. Bemis, and R.T. Pabalan. *Journal of Physical Chemistry B.* Vol. 106. p. 1,646. 2002. Copyright 2002. American Chemical Society.

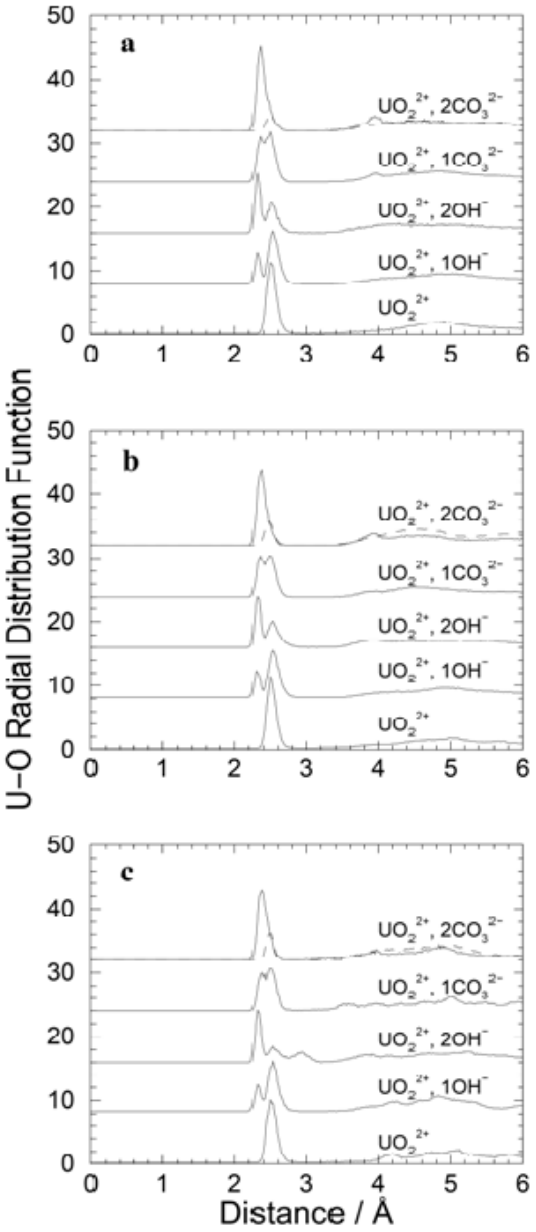

Figure 3.4-2. Plots of the U–O Radial Distribution Functions From Simulations in (a) Bulk Solution, (b) Singly Protonated Quartz (010) Surface, and (c) Partially Deprotonated Quartz (010) Surface. Ionic Species in the Aqueous Layer Are Indicated Next to Each Plot. Peaks Are Assigned in Tables 3.4-2 through 3.4-4. For the Results With 1 UO_2^{2+} and 2 CO_3^{2-}, the Dashed Line Represents the U–O_w Distribution (O_w = Water Oxygen). Reproduced With Permission From Greathouse, J.A., R.J. O'Brien, G. Bemis, and R.T. Pabalan. *Journal of Physical Chemistry B.* Vol. 106. p. 1,646. 2002. Copyright 2002. American Chemical Society.

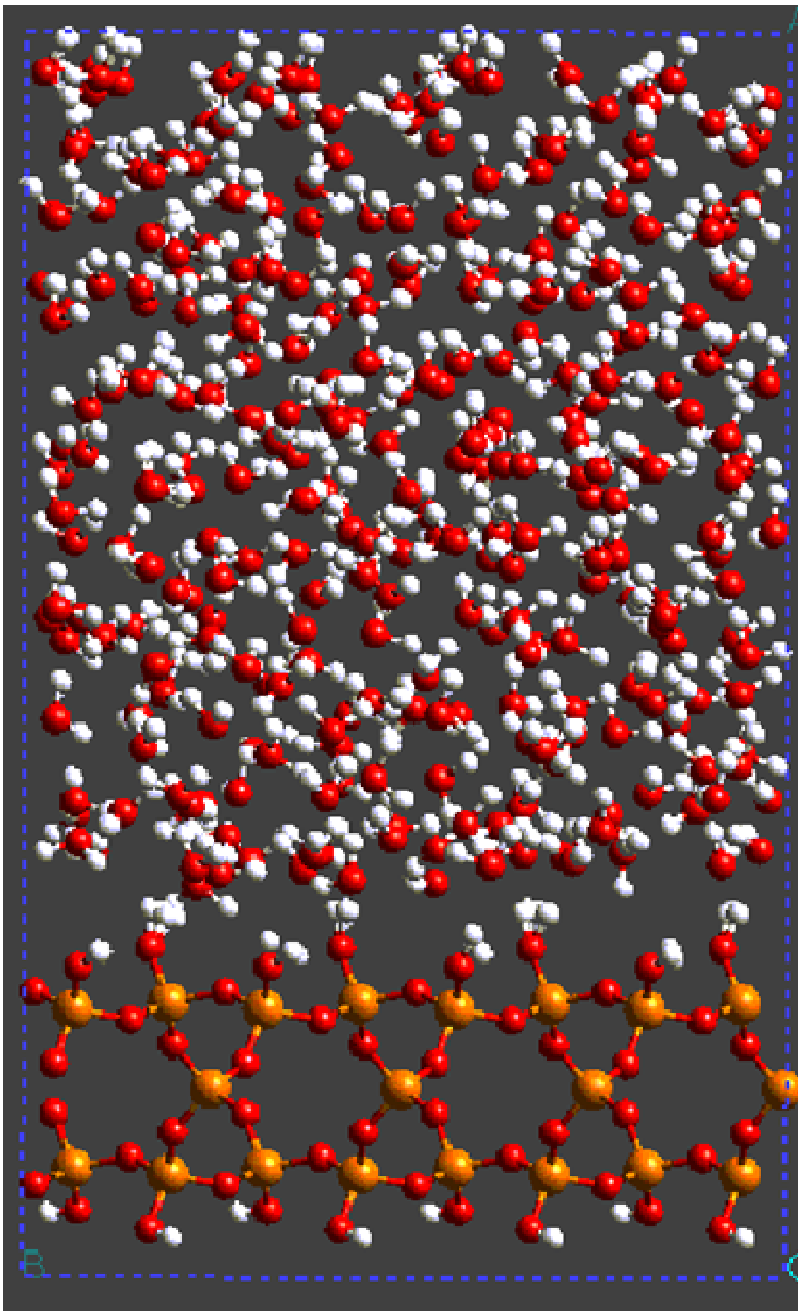

Figure 3.4-3. Equilibrium Snapshot (*x*, *z* Plane) of the Supercell Containing 300 Water Molecules and the Singly Protonated Quartz (010) Surface. The Dashed Line Represents the Supercell Boundaries, and Atomic Designations Are Si (Orange), O (Red), and H (White). Reproduced With Permission From Greathouse, J.A., R.J. O'Brien, G. Bemis, and R.T. Pabalan. *Journal of Physical Chemistry B.* Vol. 106. p. 1,646. 2002. Copyright 2002. American Chemical Society.

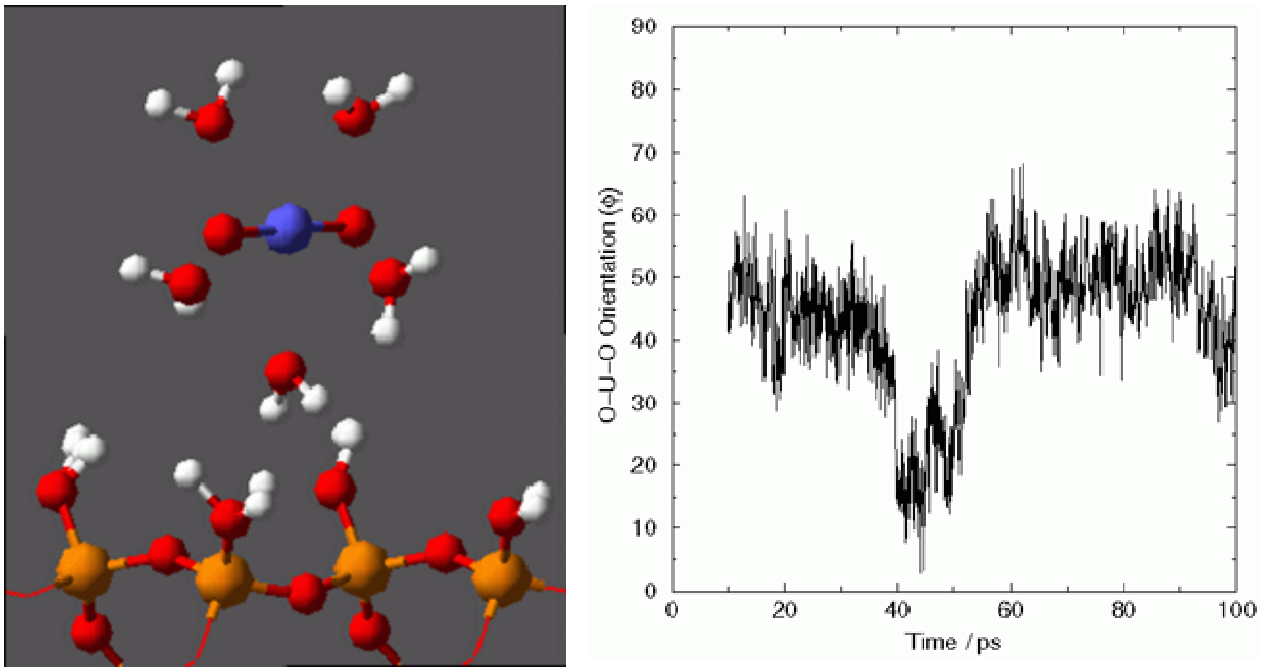

(a) (b)

Figure 3.4-4. Results From the Simulation of UO_2^{2+} and 300 Water Molecules Near the Singly Protonated Quartz (010) Surface. (a) Equilibrium Snapshot (*y*, *z* Plane) of the Outer-Sphere Surface Complex $[UO_2(H_2O)_5]^{2+}$, With Atomic Designations as in Figure 3.4-3 and U (blue). (b) Time Evolution of the O–U–O Vector Orientation to the Surface Normal. A Value of 90° Indicates That the Uranyl Ion Is Oriented Perpendicular to the Surface. Figure 4(b) Is Reproduced With Permission From Greathouse, J.A., R.J. O'Brien, G. Bemis, and R.T. Pabalan. *Journal of Physical Chemistry B.* Vol. 106. p. 1,646. 2002. Copyright 2002. American Chemical Society.

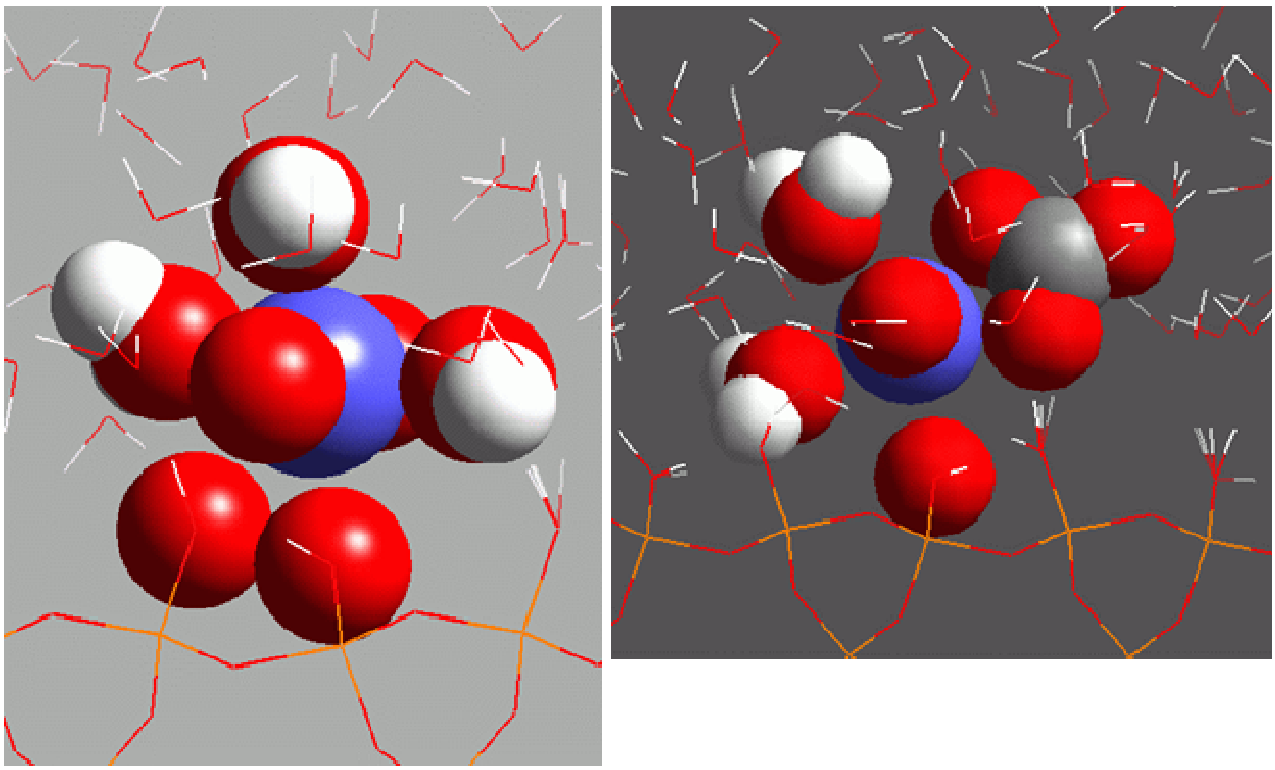

(a) (b)

Figure 3.4-5. Equilibrium Snapshot (*x*,*z* Plane) of the Inner-Sphere Surface Complexes (a) $[UO_2(H_2O)(OH)_2\{O\}_2]$ and (b) $[UO_2(H_2O)_2(CO_3)\{O\}_2]$, Both Shown as Large Spheres. Nonsolvating Water Molecules and Other Quartz Atoms Are Shown as Sticks. Atomic Designations Are Si (Orange), O (Red), U (Blue), and H (White).

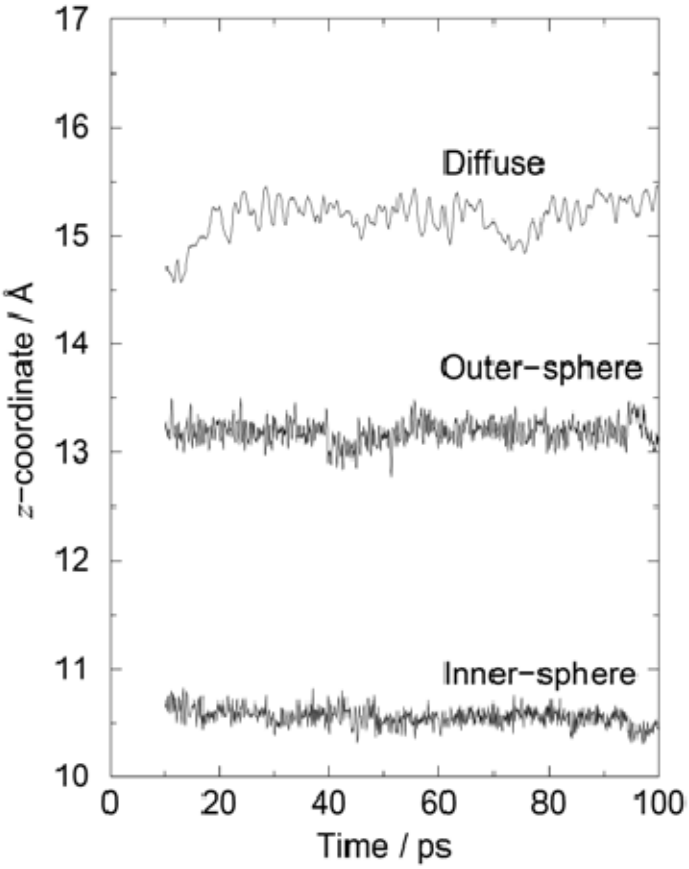

Figure 3.4-6. Equilibrium Trajectories (*z*-Direction) of Uranium Atoms in Inner-Sphere, Outer-Sphere, and Diffuse Uranyl Species. From Bottom to Top, the Three Uranyl Complexes Are $[UO_2(H_2O)(OH)_2\{O\}_2]$, $[UO_2(H_2O)_5]^{2+}$, and $[UO_2(H_2O)_3(OH)_2]$. Hydrogen Atoms at the Quartz Surface Have a z-Coordinate of Approximately 9.4 Å, so the Uranium *z*-Coordinates Shown Correspond to Average Distances of 1 Å, 4 Å, and 6 Å Above the Surface. Reproduced With Permission From Greathouse, J.A., R.J. O'Brien, G. Bemis, and R.T. Pabalan. *Journal of Physical Chemistry B.* Vol. 106. p. 1,646. 2002. Copyright 2002. American Chemical Society.

Table 3.2-1. Summary of Binary Ion-Exchange Experiments				
Experimental System	**Form of Zeolite Used**	**Ionic Strength**	**Number of Reference Solutions**	**Number of Experimental Solutions**
K^+/Cs^+	K	0.05 N	6	18
Ca^{2+}/Sr^{2+}	Ca	0.05 N	5	18
K^+/Sr^{2+}	K	0.0005 N	1	17
Na^+/Cs^+	Na	0.05 N	5	19
K^+/Na^+	K	0.05 N	7	20
K^+/Ca^{2+}	K	0.01 N	3	14

Table 3.2-2. Summary of Ternary and Quaternary Ion-Exchange Experiments				
Experimental System	**Form of zeolite Used**	**Ionic Strength**	**Number of Reference Solutions**	**Number of Experimental Solutions**
$Na^+/K^+/Cs^+$	K	0.05 N	6	18
$Na^+/K^+/Cs^+$	Na	0.005 N	29	29
$Na^+/K^+/Ca^{2+}$	Na	0.05 N	29	29
$Na^+/K^+/Ca^{2+}$	Na	0.005 N	29	29
$Na^+/K^+/Sr^{2+}$	Na	0.05 N	29	29
$Na^+/K^+/Sr^{2+}$	Na	0.005 N	29	29
$Na^+/K^+/Ca^{2+}/Sr^{2+}$	Na	0.05 N	39	39

Table 3.2-3. Model Parameters Derived From Regression of Ion-Exchange Data. Standard Errors in the Derived Parameters Are in Parentheses. The Footnotes Give the Source of Experimental Data Used in Deriving the Model Parameters.							
		Wilson Model			**Margules Model**		
Exchange Reaction	**Total Solution Concentration (N, equiv./liter)**	Λ_{12}	Λ_{21}	ln $K_{A,B}$	W_A	W_B	ln $K_{A,B}$
$Li^+ + NaL \Leftrightarrow Na^+ + LiL$	0.1*	0.439 (864)	2.277 (1967)	−1.970 (0.102)	−0.353 (0.121)	0.794 (0.435)	−1.724 (0.119)
$K^+ + NaL \Leftrightarrow Na^+ + KL$	0.005†	0.225 (2174.)	4.450 (9675.)	3.337 (0.306)	−2.179 (0.383)	−0.458 (0.127)	3.306 (0.097)
	0.05†	0.719 (0.504)	3.449 (1.888)	3.571 (0.122)	−1.844 (0.346)	−0.855 (0.104)	3.537 (0.080)
	0.5†	2.628 (0.606)	1.042 (0.518)	3.195 (0.092)	−0.860 (0.454)	−1.592 (0.133)	3.175 (0.092)
$Cs^+ + NaL \Leftrightarrow Na^+ + CsL$	0.02§	1.3051 $\times 10^{-6}$ (0.5859)	6.5211 (65)	2.7386 (8.9677)	3.1204 (0.4737)	−2.3941 (0.4850)	3.1072 (0.3311)
	0.1*	1.2744 (1.3811)	30.4197 (564)	5.9805 (17.4)	−3.3839 (2.7445)	−2.1626 (0.7933)	4.4891 (0.9082)
	1.0‡	0.7157 (2951)	1.3985 (4129)	4.1248 (1.4932)	−4.5831 (2.0340)	−1.3879 (0.6487)	5.6257 (0.7013)
	0.02§, 0.1*, 1.0‡	1.837 (2.028)	2.713 (11.428)	4.388 (2.488)	−1.666 (4.906)	−1.711 (1.542)	4.265 (1.689)
$Cs^+ + KL \Leftrightarrow K^+ + CsL$	0.1*	8.975 (9.73)	0.807 (0.804)	−0.178 (0.677)	−1.197 (0.643)	−3.221 (0.119)	0.119 (0.245)
	0.1‖	1.614 (0.504)	1.637 (0.465)	1.474 (0.073)	−1.108 (0.193)	−1.087 (0.239)	1.477 (0.072)
	0.1*,‖	0.876 (0.738)	3.013 (1.339)	0.968 (0.144)	−1.960 (0.457)	−0.480 (0.517)	1.058 (0.154)
$Cs^+ + RbL \Leftrightarrow Rb^+ + CsL$	0.1*	2.7079 (0.3987)	1.7319 (0.2456)	−0.4303 (0.0545)	−1.5890 (0.1253)	−2.0303 (0.1624)	−0.4265 (0.0465)
$NH_4^+ + NaL \Leftrightarrow Na^+ + NH_4L$	0.1¶	1.8350 (1.9340)	0.7923 (1.3641)	1.5894 (0.1500)	−0.1781 (0.4859)	−0.6679 (0.3041)	1.5833 (0.1480)
	0.1#	3.0661 (237)	0.3272 (77)	1.5476 (0.1139)	0.2536 (0.2173)	−1.4222 (0.2531)	1.6104 (0.0884)
	0.1 ¶,#	2.504 (2.901)	0.473 (1.277)	1.564 (0.087)	0.103 (0.213)	−1.014 (0.197)	1.589 (0.079)

Table 3.2-3. Model Parameters Derived From Regression of Ion-Exchange Data. Standard Errors in the Derived Parameters Are in Parentheses. The Footnotes Give the Source of Experimental Data Used in Deriving the Model Parameters (continued).

Exchange Reaction	Total Solution Concentration (N, equiv./liter)	Wilson Model			Margules Model		
		Λ_{12}	Λ_{21}	ln $K_{A,B}$	W_A	W_B	ln $K_{A,B}$
$NH_4^+ + KL \Leftrightarrow K^+ + NH_4L$	0.1¶	4.732 (2312)	0.212 (489)	−0.901 (0.303)	−0.312 (0.735)	−1.526 (0.934)	−0.849 (0.314)
$2NH_4^+ + CaL \Leftrightarrow Ca^{2+} + NH_4L_2$	0.1¶	3.472 (108)	0.290 (31.165)	5.826 (0.243)	0.298 (0.549)	−1.120 (0.177)	5.623 (0.269)
	0.05†	0.785 (0.221)	4.151 (0.518)	−1.615 (0.063)	−2.340 (0.086)	−0.527 (0.204)	−1.563 (0.058)
	0.5†	1.821 (0.324)	3.420 (0.185)	−1.863 (0.075)	−2.718 (0.708)	−1.207 (0.306)	−1.707 (0.081)
$Ca^{2+} + 2KL \Leftrightarrow 2K^+ + CaL_2$	0.05**	0.164 (54)	6.099 (328)	−8.739 (0.057)	−2.364 (0.201)	−0.568 (0.431)	−8.844 (0.160)
$Sr^{2+} + 2NaL \Leftrightarrow 2Na^+ + SrL_2$	0.005**	6.814 (1.697)	1.664 (0.214)	−1.911 (0.161)	−2.204 (0.135)	−3.241 (0.350)	−1.628 (0.096)
	0.05**	4.807 (0.712)	2.454 (0.187)	−1.231 (0.099)	−2.682 (0.090)	−3.266 (0.207)	−1.137 (0.064)
	0.5**	4.108 (0.801)	3.373 (0.169)	−1.112 (0.125)	−3.371 (0.087)	−2.731 (0.358)	−0.921 (0.095)
$Sr^{2+} + 2KL \Leftrightarrow 2K^+ + SrL_2$	0.05**	0.225 (52.1)	4.452 (231.6)	−6.385 (0.069)	−1.477 (0.131)	0.612 (0.421)	−6.108 (0.136)
$Sr^{2+} + CaL_2 \Leftrightarrow Ca^{2+} + SrL_2$	1.0††	0.820 (0.584)	5.612 (1.257)	0.342 (0.222)	−3.728 (0.296)	0.699 (0.632)	0.738 (0.191)

*Chelischev et al. (1973)
†Pabalan (1994)
‡Ames (1964a)
§Howery and Thomas (1965)
‖Ames (1968)
¶Jama and Yucel (1990)
#Townsend and Loizidou (1984)
**Pabalan and Bertetti (1999)
††Ames 1964b

Table 3.4-1. Results for Simulations in Bulk Water*

Uranyl Complex	Interatomic Distance (Å)	
	$U\text{-}O_L$	$U\text{-}O_w$
$[UO_2(H_2O)_5]^{2+}$	–	2.51
$[UO_2(H_2O)_4(OH)]^{+}$	2.31	2.53
$[UO_2(H_2O)_3(OH)_2]$	2.33	2.53
$[UO_2(H_2O)_3(CO_3)]$	2.37	2.51
$[UO_2(H_2O)(CO_3)_2]^{2-}$	2.39	2.51

*U–O and U–Si distances (Å) from peaks in the averaged RDFs for ligand (O_L) and water (O_w)

Table 3.4-2. Results for Simulations Near the Singly Protonated Quartz (010) Surface*

Uranyl Complex	Interatomic Distance (Å)		
	$U\text{-}O_L$	$U\text{-}O_w$	U-Si
$[UO_2(H_2O)_5]^{2+}$	–	2.49	6.35
$[UO_2(H_2O)_4(OH)]^{+}$	2.31	2.53	8.13
$[UO_2(H_2O)_3(OH)_2]$	2.33	2.55	8.06
$[UO_2(H_2O)_3(CO_3)]$	2.37	2.51	8.25
$[UO_2(H_2O)(CO_3)_2]^{2-}$	2.37	2.51	8.03

*U-O and U-Si distances (Å) from peaks in the averaged RDFs. Oxygen atoms from ligand (hydroxide or carbonate), and water are denoted by O_L and O_w, respectively.

Table 3.4-3. Results for Simulations Near the Partially Deprotonated Quartz (010) Surface*

Uranyl Complex†	Interatomic Distance (Å)			
	$U\text{-}O_L$	$U\text{-}O_w$	$U\text{-}O_s$	U-Si
$[UO_2(H_2O)_4\{O\}]^{2+}$	–	2.50	2.50	3.98
$[UO_2(H_2O)_2(OH)\{O\}_2]^{+}$	2.35	2.55	2.55	4.06
$[UO_2(H_2O)\ (OH)_2\{O\}_2]$	2.33	2.53	2.53, 2.91	4.46
$[UO_2(H_2O)_2(CO_3)\{O\}]$	2.35	2.49	2.49	3.79, 4.55
$[UO_2(H_2O)\ (CO_3)_2]^{2-}$	2.38	2.55	2.91	4.49

*U-O and U-Si distances (Å) from peaks in the averaged RDFs. Oxygen atoms from ligand (hydroxide or carbonate), water, and quartz surface are denoted by O_L, O_w, and O_S, respectively.

†Surface oxygen atoms in the uranium coordination shell are denoted by {O}. Charge contributions due to {O} were not included in determining the overall charge of the complex.

4 IMPLEMENTING SORPTION MODELING APPROACHES IN PERFORMANCE ASSESSMENT

4.1 Groundwater Chemistry Considerations

Results of sorption experiments on silicate, oxide, and carbonate minerals suggest that groundwater chemistry plays a primary role in determining the magnitude of surface complexation-related sorption (i.e., excluding ion-exchange reactions). For a particular element, differences in sorption behavior due to differences in the surface characteristics of minerals are minimal. The specific surface area of the mineral does influence sorption (with larger surface areas generally exhibiting greater sorption), but as discussed in Section 2.2, the surface area effects are similar across many mineral types.

The pH, carbonate content (or P_{CO2}), and redox conditions of solutions are most important in driving sorption behavior for most elements. The sorption of many contaminants, including radionuclides, is particularly sensitive to variations in pH. For actinides, sensitivity to pH values in terms of sorption is related to their typically complicated hydrolysis behavior. The concentration of carbonate species in groundwater also has a pronounced effect on complexation and sorption of actinides, particularly at pH values above about 7 (Bertetti, et al., 1998; Pabalan and Turner, 1997; Davis, 2001). The oxidation states of many metals and actinides are affected by local redox conditions in groundwater systems. For instance, technetium, neptunium, and uranium are less mobile under reducing conditions and more mobile when oxidized. Conversely, iron is more mobile when reduced and less mobile when oxidized. Work in the Center for Nuclear Waste Regulatory Analyses (CNWRA®) sorption program focused on oxidizing conditions because, as confirmed by field sampling (e.g., Bertetti, et al., 2004), those conditions predominated throughout the Yucca Mountain system.

For performance assessment modeling, an appropriate range of groundwater chemistry conditions must be identified to reasonably model the expected range of sorption values for contaminants of interest. As part of the development of a performance assessment model for Yucca Mountain, Turner, et al. (1998) screened and culled the water chemistry dataset of Perfect, et al. (1995) to represent the groundwater chemistry at Yucca Mountain. Data later developed as part of the Nye County Early Warning Drilling Program and additional U.S. Department of Energy (DOE) characterization efforts were assembled and analyzed in subsequent reports (Bertetti, et al., 2004; McMurry and Bertetti, 2005) to produce a site-specific dataset pertinent to the region of interest for radionuclide transport in groundwater at Yucca Mountain.

The important parameters pH and P_{CO2} were used from the site-specific dataset to provide a characterization of Yucca Mountain groundwater chemistry in the performance assessment model (Figure 4.1-1) (McMurry and Bertetti, 2005). The two parameters were statistically analyzed and compared to groundwater data collected from the unsaturated zone (Browning and Murphy, 2002) to develop correlation and distribution functions for use in modeling actinide sorption (McMurry and Bertetti, 2005). These distribution functions were then sampled within the performance assessment code to calculate sorption for the actinides americium, neptunium, plutonium, thorium, and uranium as described in Section 4.5.

Although the pH and P_{CO2} data were primarily used to inform the development of the U.S. Nuclear Regulatory Commission (NRC) performance assessment code, they were also

useful in developing a spatial representation of the potential for radionuclide sorption in the Yucca Mountain region (Figure 4.1-2). Because the NRC performance assessment code did not explicitly represent spatial variations in groundwater chemistry, maps such as that exemplified in Figure 4.1-2 can provide confidence in the model representation of sorption along expected flow paths.

4.1.1 References

Bertetti, F.P., J. Prikryl, and B. Werling. "Development of Updated Total-System Performance Assessment Parameter Distributions for Radionuclide Transport in the Saturated Zone." San Antonio, Texas: CNWRA. 2004.

Bertetti, F.P., R.T. Pabalan, and M.G. Almendarez. "Studies of Neptunium^{V} Sorption on Quartz, Clinoptilolite, Montmorillonite, and α-alumina. *Adsorption of Metals by Geomedia*. E.A. Jenne, ed. New York City, New York: Academic Press, Inc. pp. 131–148. 1998.

Browning, L. and W.M. Murphy. "Revised Analytical Compositions of Pore Water Collected from Yucca Mountain, Nevada, and Vicinity". San Antonio, Texas: CNWRA. 2002.

Davis, J.A. NUREG/CR–6708, "Surface Complexation Modeling of Uranium(VI) Adsorption on Natural Mineral Assemblages. Washington, DC: NRC. 2001.

McMurry, J. and F.P. Bertetti. "Selection of Sorption-Related Values for Unsaturated Zone and Saturated Zone Transport in Total-System Performance Assessment." CNWRA Letter Report. San Antonio, Texas: CNWRA. June 2005.

Pabalan, R.T. and D.R. Turner. "Uranium(6+) Sorption on Montmorillonite: Experimental and Surface Complexation Modeling Study." *Aqueous Geochemistry*. Vol. 2. pp 203–226. 1997.

Perfect, D.L., C.C. Faunt, W.C. Steinkampf, and A.K. Turner. "Hydrochemical Data Base for the Death Valley Region, California and Nevada. U.S. Geological Survey Open-File Report 94-305. 1995.

Turner, D.R., R.T. Pabalan, J.D. Prikryl, and F.P. Bertetti. "Radionuclide Sorption at Yucca Mountain, Nevada–A Demonstration of an Alternate Approach for Performance Assessment." Symposium on the Scientific Basis for Nuclear Waste Management-XXII, Materials Research Society Fall Meeting Paper, Boston, Massachusetts, November 30–December 3, 1998. Warrendale, Pennsylvania: Materials Research Society. 1998.

4.2 Empirical Models—Deterministic

4.2.1 Evaluating K_d Values for Deterministic Performance Assessments—An Example

The simplest approach to implementing sorption in radionuclide transport models supporting performance assessment is to develop preferred K_d values from available studies and apply them as single values (i.e., deterministically). The values must be defined for given spatial domains in the model (e.g., strata and lateral position) and so are preferably developed with the specific sorbing media and geochemical conditions for that domain in mind. The single-value, constant K_d values are then used in the advection-dispersion expression governing transport within that domain. CNWRA staff developed this sort of dataset as part of their charter

program Technical Assistance in Evaluating Non-High-Level Waste Determinations for the DOE in South Carolina and Idaho. In this program, CNWRA is providing technical support to NRC staff reviews of performance assessments designed to demonstrate compliance with performance objectives for retaining residual waste in high-level waste tanks and for disposing of salt wastes in the near surface. (NRC has a consultative, rather than regulatory, role in these reviews). This program is not directly related to Yucca Mountain, but as a part of the CNWRA charter program, it provides insights into how different chemical environments affect radionuclide sorption in engineered systems.

Prikryl and Pickett (2007) were tasked with recommending reasonable K_d values for various radioelements for the natural system at two general locations potentially subject to NRC waste determinations reviews: the Savannah River Site and Idaho National Laboratory. (We use the term "radioelement" here because the sorption coefficient is a chemical parameter that would, in general, apply to all isotopes of an element.) The report was mainly intended to be useful as a review tool for the NRC and CNWRA staffs in evaluating K_d single values or probability distributions used in DOE performance assessments supporting waste determinations. The output of the report was a set of single recommended K_d values for each important radioelement in (i) each relevant hydrostratigraphic unit at Savannah River Site and (ii) each relevant aquifer rock type at Idaho National Laboratory. For example, values were recommended for the Gordon Aquifer at Savannah River Site and for alluvium at Idaho National Laboratory. The report also often included ranges of values the authors considered reasonable, but did not recommend that those ranges explicitly be used to develop probability distributions. The radioelements covered in the report were carbon, nickel, selenium, strontium, niobium, technetium, tin, iodine, cesium, lead, uranium, neptunium, plutonium, americium, and curium.

The authors surveyed project reports and the literature for site-specific experimental data and considered other sources when site-specific data were lacking or inadequate. To paraphrase Prikryl and Pickett (2007, Section 1.3), the analysis of sorption coefficients followed this procedure for each site:

- The mineralogical and hydrogeochemical characteristics of subsurface units along transport pathways were described.
- The radioelements of concern were designated.
- For each radioelement the chemistry and important sorptive characteristics of the radioelement were described.
- Site-specific measurements of K_d values for the various transport media and/or measurements of K_d values under analogous conditions were summarized.
- Literature-based reference K_d estimates and recommendations for previous assessments at the site were reviewed.
- K_d values from compendia of sediment and rock types comparable to subsurface units at the site were discussed (e.g., Sheppard and Thibault, 1990; Looney, et al., 1987).
- Based on the data review, a recommended K_d value was designated.

The report went on to discuss how K_d measurements could be evaluated and compared (e.g., batch versus column versus *in situ*) and discuss the general effects of environmental

factors (e.g., pH and clay content) on sorption behavior. The report also made the following point about conservatism (Prikryl and Pickett, 2007, p. 1–2):

> Because these lithologic and hydrogeochemical factors are not always well constrained for a given transport model, it is often necessary to make conservative selections of K_d values that are at the low end of reasonable ranges. In this way, the model is less likely to overpredict the favorable effects of sorption. Such an approach is useful in the case of spatial and temporal variation. This approach also addresses the uncertainties inherent in the K_d values themselves, apart from environmental uncertainty and variation.

This statement about conservatism, generally accepted by the scientific community at the time, applies only to transport and minimum time of arrival of the radionuclide of interest at a specified compliance boundary. The adoption of low K_d values may not necessarily be conservative with respect to dose when other factors such as the effects of daughter ingrowth are considered. Moreover, spatial and temporal variation in water chemistry and other factors influencing sorption may result in significant variations in the spatial and temporal concentrations of the radionuclide of interest. These variations may result in unexpected effects on dose that are not well described by the use of single K_d values. The full range of expected K_d values for each radionuclide, which affects the expected time of transport, and the concentrations of radionuclides at the receptor location should be considered before an assumption of conservatism is associated with use of low K_d values.

4.2.2 References

Looney, B.B., M.W. Grant, and C.M. King. "Estimation of Geochemical Parameters for Assessing Subsurface Transport at the Savannah River Plant." Environmental Information Document DPST–85–904. Aiken, South Carolina: E.I. du Pont de Nemours and Company, Savannah River Laboratory. 1987.

Prikryl, J.D. and D.A. Pickett. "Recommended Site-Specific Sorption Coefficients for Reviewing Non-High-Level Waste Determinations at the Savannah River Site and Idaho National Laboratory." San Antonio, Texas: CNWRA. 2007.

Sheppard, M.I. and D.H. Thibault. "Default Soil Solid/liquid Partition Coefficients, K_ds, for Four Major Soil Types: A Compendium." *Health Physics*. Vol. 59, No. 4. pp. 471–482. 1990.

4.3 Using Site-Specific Groundwater Chemistry To Develop Probability Density Function Statistics

After evaluating the different surface complexation model approaches, CNWRA staff focused on using a relatively simple DLM to model sorption for the range in water chemistries at Yucca Mountain (Turner, et al., 1998a; Turner and Pabalan, 1999). The initial effort focused on a regional water chemistry database Perfect, et al. (1995) developed.

As described previously, this modeling approach used several assumptions, including the following

- Sorption behavior as a function of pH and carbonate concentration is similar for aluminosilicate minerals when expressed in terms of $K_{A,eff} = K_d/A_{eff}$, where A_{eff} is the effective surface area (BET surface area in the case of nonporous minerals, 10 percent

of BET in the case of sheet minerals such as montmorillonite, gibbsite, and kaolinite). Also implicit in this assumption is that aluminosilicate minerals will dominate sorption in the tuff units at Yucca Mountain.

- The effect outlined previously has been demonstrated for U(VI) and Np(V) (Pabalan, et al., 1998; Bertetti, et al., 1998). It is assumed that it is also true for other actinides such as Am(III), Pu(V), and Th(IV).

- The water chemistries of Perfect, et al. (1995) as screened in Turner, et al. (1998a) represent the likely range in water chemistry at Yucca Mountain. These data were subsequently modified as the Nye County Early Warning Drilling Program and DOE developed additional water chemistry data for the Fortymile Wash region (McMurry and Bertetti, 2005).

4.3.1 Steps in Applying the Model

The steps involved in this modeling exercise include the following

- Identify sorption experiments that can be used to calibrate the diffuse layer model parameters. We used the sorption experiments of Righetto, et al. (1991, 1988) for Am(III), Th(IV), and Pu(V) sorption on γ-alumina and those of Turner, et al. (1998b) and Pabalan and Turner (1997)] for Np(V) and U(VI) sorption on montmorillonite. Diffuse layer model parameters were determined assuming A_{eff} = 10 percent of BET measured area for both γ-alumina (BET = 130 m^2/g; A_{eff} = 13.0 m^2/g) and montmorillonite (BET = 97 m^2/g; A_{eff} = 9.7 m^2/g).

- Determine the diffuse layer model parameters for these experiments.

- The diffuse layer model parameters in Turner, et al. (1998b) and Pabalan and Turner (1997) were used for Np(V)- and U(VI)-montmorillonite. Diffuse layer model parameters for Am(III)-, Pu(V)-, and Th(IV)-γ-alumina were developed in Turner (1995) for γ-alumina (130 m^2/g). We reinterpreted the data using A_{eff} = 13.0 m^2/g and the Nuclear Energy Agency thermodynamic database for americium, plutonium, neptunium, and uranium.

- With the parameters developed, the diffuse layer model was applied to the 460 analyses in the culled Perfect, et al. (1995) database (Turner, et al., 1998a). Running these models allows generation of sorption coefficients for the observed ranges in water chemistry for the five radionuclide-mineral systems considered here. Normalized to effective surface area $K_{A,eff}$ of the minerals is used in the calibration experiments, and assuming that the pH- and P_{CO2}-dependent sorption behavior is similar for aluminosilicates, these sorption coefficient distributions were then recast in terms of K_d for each of the hydrostratigraphic units used in the TPA code.

- The distributions for each radionuclide appeared to be lognormal, although the kurtosis of the distributions varies (Turner, et al., 1998a; Turner and Pabalan, 1999). The final step in using this information in TPA is to apply this distribution to each hydrostratigraphic unit and transform the $K_{A,eff}$ into K_d (in mL/g). Assuming that aluminosilicates will dominate sorption in these units, it follows that the chemical-dependent sorption behavior, and therefore these distributions, should hold for each unit. The key parameter for each transform to $K_{A,eff}$ will therefore be the effective surface area.

Note that for a given radionuclide, the method used here results in the same distribution for each hydrostratigraphic unit, because K_d is determined by multiplying $K_{A,eff}$ by a unit-specific constant (A_{eff}). It is also possible to use this information to develop correlation coefficients between each of the radionuclides.

4.3.2 Correlations Among Radionuclides

In addition to constraining probability distribution functions for a given radioelement, the application of mechanistic sorption models offers a way of explicitly developing a multivariate correlation among sorption parameter PDFs that reflects the underlying effects of geochemistry on sorption. For example, calculating a distribution for Np(V)- and U(VI)-montmorillonite sorption can provide a direct means of testing the bivariate correlation between Np(V) and U(VI) sorption that results from the effects of chemical variability. The relationship is not 1:1 due to differences in the aqueous speciation that control sorption of Np(V) and U(VI).

Using this method, the correlation coefficient for log K_d calculated for Np(V) and U(VI) is about 0.6, indicating a positive correlation in sorption behavior for these two actinides due to geochemical effects. The correlation is weak ($r^2 = 0.4$), however, due to the different speciation behavior of these two actinides, and is also likely influenced by a few outlier points. Nevertheless, correlation coefficients calculated in a similar manner for multiple pairings of radioelements can be included as input into the performance assessment sampling routine; in this way, the value selected for one radioelement sorption parameter is conditioned by its statistical (and therefore geochemical) relationship to the other radioelements. These types of correlations can also be used to examine the justification for using chemical analogues in performance assessment to supplement limited sorption data for some radionuclides.

4.3.3 Caveats to the Groundwater Chemistry Modeling Approach

Some caveats should be kept in mind when using this approach:

- The models were calibrated based on a limited number of single mineral, end member, batch experiments. This is particularly true for Am(III), Th(IV), and Pu(V) where only a single set of experimental conditions has been used to calibrate and test the model.

- A simplified diffuse layer model was used to generate the sorption coefficients. Competitive sorption reactions are not included in the model, although there is allowance for aqueous speciation of the radionuclide of interest with ligands (e.g., CO_3^{2-}, F^-, Cl^-, and SO_4^{2-}).

- In the absence of detailed site-specific information, many of the diffuse layer model parameters were assumed. These include M/V, radionuclide concentration, and site density (Turner and Sassman, 1996).

- In converting the $K_{A,eff}$ values to K_d, empirical measures of specific surface areas were assumed based on porosity, density, and pore aperture. These surface areas were expressed in terms of m^2/g and do not explicitly take into account the potential effects of conditions such as wetted surface area and dead-end pore space. The surface areas are not based on site-specific measured surface area and for this reason should be used with caution.

- Other than assuming that the minerals were some type of aluminosilicate, no specific mineral was assumed. Although mineral-specific experiments were used in calibrating the models and in developing the $K_{A,eff}$ distributions, the empirical surface area presumed no specific mineral type.

- Many of the K_ds calculated here were too high to be reliably measured in experiments [e.g., K_d for Am(III) up to 10^{10} mL/g].

- Given these caveats, retardation predicted using these parameters is best viewed as a "defense-in-depth" strategy to reduce uncertainty in parts of the transport codes.

4.3.4 References (Section 4.3)

Bertetti, F.P., R.T. Pabalan, and M.G. Almendarez. "Studies of Neptunium^{V} Sorption on Quartz, Clinoptilolite, Montmorillonite, and α-alumina. *Adsorption of Metals by Geomedia*. E.A. Jenne, ed. New York City, New York: Academic Press, Inc. pp. 131–148. 1998.

McMurry, J. and F.P. Bertetti. "Selection of Sorption-Related Values for Unsaturated Zone and Saturated Zone Transport in Total-System Performance Assessment." San Antonio, Texas: CNWRA. 2005.

Pabalan, R.T., D.R. Turner, F.P. Bertetti, and J.D. Prikryl. "Uranium^{VI} Sorption onto Selected Mineral Surfaces." *Adsorption of Metals by Geomedia*. E.A. Jenne, ed. New York City, New York: Academic Press, Inc. pp. 99−130. 1998.

Pabalan, R.T. and D.R. Turner. "Uranium(6+) Sorption on Montmorillonite: Experimental and Surface Complexation Modeling Study." *Aqueous Geochemistry*. Vol. 2. pp. 203-226. 1997.

Perfect, D.L., C.C. Faunt, W.C. Steinkampf, and A.K. Turner. "Hydrochemical Data Base for the Death Valley Region, California and Nevada. U.S. Geological Survey Open-File Report 94-305. 1995.

Righetto, L., G. Bidoglio, B. Marcandalli, and I.R. Bellobono. "Surface Interactions of Actinides With Alumina Colloids." *Radiochimica Acta*. Vol. 44/45. pp. 73–75. 1988.

Righetto, L., G. Bidoglio, G. Azimonti, and I.R. Bellobono. "Competitive Actinide Interactions in Colloidal Humic Acid-Mineral Oxide Systems." *Environmental Science and Technology*. Vol. 25. pp. 1,913–1,919. 1991.

Turner, D.R. "A Uniform Approach to Surface Complexation Modeling of Radionuclide Sorption." CNWRA 95–001. San Antonio, Texas: CNWRA. 1995.

Turner, D.R. and S.A. Sassman. "Approaches to Sorption Modeling for High-Level Waste Performance Assessment." *Journal of Contaminant Hydrology*. Vol. 21 pp. 311–332. 1996.

Turner, D.R. and R.T. Pabalan. "Abstraction of Mechanistic Sorption Model Results for Performance Assessment Calculations at Yucca Mountain, Nevada. *Waste Management.* Vol. 19. pp. 375–388. 1999.

Turner, D.R., R.T. Pabalan, J.D. Prikryl, and F.P. Bertetti. "Radionuclide Sorption at Yucca Mountain, Nevada–A Demonstration of an Alternate Approach for Performance Assessment."

Symposium on the Scientific Basis for Nuclear Waste Management-XXII, Materials Research Society Fall Meeting Paper, Boston, Massachusetts, November 30–December 3, 1998. Warrendale, Pennsylvania: Materials Research Society. 1998a.

Turner, D.R., R.T. Pabalan, and F.P. Bertetti. "Neptunium(V) Sorption on Montmorillonite: An Experimental and Surface Complexation Modeling Study." *Clays and Clay Minerals*. Vol. 46. pp. 256−269. 1998b,

4.4 Thermodynamic Model—Response Surface

4.4.1 Description of a Response Surface Approach

As described previously in Section 1.3, another method the CNWRA staff used to abstract detailed geochemical sorption models for the purposes of performance assessment was to develop sorption response surfaces using a simplified diffuse layer model approach (Figure 4.4-1) that correlated K_d values with variations in pH and P_{CO2} (Turner, et al., 2006, 2002; McMurry and Bertetti, 2005). After calibrating the model and running it over a wide range in geochemical conditions, the simulated sorption curve for discrete values was parameterized for the purposes of interpolating geochemical conditions using different polynomial expressions (Figure 4.4-2). The sorption response surfaces were for the actinides americium, neptunium, plutonium, thorium, and uranium; surface complexation models were applied over a wide range of geochemical conditions to generate a set of effective surface area normalized distribution coefficients ($K_{A,eff}$) (Turner, et al., 2006, 2002), which are in turn converted to K_d values using the specific surface area properties of the hydrostratigraphic layers. Probability distribution functions for the key geochemical parameters pH and P_{CO2} were developed based on site-specific hydrochemical data (McMurry and Bertetti, 2005; Bertetti, et al., 2004)

In a stochastic performance assessment simulation, each realization samples specific correlated values for pH and P_{CO2} that, in turn, are used to select the appropriate $K_{A,eff}$ from the response surface lookup table. Although the approach does not explicitly incorporate geochemistry in the performance assessment transport calculations, it correlates the calculation of K_d values with two key geochemical parameters that affect sorption behavior, providing a stronger technical basis for the treatment of transport for these five significant actinides. In any particular realization of the code, the K_d values for the actinides are calculated separately, but the calculations for all five are consistent because each value is associated with the same specified pH and P_{CO2} parameter values (Figure 4.4-3). This approach was used in developing the sorption coefficients for TPA Version 5.1 (Durham, et al., 2007).

4.4.2 References (Section 4.4)

Bertetti, F.P., J. Prikryl, and B. Werling. "Development of Updated Total-System Performance Assessment Parameter Distributions for Radionuclide Transport in the Saturated Zone." San Antonio, Texas: CNWRA. 2004.

Durham, J., C. Grossman, and B. Leslie. "Total-System Performance Assessment (TPA) Version 5.1 Code Module Descriptions And User Guide." San Antonio, Texas: CNWRA. July 2007.

Hsi, C-K.D. and D. Langmuir. "Adsorption of Uranyl Onto Ferric Oxyhydroxides: Application of the Surface Complexation Site-Binding Model." *Geochimica et Cosmochimica Acta*. Vol. 49, No. 1. pp. 931–1,941. 1984

McMurry, J. and F.P. Bertetti. "Selection of Sorption-Related Values For Unsaturated Zone and Saturated Zone Transport In Total-System Performance Assessment." CNWRA Letter Report. San Antonio, Texas: CNWRA. June 2005.

Turner, D.R., F.P. Bertetti, and R.T. Pabalan. "The Role of Radionuclide Sorption in High-Level Waste Performance Assessment: Approaches for the Abstraction of Detailed Models. Soil Science Society of America Proceedings Volume: *Soil Geochemical Processes of Radionuclides*. Pittsburgh, Pennsylvania: Soil Science of America. pp. 211–252. 2002.

Turner, D.R., R.T. Pabalan, and F.P. Bertetti. "Applying Surface Complexation Modeling to Radionuclide Sorption." *Surface Complexation Modeling*. F. Lützenkirchen, ed. Amsterdam: Elsevier, Ltd. pp. 553–604. 2006.

Turner, D.R., R.T. Pabalan and F.P. Bertetti. "Neptunium(V) Sorption on Montmorillonite: An Experimental and Surface Complexation Modeling Study." *Clays and Clay Minerals*. Vol. 46. pp. 256−269. 1998.

4.5 In-Package Radionuclide Transport in Total System Performance Assessment

In reviewing the license application for the proposed repository at Yucca Mountain, and in prelicensing interactions, the CNWRA and NRC staffs recognized the potential risk significance of actinide sorption onto surfaces inside the waste package. This process was not included in the independent NRC performance assessment, but DOE did implement it in Total System Performance Assessment. The modeled in-package sorptive medium was the surface of iron oxyhydroxides resulting from the corrosion of steel components, such as the basket holding fuel assemblies and the surface of the stainless steel internal container.

In Total-system Performance Assessment, DOE modeled actinide sorption on corrosion products using a surface complexation model to develop effective K_ds appropriate for the modeled chemical conditions. The K_ds were then used in a mixing cell model to simulate equilibrium delay of release of some actinides (uranium, neptunium, and thorium) from the waste package. In contrast, kinetic reversible sorption onto corrosion products was modeled for americium and plutonium, also based on the K_ds derived from the surface complexation model.

To develop the K_d distributions used in Total-system Performance Assessment, DOE performed multiple surface complexation model simulations intended to represent the range of (i) surface properties and (ii) potential water chemistries inside the package and used multiple regressions to produce functions that calculated actinide sorption as a function of key geochemical properties. In this way, DOE sought to incorporate into the K_d distributions uncertainty for appropriate key geochemical properties, such as pH and P_{CO2}, and surface properties related to sorption site concentration, such as site density, surface area, and solid mass.

There is not an abundance of experimental evidence regarding the sorption of risk-significant radionuclides such as plutonium onto steel corrosion products. DOE, therefore, compared its modeled K_d distributions to ranges of soil data compiled by the U.S. Environmental Protection Agency.

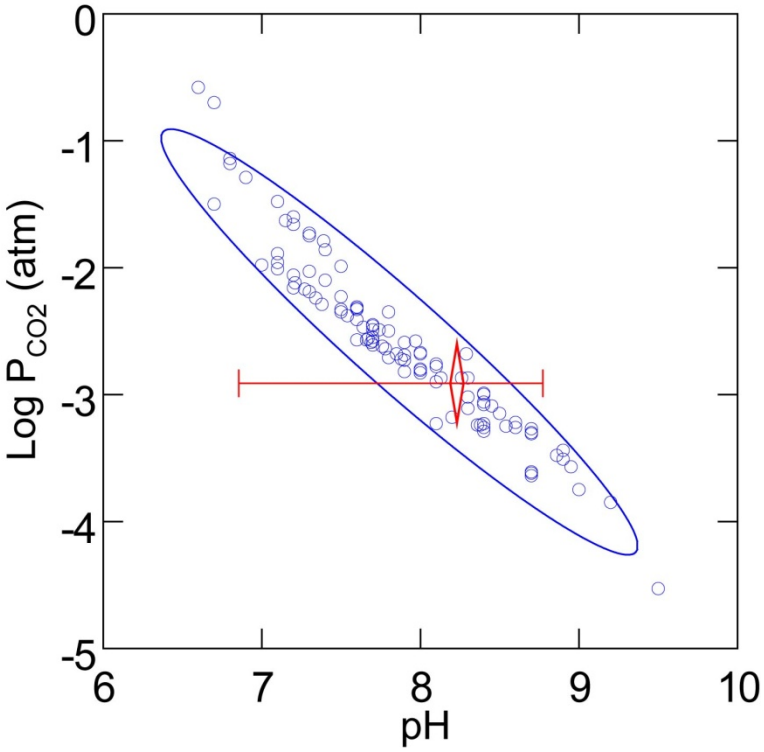

Figure 4.1-1. Plot of Water Chemistry Data From Wells (107 Samples) Located Within the Site-Scale Model area in the Yucca Mountain Vicinity (McMurry and Bertetti, 2005). The 95 Percent Confidence Ellipse (Blue Line) Is Shown for the pH and CO_2 Data. The Red Bar Indicates the Range of pH Values From an Analysis of Unsaturated Zone Waters (103 Samples) From Yucca Mountain (Browning and Murphy, 2002), While the Red Diamond Indicates the Median pH Value From the Same Study.

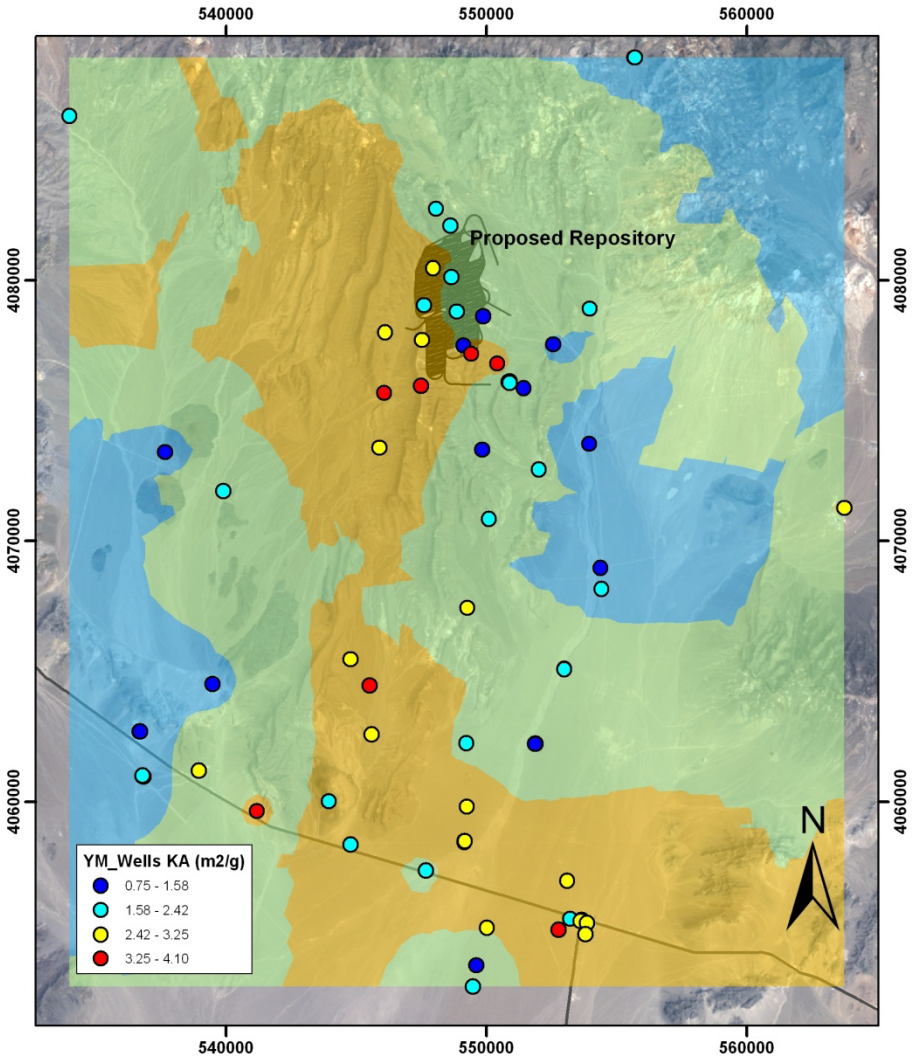

Figure 4.1-2. Map of Calculated Neptunium $K_{A,eff}$ (See Section 2.4.3) Sorption Values for Selected Wells Plotted Along With a Geostatistical Prediction Map of Neptunium $K_{A,eff}$ Sorption Values for the Yucca Mountain Region

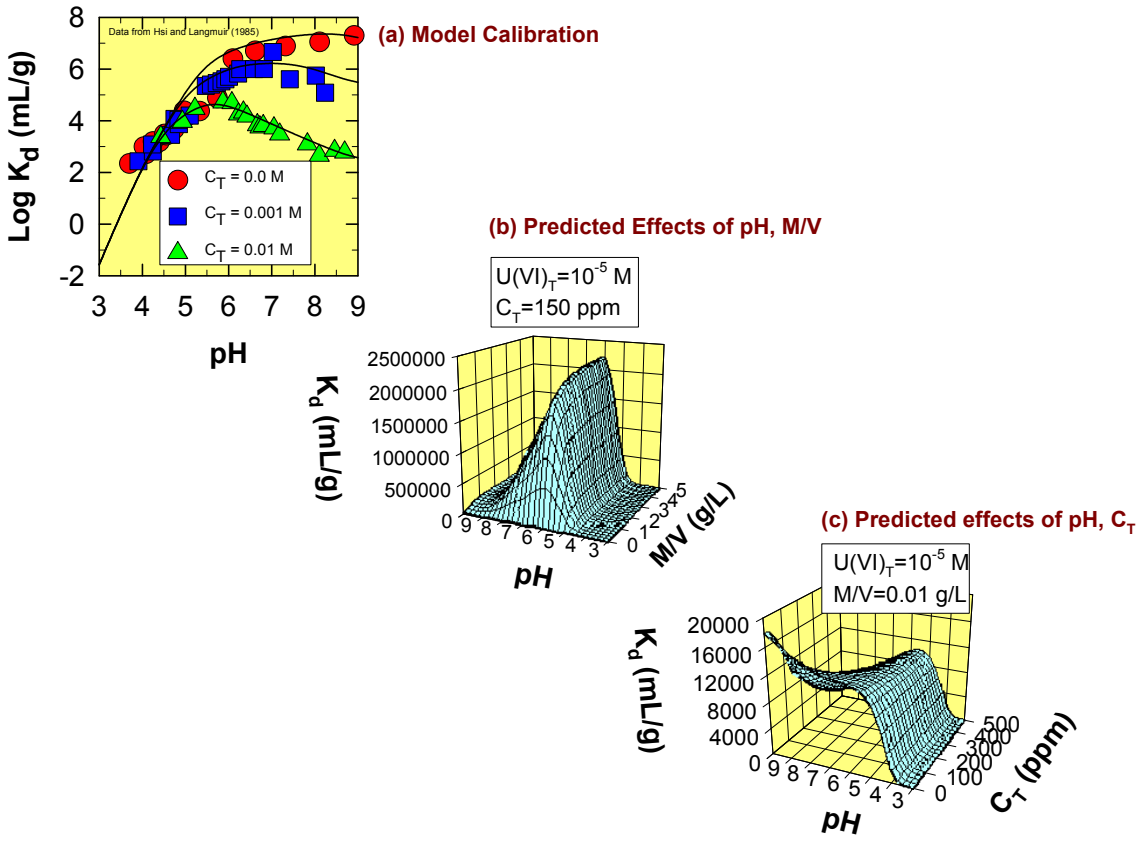

Figure 4.4-1. Developing a Response Surface Using the Simplified Diffuse-Layer Model Approach. (a) U(VI)-Goethtite Sorption Data of Hsi and Langmuir (1985) Used to Calibrate Model. (b) Sorption (K_d) Expressed as a Function of pH and M/V as a Surrogate for Site Concentration. (c) Sorption (K_d) Expressed as a Function of pH and Inorganic Carbon. Reproduced with Permission From. Turner, D.R., F.P. Bertetti, and R.T. Pabalan. "Role of Radionuclide Sorption in High-Level Waste Performance Assessment: Approaches for the Abstraction of Detailed Models." Soil Science Society of America Special Publication No. 59. 2002. Copyright 2002. Soil Science Society of America, Inc.

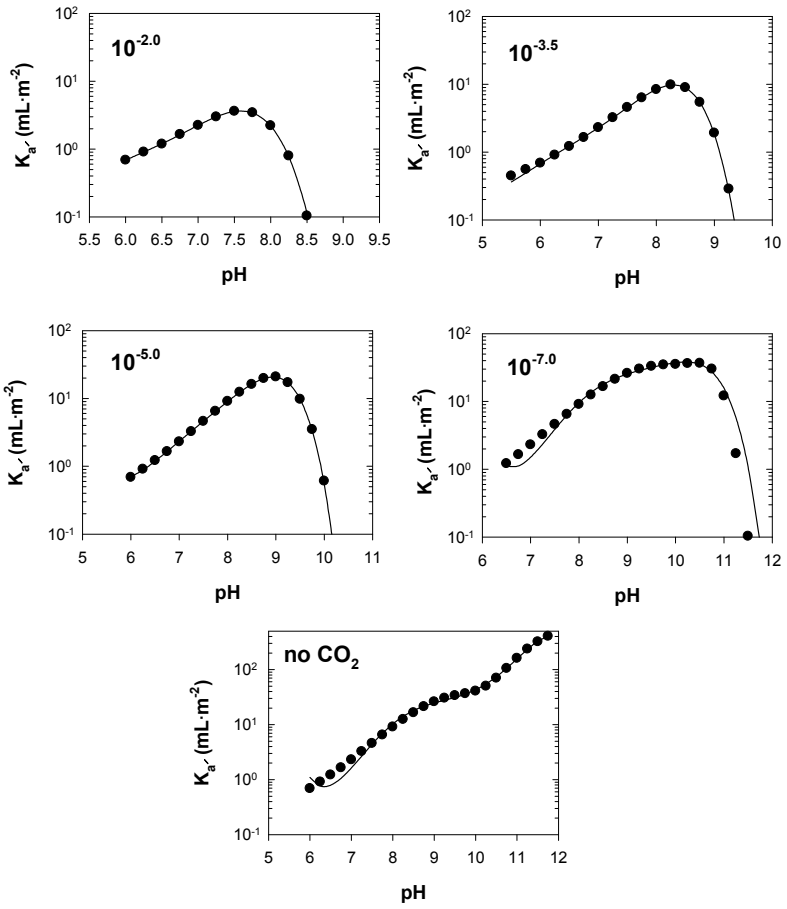

Figure 4.4-2. Developing Parametric Expressions to Simulate Np(V)-Montmorillonite Sorption Surfaces for a Range in P_{CO2} From 0 to 10^{-2} atm. Simplified Diffusive-Layer Model Calibrated Using Np(V)-Montmorillonite Sorption Data (Turner, et al., 1998). Reproduced with Permission From. Turner, D.R., F.P. Bertetti, and R.T. Pabalan. "Role of Radionuclide Sorption in High-Level Waste Performance Assessment: Approaches for the Abstraction of Detailed Models." Soil Science Society of America Special Publication No. 59. 2002. Copyright 2002. Soil Science Society of America, Inc.

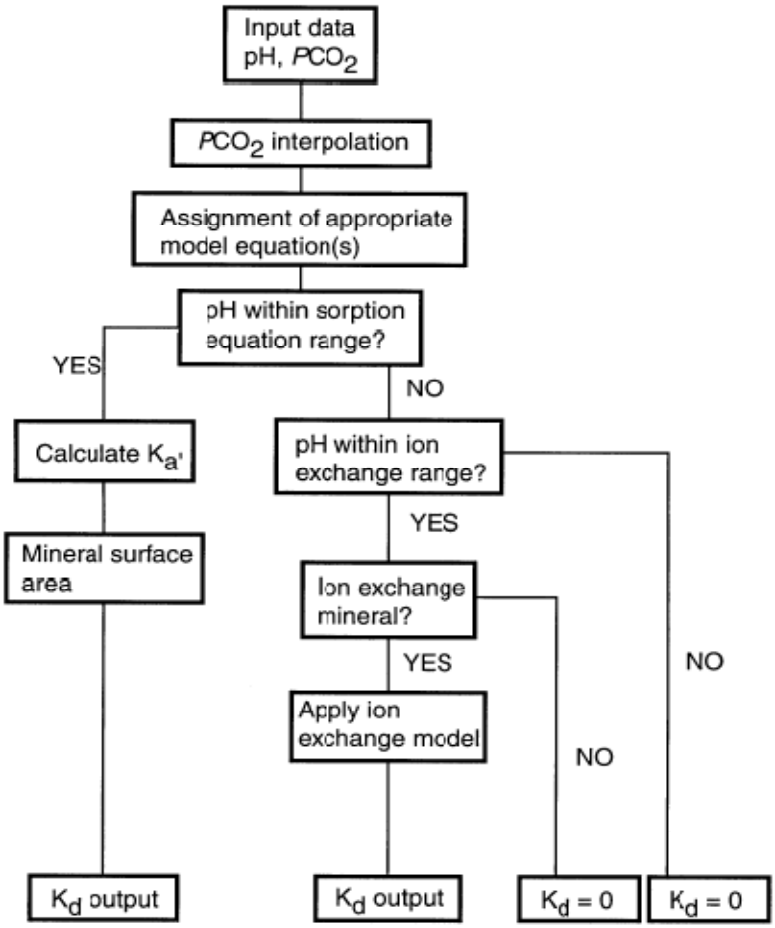

Figure 4.4-3. Flow Diagram for Implementing a Sorption Response Surface in Performance Assessment. Reproduced with Permission from. Turner, D.R., F.P. Bertetti, and R.T. Pabalan. "Role of Radionuclide Sorption in High-Level Waste Performance Assessment: Approaches for the Abstraction of Detailed Models." Soil Science Society of America Special Publication No. 59. 2002. Copyright 2002. Soil Science Society of America, Inc.

5 SUMMARY AND CONCLUSIONS

5.1 Summary

The potential release of radionuclides as dissolved constituents in groundwater is a primary concern in performance assessment of proposed high-level nuclear waste geologic repositories. Sorption onto mineral surfaces is an important mechanism for reducing radionuclide concentrations along groundwater flow paths and retarding radionuclide migration to a receptor location [such as the reasonably maximally exposed individual (RMEI)]. The Center for Nuclear Waste Regulatory Analyses (CNWRA®) has been engaged in studying radionuclide sorption processes for more than 20 years, including experimental analysis, process modeling, and abstracting detailed sorption models for performance assessment calculations.

This knowledge capture report summaries some of the technical assistance work undertaken on behalf of the U.S. Nuclear Regulatory Commission (NRC). In addition, it provides as an attachment a listing of journal articles, reports, abstracts, and scientific notebooks the CNWRA staff produced since 1990 to document the results of this work.

5.2 Key Uncertainties and Future Work

5.2.1 Development of Sorption Coefficient Databases

Sorption coefficient databases can range from simple tabulations, to probability distributions, to complex interrelational computerized datasets. Historically, the tendency has been to use these databases as a source of individual sorption coefficients for the contaminant of interest. It is important, however, that the users of these compilations understand the assumptions and adequacy of experimental data (including quality assurance) that form the basis for the values presented in the database. This understanding is necessary for the user to characterize the limitations, conservatisms, and uncertainties inherent in the dataset and make an informed decision with regard to selecting values that are appropriate to different systems. Special care should be taken in selecting sorption coefficients for contaminants that are sensitive to geochemical and physical conditions. Experimental and modeling work at CNWRA has shown different ways to address the uncertainties due to these types of natural variability in geochemical systems. However, these approaches are generally calibrated based on batch sorption experiments using pure end-member minerals. More realistic approaches should be investigated to examine the extent to which these relatively simple surface complexation models and ion-exchange models can be productively applied to natural materials and mineral mixtures likely to be encountered along the groundwater flow path.

5.2.2 Steel Corrosion Product Sorption

As discussed in Section 4.6.1, products of corrosion of in-package steel components may play a role in radionuclide release from nuclear waste containers. Important uncertainties in modeling transport through the container include.

- Temporal evolution of corrosion product mineralogy
- The nature and temporal evolution of physical characteristics of the corrosion products, including surface area, crystallinity, and the potential for preferential pathways through the corrosion products or pathways that bypass them

- Temporal evolution of aqueous chemical conditions in the waste package
- Sorption coefficients on steel corrosion products
- Sorption kinetics
- Sorption competition

The CNWRA staff initiated a study of plutonium sorption onto goethite as an independent confirmatory analysis of the effectiveness of steel corrosion products at delaying waste package release. That work continues now under the Integrated Spent Nuclear Fuel Regulatory Activities program because it has application in a wide variety of potential geologic repository settings.

5.2.3 Radionuclide Systems

CNWRA sorption work has focused on actinides in general, and uranium and neptunium in particular. Other radionuclides that can have an effect on performance include plutonium, americium and thorium and fission products such as technetium and iodine. Particularly for plutonium, there is a general lack of suitable experimental data from which to apply the methods outlined in this report. Additional work will be needed to provide sorption results over a suitably wide range in geochemical conditions to allow model calibration and testing through model predictions.

APPENDIX

LIST OF CENTER FOR NUCLEAR WASTE REGULATORY ANALYSES (CNWRA®) SORPTION-RELATED PRODUCTS

Bertetti, F.P., J. Prikryl, and B. Werling. "Development of Updated Total-System Performance Assessment Parameter Distributions for Radionuclide Transport in the Saturated Zone." San Antonio, Texas: CNWRA. 2004.

Bertetti, P. and D.R. Turner. "Review of U.S. Department of Energy (DOE) Study Plan 8.3.1.3.4.2—Biological Sorption and Transport." San Antonio, Texas: CNWRA. 1993.

Bertetti, F.P. and B. Werling. "Predecisional for Official Use Only: Sorption of Neptunium-237 on Alluvium Collected from Fortymile Wash, Nye County, Nevada." San Antonio, Texas: CNWRA. 2005.

McMurry, J. and F.P. Bertetti. "Selection of Sorption-Related Values for Unsaturated Zone and Saturated Zone Transport in Total-System Performance Assessment." San Antonio, Texas: CNWRA. 2007.

McMurry, J. and F.P. Bertetti. "Draft: Selection of Sorption-Related Values for Unsaturated Zone and Saturated Zone Transport in Total-System Performance Assessment." San Antonio, Texas: CNWRA. 2007

Pabalan, R. and D.R. Turner. "Center for Nuclear Waste Regulatory Analyses Review of the Nuclear Waste Management Organization (NWMO) Report: Sorption in Highly Saline Solutions—State-of-Science Review." San Antonio, Texas: CNWRA. 2009

Pabalan, R.T. "Report on the Peer Review of the Sorption Modeling for High-Level Performance Assessment Research Project." CNWRA 95-023. San Antonio, Texas: CNWRA. 1995.

Prikryl, J.D. and R.T. Pabalan. "Proposal 20-20026: Radionuclide Sorption on Surfactant-Modified Natural Zeolites." San Antonio, Texas: CNWRA. 1996.

Prikryl, J.D. and D.A. Pickett. "Recommended Site-Specific Sorption Coefficients for Reviewing Non-High-Level Waste Determination at the Savannah River Site and Idaho National Laboratory." Rev. 1. San Antonio, Texas: CNWRA. 2007

Turner, D.R. "Center for Nuclear Waste Regulatory Analyses Input to the Nuclear Energy Agency Phase II Sorption Modeling Project." San Antonio, Texas: CNWRA. 2002.

Turner, D.R. "Radionuclide Sorption in Fractures at Yucca Mountain, Nevada: A Preliminary Demonstration of Approach for Performance Assessment." San Antonio, Texas: CNWRA. 1998.

Turner, D.R. "A Uniform Approach to Surface Complexation Modeling of Radionuclide Sorption." CNWRA 95-001. San Antonio, Texas: CNWRA. 1995.

Turner, D.R. "Mechanistic Approaches to Radionuclide Sorption Modeling." CNWRA 93-019. San Antonio, Texas: CNWRA. 1993.

Turner, D.R. "Sorption Modeling for High-Level Waste Performance Assessment: A Literature Review." CNWRA 91-011. San Antonio, Texas: CNWRA. 1991.

Turner, D.R. "Effects of Variable Hydrologic Saturation on Sorption Modeling for High-Level Waste Performance Assessment: A Literature Review." CNWRA 91-016. San Antonio, Texas: CNWRA. 1991.

Turner, D.R., F.P. Bertetti, and R.T. Pabalan. "Applying Surface Complexation Modeling to Radionuclide Sorption." San Antonio, Texas: CNWRA. 2005.

Turner, D., B. Sagar, and W. Ott. "Trip Report: Attendance at the Workshop on Sorption: Conclusion of the Nuclear Energy Agency (NEA) Sorption Project II on Use of Thermodynamic Sorption Models (TSM) in Performance Assessment held at Paris, France, October 10–11, 2005." San Antonio, Texas: CNWRA. 2005

Turner, D., G. Wittmeyer, and P. Bertetti. "Radionuclide Sorption in the Alluvium at Yucca Mountain, NV—A Preliminary Demonstration of an Approach for Performance Assessment—Letter Report." San Antonio, Texas: CNWRA. 1998.

Abstracts/Posters/Presentations

Bertetti, F.P., R. Pabalan, D.R. Turner, and M.G. Almendarez. "Studies of Neptunium(V) Sorption on Montmorillonite, Clinoptilolite, Quartz and a-Alumina." American Chemical Society Annual Meeting Abstract, New Orleans, Louisiana, March 24–28, 1995. Washington, DC: American Chemical Society. 1996.

Bertetti, F.P., R.T. Pabalan, and D.R. Turner. "Neptunium (V) Sorption Behavior on Clinoptilolite, Quartz and Montmorillonite." Materials Research Society Fall Meeting Abstract. Boston, Massachusetts, November 27–December 1, 1995. Warrendale, Pennsylvania: Materials Research Society. 1996.

Bertetti, F.P., R.T. Pabalan, and M.G. Almendarez. "Studies of Neptunium(V) Sorption on Quartz, Clinoptilolite, Montmorillonite, and A-Alumina." Proceedings of the American Chemical Society Symposium Abstract, New Orleans, Louisiana, March 26–29, 1996; and 211th American Chemical Society Symposium on Sorption of Metals on Earth Material: Factors, Rates, Mechanisms, and Model Applications, New Orleans, Louisiana, March 26–29, 1996. Washington, DC: American Chemical Society. 1996.

Bertetti, F.P., R.T. Pabalan, D.R. Turner, and M.G. Almendarez. "Experimental Studies of Neptunyl Sorption on Quartz, Clinoptilolite, and Montmorillonite." Annual Meeting of the Geological Society of America Abstract, New Orleans, Louisiana, November 6–9, 1995. Washington, DC: Geological Society of America. 1995.

Bertetti, F.P., R.T. Pabalan, D.T. Turner, and M.G. Almendarez. " Neptunium(V) Sorption Behavior on Clinoptilolite Quartz and Montmorillonite." Materials Research Society Meeting Paper, Boston, Massachusetts, November 27–December 1, 1995. Warrendale, Pennsylvania: Materials Research Society. 1995.

Bertetti, P.F., R.T. Pabalan, D.R. Turner, and M. Almendarez. "Experimental Study of Uranium (+6) Sorption on Quartz Sand. Geological Society of America (GSA) Annual Meeting Abstract, Seattle, Washington, October 24–27, 1994. Washington, DC: Geological Society of America. 1994.

Greathouse, J. and R.T. Pabalan. "Molecular Simulation of Uranium(6+) Adsorption on Quartz Surfaces." Proceedings of the 24th International Symposium on the Scientific Basis for Nuclear Waste Management Abstract, Sydney, Australia, August 27–31, 2000. Warrendale, Pennsylvania: Materials Research Society. 2000.

Jain, A., J.D. Prikryl, R.T. Pabalan, and D.R. Turner. "Experimental and Modeling Studies of Uranyl Adsorption Onto Binary Mixture of Silicate Minerals." Proceedings of the 217th American Chemical Society National Meeting Abstract, Anaheim, California, March 21–25, 1999. Washington, DC: American Chemical Society. 1999.

Pabalan, R.T. "Radionuclide Sorption in High-Level Waste Performance Assessment: Abstraction of Results From Experiments and Surface-Complexation Models." Workshop on Conceptual Model Development for Subsurface Reactive Transport Modeling of Inorganic Contaminates, Radionuclides, and Nutrients Presentation, Albuquerque, New Mexico, April 20–22, 2004. Washington, DC: NRC. 2004.

Pabalan, R., F.P. Bertetti, J.D. Prikryl, and D.R. Turner. "Uranium(VI) Sorption Onto Selected Mineral Surfaces: Key Geochemical Parameters." Chapter 3. E. Jenne, ed. American Chemical Society Annual Meeting Abstract/Presentation, New Orleans, Louisiana, March 24–29, 1996. San Diego, California: American Chemical Society. pp. 100–130. 1996.

Pabalan, R.T. and M. Lupkowski. "Molecular Dynamics Simulation of Uranyl Sorption on Mineral Surfaces." Spring Meeting, American Geophysical Union Abstract, Baltimore, Maryland, May 23–27, 1994. Washington, DC: American Geophysical Union. 1994.

Pabalan, R.T. and M. Lupkowski. "Molecular Dynamics Simulation of Uranyl Sorption on Mineral Surfaces." Geological Society of America Annual Meetings Article, Boston, Massachusetts, October 25–28, 1993. Washington, DC: Geological Society of America. 1993.

Pabalan, R.T. and D.R. Turner. "Uranium (6+) Sorption on Montmorillonite: Effect pH, EU, and M/V." Symposium on Clays, Surfaces, and the Environment 32nd Annual Meeting of the Clay Minerals Society Abstract, Baltimore, Maryland, June 3–8, 1995. Chantilly, Virginia: Clay Minerals Society. 1995.

Pabalan, R.T., D.R. Turner, and F.P. Bertetti. "Radionuclide Sorption in High-Level Waste Performance Assessment: Abstraction of Results From Experiments and Surface-Complexation Models." Workshop on Conceptual Model Development for Subsurface Reactive Transport Modeling of Inorganic Contaminates, Radionuclides, and Nutrients, Sponsored by the Working Group on Subsurface Reactive Solute Transport; Federal Interagency Collaboration on Multimedia Environmental Models, Abstract, Albuquerque, New Mexico, April 20–22, 2004. Washington, DC: NRC. 2004.

Pabalan, R.T., M. Miller, and M. Lupkowski. "Molecular Dynamics Simulation of Uranyl Adsorption on Quartz Surfaces." Proceedings of the 217th American Chemical Society National Meeting Abstract, Anaheim, California, March 21–25, 1999. Washington, DC: American Chemical Society. 1999.

Pabalan, R.T., D.R. Turner, F.P. Bertetti, and J.D. Prikryl. "Uranium(VI) Sorption Onto Selected Mineral Surfaces: Key Geochemical Parameter." Proceedings of the 211th American Chemical Society Symposium on Sorption of Metals on Earth Material: Factors, Rates, Mechanisms, and Model Applications Article, New Orleans, Louisiana, March 26–29, 1996. Washington, DC: American Geochemical Society. 1996.

Pabalan, R.T., F.P. Bertetti, and J.D. Prikryl. "Geochemical Controls on the Sorption of Uranium (6+) onto Mineral Surfaces." Spring Meeting, American Geophysical Union Abstract, Washington, DC, May 29–June 2, 1995. Washington, DC: American Geophysical Union. 1995.

Pabalan, R.T., T.B. Dietrich, and B.W. Leslie. "The Effects of pH, EU, and Ionic Strength on the Sorption of Uranium (VI) on Clinopilolite." Proceedings of the 4th International Conference on the Chemistry and Migration Behavior of the Actinides and Fission Products in the Geosphere, MIGRATION '93 Abstract, Charleston, South Carolina, December 12–17, 1993.

Pabalan, R.T., J.D. Prikryl, P.M. Muller, and T.B. Dietrich. "Experimental Study of Uranium (6+) Sorption on the Zeolite Mineral Clinoptilolite." Symposium V 1992 Materials Research Society Fall Meeting Article, Boston, Massachusetts, November 30–December 4, 1992. Warrendale, Pennsylvania: Materials Research Society. 1992.

Pabalan, R.T., J.D. Prikryl, and P.M. Muller. "Experimental Study of U6+ Sorption on the Zeolite Mineral Clinoptilolite." Proceedings of the Seventh International Symposium on Water-Rock Interaction, Abstract. Research Triangle Park, North Carolina: International Association of GeoChemistry. 1991.

Painter, S., V. Cvetkovic, D. Pickett, and D. Turner. "Significance of Kinetics for Sorption on Inorganic Colloids: Modeling and Data Interpretation Issues." American Geophysical Union Fall Meeting Abstract, San Francisco, California, December 10–14, 2001. Washington, DC: American Geophysical Union. 2001.

Prikryl, J. and R. Pabalan. "Sorption of Uranium (VI) and Neptunium (V) by Surfactant Modified Natural Zeolites." Proceedings of the Materials Research Society Symposium on the Scientific Basis for Nuclear Waste Management Abstract, Boston, Massachusetts, November 30–December 4, 1998. Warrendale, Pennsylvania: Materials Research Society. pp. 1,035–1,042. 1998.

Prikryl, J.D., A. Jain, D.R. Turner, and R.T. Pabalan. "Uranium(VI) Sorption Behavior on Silicate Mineral Mixtures." Proceedings of the Seventh International Conference on the Chemistry and Migration Behavior of Actinide and Fission Products in the Geosphere, Article, Lake Tahoe, Nevada, September 26–October 1, 1999. Munich, Germany: Oldenbourg Verlag. 1999.

Prikryl, J.D., F.P. Bertetti, and R.T. Pabalan. "Effects of Surfactant Modification on the Sorption Behavior of Natural Zeolites for Strontium (2+) and Uranium (6+)." Proceedings of the Materials Research Society Symposium on the Scientific Basis for Nuclear Waste Management Abstract, Boston, Massachusetts, November 29–December 3, 1999. Warrendale, Pennsylvania: Materials Research Society. 1999.

Prikryl, J.D., P. Bertetti, and R.T. Pabalan. "Effects of Surfactant Modification on the Sorption Behavior of Natural Zeolites for Strontium (2+) and Uranium (6+)." R. Smith, and D. Shoesmith eds. Scientific Basis for Nuclear Waste Management XXIII 608, Article. Warrendale, Pennsylvania: Materials Research Society. pp. 281–286. 1999.

Prikryl, J.D., R.T. Pabalan, D.R. Turner, and B.W. Leslie. "Uranium Sorption on Alumina: Effects of pH and Surface-Area/Solution—Volume Ratio." Fourth International Conference on the Chemistry and Migration Behavior of Actinides and Fission Products in the Geosphere, Article, MIGRATION '93, Charleston, South Carolina, December 12–17, 1993. Munich, Germany: Oldenbourg Verlag. 1993.

Sagar, B. "Thermodynamic Sorption Models in Safety Assessments: Regulatory View." Nuclear Energy Agency (NEA) Sorption Project Workshop, Article, Paris, France, October 10–11, 2005. Paris, France: Nuclear Energy Agency. 2005.

Turner, D.R. "The Role of Radionuclide Sorption in High-Level Waste Performance Assessment: Approaches for the Abstraction of Detailed Models." Annual Meeting of the Soil Science of America Annual Meeting, Abstract. Salt Lake City, Utah: October 31–November 4, 1999.

Turner, D. "Approaches to Sorption Modeling for High-Level Waste Performance Assessment." Fourth International Conference Chemistry and Migration Behavior of the Actinides and Fission Products in the Geosphere, Article, MIGRATION '93, Charleston, South Carolina, December 12–17, 1993. Munich, Germany: Oldenbourg Verlag. 1993.

Turner, D. "Radionuclide Sorption Modeling Using the MINTEQA2 Speciation Code." Sixteenth International Symposium on the Scientific Basis for Nuclear Waste Management, Abstract, Boston, Massachusetts, November 30–December 4, 1992. Pittsburgh, Pennsylvania: Material Research Society. 1992.

Turner, D.R. and R.T. Pabalan. "Abstraction of Mechanistic Sorption Models for Performance Assessment Calculations at Yucca Mountain, NV." Proceedings of the Waste Management '99 Conference Paper, Tucson, Arizona, February 28–March 4, 1999. Published on CD ROM. Tucson, Arizona: WM Symposia, Inc. 1999.

Turner, D.R. and R.T. Pabalan. "Sorption Modeling for Performance Assessment at the Center for Nuclear Waste Regulatory Analyses." Nuclear Energy Agency (NEA), Abstract, Cambridge, United Kingdom, May 5–8, 1997. Paris, France: Nuclear Energy Agency. 1997.

Turner, D. and S.A. Sassman. "Approaches to Sorption Modeling for High-Level Waste Performance Assessment." Fourth International Conference on the Chemistry and Migration Behavior of Actinides and Fission Products in the Geosphere, Article, Charleston, South Carolina, December 12–17, 1993.

Turner, D.R., F.P. Bertetti, J. McMurry, and R.T. Pabalan. "Applying Thermodynamic Radionuclide Sorption Models to Performance Assessment." Nuclear Energy Agency (NEA) Sorption Workshop Presentation, Paris, France, October 10–11, 2005. Paris, France: Nuclear Energy Agency. 2005.

Turner, D.R., R.T. Pabalan, and F.P. Bertetti. "Developing Thermodynamic Radionuclide Sorption Models: Experimental and Modeling Results." Nuclear Energy Agency (NEA) Sorption Workshop Presentation, Paris, France, October 10–11, 2005. Paris, France: Nuclear Energy Agency. 2005.

Turner, D.R., F.P. Bertetti, and R.T. Pabalan. "The Role of Radionuclide Sorption High-Level Waste Performance Assessment." *Soil Geochemical Processes of Radionuclides*. Proceedings of the 2001 Soil Science Society of America. Madison, Wisconsin: Soil Science Society of America. 2001.

Turner, D.R., R.T. Pabalan, J.D. Prikryl, and F.P. Bertetti. "Radionuclide Sorption at Yucca Mountain, Nevada—A Demonstration of an Alternate Approach for Performance Assessment." Symposium on the Scientific Basis for Nuclear Waste Management XXII, Materials Research Society Fall Meeting Paper, Boston, Massachusetts, November 30–December 3, 1998. Warrendale, Pennsylvania: Materials Research Society. 1998.

Turner, D.R., R.T. Pabalan, P. Muller, and F.P. Bertetti. "Uniform Surface Complexation Approaches to Radionuclide Sorption Modeling." Proceedings of the Sixth Annual International Conference on High-Level Radioactive Waste Management Paper, Las Vegas, Nevada, May 1995. La Grange Park, Illinois: American Nuclear Society. 1995.

Turner, D.R., T. Griffin, and T.B. Dietrich. "Radionuclide Sorption Modeling Using the MINTEQA2 Speciation Code." Symposium V 1992 Materials Research Society Fall Meeting Paper, Boston, Massachusetts, November 30–December 4, 1992. Warrendale, Pennsylvania: Materials Research Society. 1992.

Zaidan, O.F., J.A. Greathouse, and R.T. Pabalan. "Computer Simulation of Uranyl Adsorption on Montmorillonite Clay." 12th Annual V.M. Goldschmidt Conference Abstract, Davos, Switzerland, August 18–23, 2003. Oxford, United Kingdom: Cambridge Publications. 2003.

Journal Articles/Book Chapters

Bertetti, P.F., R.T. Pabalan, D.R. Turner, and M. Almendarez. "Experimental and Modeling Study of Uranium (6+) Sorption on Quartz." *Journal Applied Geochemistry*. 1995.

Cvetkovic, V. and S. Painter. "Final Journal Article: Field-Scale Transport Implications of Sorption Kinetics with Multiple Rates." *Journal of Waters Resources Research.* 2008.

Jarzemba, M.S. "An Improved Method for Modeling Sorption of Radionuclides During Liquid Phase Transport for Performance Assessments of High-Level Waste Repositories." *Nuclear Technology*. 1995.

Pabalan, R.T. and D.R. Turner. "Uranium (+6) Sorption on Montmorillonite: Experimental and Surface Complexation Modeling Study." *Aquatic Geochemistry*. 1995.

Painter, S., V. Cvetkovic, D. Pickett, and D.R. Turner. "Significance of Kinetics for Sorption on Inorganic Colloids: Modeling and Experiment Interpretation Issues." *Environmental Science and Technology*. Vol. 36. pp. 5,369–5,375. 2002.

Prikryl, J.D., A. Jain, R.T. Pabalan, and D.R. Turner. "Uranium (VI) Sorption Behavior on Mixed Silicate Minerals." *Journal of Contaminant Hydrology*. Vol. 47, Issues 2–4. pp. 241–253. 1999.

Turner, D.R., R.T. Pabalan, and F.P. Bertetti. "Neptunium(V) Sorption on Montmorillonite: Experimental and Surface Complexation Modeling Study." *Environmental Science and Technology*. 1996.

Wang, P., A. Anderko, and D.R. Turner. "Thermodynamic Modeling of the Adsorption of Radionuclides on Selected Minerals II: Anions." *Geochimica et Cosmochimica Acta*. 2000.

Wang, P., A. Anderko, and D.R. Turner. "Thermodynamic Modeling of the Adsorption of Radionuclides on Selected Minerals I: Cations." *Geochimica et Cosmochimica Acta*. 2000.

Zaidan, O.F., J.A. Greathouse, and R.T. Pabalan. "Monte Carlo and Molecular Dynamics Simulation of Uranyl Adsorption on Montmorillonite Clay." *Clays and Clay Minerals*. Vol. 51. pp. 372–381. 2002.

Scientific Notebooks

Bertetti, P. "Neptunium Sorption Experiments (03/18/1999–03/27/2002)." Scientific Notebook No. 309. San Antonio, Texas: CNWRA. 2002.

Browning, L. "Development of a New Sorption Database for the Geochemist's Workbench (GWB), Release 3.0 (06/01/1999–04/06/2000)." Scientific Notebook No. 331. San Antonio, Texas: CNWRA. 2000.

CNWRA. "Supplemental Material, Technical Activity Supporting Documentation: Experimental Data for Uranium Sorption on a-alumina Experiments B–8005, B–8006, and B–8007 (1993). San Antonio, Texas: CNWRA. 2004.

Jain, A. and D.Turner. "Radionuclide Transport Sorption Experiments (08/11/1999–08/24/2000)." Scientific Notebook No. 365. San Antonio, Texas: CNWRA. 1999.

Nugent, M. and D. Turner. "Sorption Experiments with Clinoptilolite and Montmorillonite (10/08/1999 through 08/28/2000)." Scientific Notebook No. 370. San Antonio, Texas: CNWRA. 1999.

Pabalan, R., R. Ghubash, J.D. Prikryl, and P. Bertetti. "Geochemistry Project: Zeolite Sorption Experiments (GC-10) (06/08/1993–01/08/1997). Scientific Notebook No. 061. San Antonio, Texas: CNWRA. 1997.

Pabalan, R.T. "Geochemistry Research Laboratory Notebook: Ion Exchange and Sorption Experiments (06/11/1991-03/21/1992)." *Vol. GC–05, Geochemistry Research Laboratory Notebook: Ion Exchange and Sorption Experiments (06/11/1991–03/21/1992).* Scientific Notebook No. 026. San Antonio, Texas: CNWRA. 1992.

Pabalan, R.T., P. Muller, and T. Dietrich. "Vol. GC–07 Geochemistry Research Laboratory Notebook: Ion Exchange and Sorption Experiments (03/21/1992–06/09/1993)." Scientific Notebook No. 037-1. San Antonio, Texas: CNWRA. 1993.

Pabalan, R.T., P. Muller, T. Dietrich, and J. Prikryl. "Vol. GC–06 Geochemistry Research Laboratory Notebook: Ion Exchange and Sorption Experiments (03/21/1992–12/10/1996)." Scientific Notebook No. 038. San Antonio, Texas: CNWRA. 1996.

Pickett, D. "Actinide Sorption Experiments (02/07/1995–02/23/2007)." Scientific Notebook No. 133. San Antonio, Texas: CNWRA. 2007.

Prikryl, J. "Focused Research Proposal-Radionuclide Sorption on Surfactant Modified Natural Zeolites (11/04/1996–02/04/2000). Scientific Notebook No. 200. San Antonio, Texas: CNWRA. 1996.

Sabido, L. "Modeling Np (V) Sorption to Calcite Based on Batched Sorption Experiments and Surface Complexation Modeling Performed by Zarvin, et al., 2004 (04/27/2007–02/14/2008)." Scientific Notebook No. 874E. San Antonio, Texas: CNWRA. 2008.

Turner, D. "Sorption Modeling for High-Level Waste Performance Assessment (06/02/1992–01/13/1997)." Scientific Notebook No. 046. San Antonio, Texas: CNWRA. 1997.

Turner, D. "Sorption Modeling for Performance Assessment (06/16/1992–09/09/1994)." Scientific Notebook No. 057. San Antonio, Texas: CNWRA. 1995.

Turner, D.R. and P.M. Muller. "Sorption Modeling of Radionuclide Sorption Using Surface Complexation Modeling Techniques (09/09/1994–01/20/1996)." Scientific Notebook No. 123. San Antonio, Texas: CNWRA. 1996.

Turner, D., J. Prikryl and A. Jain. "Uranium Sorption Experiments (04/21/1998–06/13/2000)." Scientific Notebook No. 266. San Antonio, Texas: CNWRA. 1998.

Werling, B. "Cation and Anion Analyses of Solutions From Sorption Experiments 19 and 22 CAL Series 1." Scientific Notebook No. 830. San Antonio, Texas: CNWRA. 2006.

Werling, B. "Neptunium/Calcite Sorption Experiments (05/29/2001–0/21/2002)." Scientific Notebook No. 463. San Antonio, Texas: CNWRA. 2001.

Werling, B. and M. Roberts. "Np Sorption on Consolidated With Simulated Waters (With and Without Calcium) Over a pH Range—Identified as CAL (Consolidated Alluvium) Series 5 and 6—(06/06/2005–08/30/2005)." Scientific Notebook No. 711. San Antonio, Texas: CNWRA. 2005.

Werling, B. and S. Watson. "Cation and Anion Analyses of Solutions from Sorption Experiments 19 and 22 CAL Series 1 (08/080/2006–11/06/2006). Scientific Notebook No. 812. San Antonio, Texas: CNWRA. 2006

Werling, B., M. Roberts, R. McGinnis, and P. Bertetti. "Cation Analyses of Experimental Solutions from Sorption Experiments CAL Series 7 and 8 (08/30/2005–08/31/2006)." Scientific Notebook No. 733. San Antonio, Texas: CNWRA. 2006

Werling, B., J. Brown, and P. Bertetti. "Neptunium-Calcite Sorption Experiments (06/25/2002–03/14/2003)." Scientific Notebook No. 463. San Antonio, Texas: CNWRA. 2002.